CATALYTIC RECYCLING OF CARBON FIBER REINFORCED THERMOSET POLYMERS (CFRPs)

Dissertation for the award of the academic degree

- Dr. rer. nat. –

Submitted to the Faculty of Natural Sciences at Paderborn University

by

Najmeh Filvan Torkaman

born on 01.03.1984 in Tehran (Iran)

Paderborn University

Faculty of Natural Sciences

Department of Chemistry

Coatings, Materials & Polymers

Reviewers: Prof. Dr. Wolfgang Bremser, Prof. Dr. Rene Wilhelm, AOR. Dr. Ilona Horwath

Acknowledgement

First of all, I would like to thank Professor Bremser and Professor Wilhelm for all their consistent support and guidance on the way to my doctoral degree. Also special thanks to Dr. Horwath from the Technik and diversity research group for all her support and advice. I would like to express my sincere gratitude to the FKLEM program for letting me be a part of such an incredible network and especially thanks to all colleagues in the recycling cluster of FKLEM. A big thanks to all my colleagues at CMP research group. I spent great moments with them in the laboratory and exchange meetings. Furthermore, special thanks to Dr. Oliver Seewald and Dr. Horst Hintze-Bruening for all their assistance. I would like also to thank Mr. Moritz Ostermann for analyzing the survey results and collecting the data.

I should also thank some colleagues at LiA who were always available to help me working with the machines in the mechanical engineering lab.

At the end, thank you is the smallest word to appreciate my amazing husband. I deeply thank him for being beside me in every situation and for all his kindness and support. I can confidently say that he paved the way for me to move forward strongly without any fear. Thanks also to my two sons that their love is always a great motivation for me. On the other hand, thanks to my parents who live far away from me, but always send me hope, motivation and encourage me.

Abstract

The aim of this PhD research was to investigate a sustainable approach of light weight engineered materials. According to this goal, two paths were examined. Recycling of the CFRPs composite made out the prepreg and also make a recyclable graphene composite via a reversible Diels-Alder cycloaddition reaction on graphite. The recycling of the CFRPs was done successfully. Making a recyclable graphene composite was partially successful.

According to the high demand of CFRPs composite in many applications especially prepreg, and also the properties of epoxy matrix which is thermoset and is not able to reshape after curing, the recycling method at mild condition without destroying the chemical and mechanical properties of carbon fiber is of huge importance, thus, this approach was performed to recycling CFRPs made out of prepreg by utilizing catalyst in DMAc(Dimethylacetamide) solvent at 160°c for 5 hours. Two catalysts, Aluminum nitrate nonahydrate and Iron nitrate nonahydrate display high efficiency to cleavage the C-N bond in cured composite with 100% degradation ratio of carbon fiber, but aluminum nitrate exhibited better results and the properties of the recycled fibers are comparable with the virgin carbon fibers in the prepreg. At the end, solvent was recycled too and reused several times in the recycling process. Degradation product was used as co-hardener in the new cured epoxy due to the existence of nitrogen in the structure of degradation product.

Furfurylamine was successfully grafted to the graphite, mostly at the edges, by DA reaction and consequently by raising the temperature, retro DA occurred. DA and R-DA were confirmed by several analytical methods.

Sustainable and responsible engineering, inter and transdisciplinary concepts were another topic during this PhD study that was part of research in Technik and Diversity research group. By conducting survey and also by cooperation with industry, the connection between society and science was made.

Contents

Chapter 1 Introduction

Besides conventional materials, advanced materials recently enhance the standards of our life. They are divided into four categories based on their structure and characteristics and their application area: ceramics, metals, plastics, and composites. Among them, composite materials, which are composed of multi-materials, exhibit the combination of the best properties of each of the components that are not displayed by any single one. Therefore, composites have been turned into common and useful engineered materials and provide unlimited opportunities for developed products and raise the global market competition especially in lightweight components. [1]

Lightweight design is reaping notable benefits along with various applications, so it has been turned into a hot topic in product design in several industries. Global trends toward CO_2 and greenhouse gas (GHG) reduction, energy saving, and resource efficiency have dramatically increased the importance of this topic over the last years. Especially the automotive industry is of particular importance in this issue, while lightweight materials are being used to enhance vehicle fuel economy as well. In fact, a 10% increase in the curb weight of the vehicle can be led to a 6.4% increase in fuel consumption. [2,3]

1.1. Carbon Fiber Reinforced Polymers composite (CFRPs)

CFRPs are prominent lightweight composites that are formed by carbon fiber as reinforcement embedded or bonded to a matrix resin with distinct interfaces (boundaries) between them. In this form, both fibers and matrix retain their physical and chemical identities and they produce a mixture of properties that cannot be gained with either of the components acting alone. In fact, fibers are the principal load-carrying constituent, while the surrounding matrix firmly keeps them in the desired orientation, acts as a load transfer medium between them, and protects them from environmental damage due to elevated temperatures and humidity. Thus, even though the fibers provide reinforcement for the matrix, the latter also offers several useful functions in a fiber-reinforced composite material. [4,5,6]

CFRPs exhibit exceptional properties such as a high strength-to-weight ratio and high wear resistance, high durability, stiffness, thermal stability, fatigue resistance and light weight which give them an advantage over other conventional materials such as concrete and steel. [7,8] Additionally, CFRP composites are highly adaptable, making them ideal for complex structures [9]. Carbon fibers have the flexibility to be interwoven into a variety patterns and orientations, resulting in a material tailored to meet precise structural demands. This enables the creation of structures that are both durable and lightweight, as well as aesthetically pleasing. [10]

Reinforcement provides the strength and rigidity that is needed, and which helps to support the structural load. The matrix or the binder helps to maintain the position and orientation of the reinforcement and is somewhat more brittle.

These unique properties have led to widely used of CFRPs in variety of applications, for instance in the Automotive [11,12] and Marine industries [13], aerospace [14,15] ,medical technology [16,17,18], wind energy [19,20] , robotics [21,22], sports and leisure sector [23,24,25], construction [26] and so on.

1.1.1. Properties and Structure of Carbon Fiber

Carbon fibers can be defined as fibers with a carbon content of 90% or above. They are transformed by thermal treatment of organic matters with a lower carbon content such as

polyacrylonitrile (PAN) containing several thousand filaments with diameter between 5 and 10 μm. Though cellulose was the early precursors used for carbon fiber, but todays, over 90% of commercial carbon fibers are produced from polyacrylonitrile (PAN) precursors, due to its combination of tensile and compressive properties as well as the carbon yield [27]. The primary reason for this widespread use of PAN is the fact that PAN polymer does not melt but can be dissolved in suitable solvents. Consequently, PAN precursors can be solution-spun into thin fibers that can be thermally processed into intractable fibers because PAN does not melt. It undergoes crosslinking and ladder-formation reactions before melting, and leads to the formation of intractable fibers, which can be further heat treated to temperatures in the 1000–1500 °C range to obtain carbon fibers. The final properties of the fibers depend on the processing details and also whether the fibers undergo a final graphitization heat-treatment. The finished PAN fibers have diameters between 5−10 μm. As shown in **Figure 1**, The surface finish is reminiscent of tree bark. Additional processing can strip off the 'bark', leaving smoother and smaller diameter fibers that can be packed into smaller spaces in the matrix, and hence provide higher stiffness per cross-sectional area. However, these fibers are more expensive owing to the additional processing.

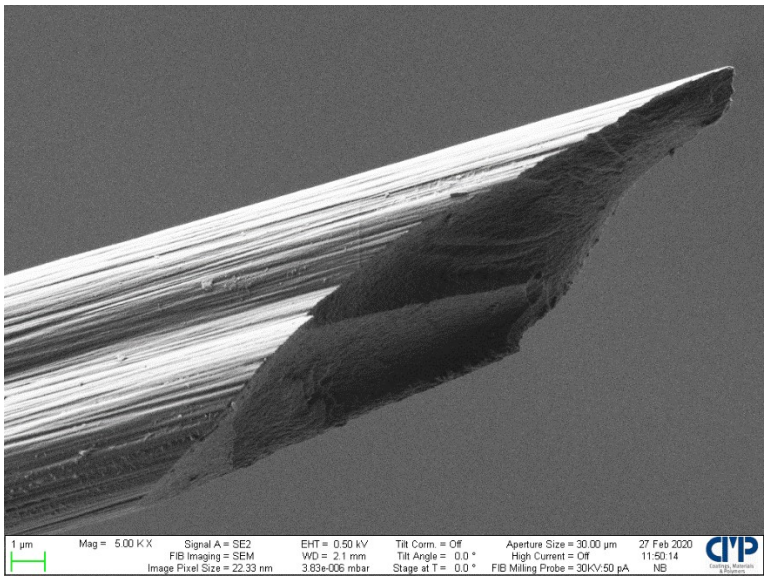

Figure 1. Carbon fibers viewed in the Scanning Electron Microscope (SEM)

Carbon fibers generally have excellent tensile properties, low densities, high thermal and chemical stabilities in the absence of oxidizing agents, good thermal and electrical conductivities, and excellent creep resistance.

In terms of final mechanical properties, carbon fibers can be roughly classified into ultra-high modulus (>500 GPa), high modulus (>300 GPa), intermediate modulus (>200 GPa), low modulus (100 GPa), and high strength (>4 GPa) carbon fibers [28,29] .The atomic structure of a carbon fiber is similar to that of graphite, consisting of carbon atom layers (graphene sheets) arranged in a regular hexagonal pattern, depending upon the precursors and manufacturing processes, layer planes in carbon fibers may be either turbostratic, graphitic, or a hybrid structure. In graphitic crystalline regions, the layer planes are stacked parallel to one another in a regular fashion. The atoms in a plane are covalently bonded through SP^2 bonding while the interaction between the sheets is relatively weak Van der Waals forces, giving the graphite its soft and brittle properties. In a single graphitic crystal, d-spacing between two graphene layers (d002) is about 0.335 nm. In a turbostratic structure, the parallel graphene sheets are stacked irregularly or haphazardly folded, tilted, or split. It has been reported that the irregular stacking and the presence of SP^3 bonding can increase d-spacing to 0.344 nm. Turbostratic carbon fibers usually show higher elastic modulus but lower tensile strength than graphitic carbon fibers.

Generally, carbon fibers are made from Poly Acrylo Nitrile (PAN) based and pitch-based formulation. One difference is the different distribution of π-orbital-oriented domains, as well as the diameter and cross-sectional shape of the fibers that has impact on mechanical properties of carbon fibers. **Figure 2** shows the, that the size and distribution of the π-orbital-oriented domains were different between the PAN- and pitch-based CFs. The white arrows represent the direction of graphene sheets along the fibers and the green ones within the fiber cross section. The direction of the graphene sheets in the PAN-based CFs is parallel to the axis of the fibers that are randomly oriented within the cross section. The size of the π-orbital-oriented domains, if it exists, is less than approximately 50 nm. By contrast, the pitch-based CFs consist of π-orbital-oriented domains whose sizes are approximately 100 nm^{-1} μm. The direction of the graphene sheets in the pitch-based CFs is also parallel to the axis of the fibers.[30]

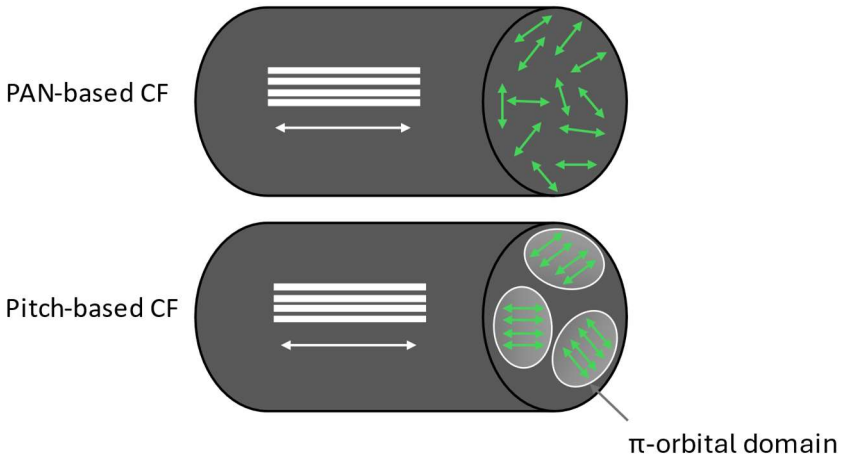

Figure 2. The difference between PAN and Pitch-based CF[30]

1.1.2. Polymers as matrix in CFRPs

Fiber-reinforced plastics utilize two types of matrix materials: Thermoset and Thermoplastic. Thermoplastics, like metals, softening and melting as more heat is applied, and re-hardening with cooling. This process of crossing the softening and/or melting threshold (Tg) can be repeated as often as desired without any appreciable effect on the material properties in either state. Common thermoplastics include acrylic, nylon, polyester, polypropylene, polystyrene, and Teflon, polyethylene (PE), polycarbonate (PC), and polyvinyl chloride (PVC), polyamides. Typical thermoplastics used in structural composites parts include Acrylonitrile Butadiene Styrene (ABS), is an opaque engineering thermoplastic widely used in electronic housings, auto parts, consumer products, pipe fittings, Lego toys, and many more**,** Polyaryletherketones (PAEK) are semicrystalline polymers. They exhibit good stability and mechanical strength at high temperatures. PAEK is extremely resistant to chemicals and hydrolysis, making them ideal for medical applications, oil drilling components, automotive gears, etc**,** Polyetheretherketone (PEEK) is a semi-crystalline, high-performance engineering thermoplastic. This rigid opaque (grey) material offers a unique combination of mechanical properties, resistance to chemicals, wear, fatigue, and creep as well as exceptionally high-temperature resistance, up to 260°C (480°F). It is extensively used in demanding applications such as aerospace, automotive, electrical, medical, etc.

The ability to reform thermoplastic components shows tremendous promise for the future of recycling/repurposing thermoplastic composite products when their original use ends.

Thermosetting materials, or 'thermosets', are formed from a chemical reaction in situ, where the resin and hardener/catalyst are mixed and then undergo a non-reversible chemical reaction to form a hard, infusible product. Thermoset plastics and polymers include epoxy, polyurethane, phenolic and silicone as well as materials such as polyester (which can also occur in a thermoplastic form). thermoset resins include some beneficial qualities, for instance: Excellent resistance to solvents and corrosives, high strength to weight ratio, good fiber wetting, resistance to heat and high temperature, High fatigue strength, tailored elasticity and excellent adhesion but thermoset resins, once cured, cannot be reversed or re-shaped, Because of this, the recycling of thermoset composites is extremely difficult and expensive. The most widely used thermosets for aircraft structures are epoxy resins, since they are readily processed and have good chemical and mechanical properties. They also undergo a low viscosity stage during cure, thereby enabling liquid resin-forming techniques like resin transfer molding (RTM). [31]

Another way of observing the behavioral difference between thermosets and thermoplastics is via their molecular weight. As we compare both polymer types, thermosets stand out in how their molecular weight drastically increases upon curing. Thermoplastics are known to have higher molecular weight values than uncured thermosets. However, when crosslinking occurs between two thermosets, a polymer network is formed of molecular weight almost double the weight when the two were separate. As the number of linked molecules increases, the molecular weight continues to rise, exceeding that of thermoplastics. This drastic increase in molecular weight causes major changes in material properties, such as an increased melting point. With a continuous increase in molecular weight due to crosslinking, the melting point can rise and reach a point that exceeds the decomposition point. In that case, a thermoset polymer would have a very high molecular weight that would decompose before it can melt, which defines why thermoset processing is irreversible [32].

Because thermoplastics have a low melting point, they are ideal for applications that use recycled materials. Thermoset plastics, in contrast, are able to withstand high temperatures without losing their shape, making them more durable (**Table 1**).

Thermosets	Thermoplastics
Main Features	
➢ undergo chemical change when cured ➢ low strain to failure ➢ low fracture energy ➢ irreversible processing ➢ very low viscosity possible ➢ absorbs moisture ➢ highly resistant to solvents	➢ non-reacting, no cure required ➢ high strain to failure ➢ high fracture energy ➢ very high viscosity ➢ processing is reversible ➢ absorbs little moisture ➢ limited resistance to organic solvents, in some cases
Advantages	
➢ relatively low processing temperature ➢ good fiber wetting ➢ formable into complex shapes ➢ liquid-resin manufacturing feasible ➢ resistant to creep	➢ short processing times possible ➢ reusable scrap ➢ post-formable: can be reprocessed ➢ unlimited shelf life without refrigeration ➢ high delamination resistance
Disadvantages	
➢ long processing time ➢ long cure (~ 1-2 hours) ➢ restricted storage life (requires refrigeration)	➢ lower resistance to solvents ➢ requires high temperature (300-400ºC) and pressure ➢ can be prone to creep ➢ very poor drapability and tack

Table1. Thermoset and thermoplastic comparison

1.2. CFRPs manufacturing methods

The conventional prepreg and lay-up processing are still the most widely used routes for manufacturing products in aerospace and sport (40%) applications. [33] Pultrusion and filament winding are prevalent in wind turbine blade fabrication and rotary part construction, accounting

for 26% of the share. Molding compounds based on discontinuous carbon fiber reinforced polymer composites such as sheet molding compound (SMC) are prevalent in automotive applications. Out-of- 6 autoclave methods such as resin transfer molding (RTM) and its variations, especially high-pressure RTM, is gaining acceptance in automotive production because of its potential to reduce cycle times to 10 min, albeit an associated high tooling cost that inhibits its progression in industrial adoption (**Figure 3**). [34]

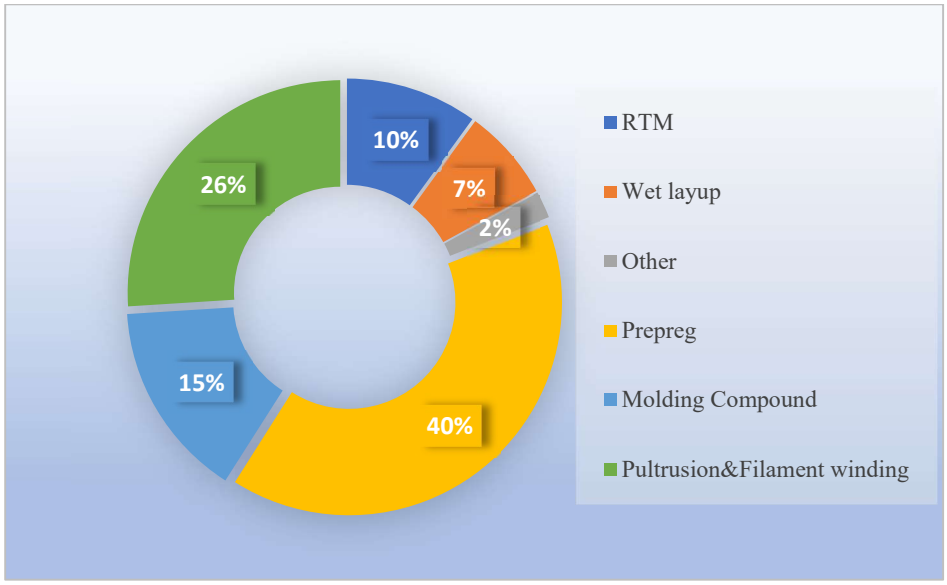

Figure 3. Global carbon fiber demand by manufacturing processes in 2020 [33]

Common Carbon Fiber Manufacturing Methods:

- RTM (Resin Transfer Molding) is categorized within the liquid composite molding processes. Typically, thermosetting resins are chosen as the matrix material owing to their low viscosity, usually in the range of 0.1-0.5 Pa.s. The process involves stacking dry fiber fabrics, which are adept at fitting onto the first mold, and placing them in position. Subsequently, a second mold half, mirroring the shape of the first mold, is clamped over it. A low-viscosity resin from a reservoir is then pumped into the space between the molds, infiltrating and filling the gaps between the fibers. Any air present in the molds is displaced and vented out. Once the fabrics are thoroughly saturated, the resin inlets are sealed, initiating the curing process. Both the injection and curing procedures can be carried out either at elevated temperatures or at ambient temperature. [35]

-In the Wet Lay-up process, carbon fibers are placed onto a mold, saturated with resin, and then rolled or squeegeed to eliminate excess resin. The layup can either remain uncovered or be enclosed with a vacuum bag. Subsequently, it undergoes curing under room temperature or with the application of heat and pressure to produce a carbon fiber composite component. This method is commonly employed for smaller volumes and intricate, challenging-to-mold parts.

Vacuum bagging evolved as an extension of the traditional wet lay-up technique, where carbon fibers are manually impregnated with consolidation rollers. In vacuum bagging, an enhanced impregnation and consolidation process is achieved by covering the wet laid-up fabrics with a plastic film and sealing them onto the tooling plate. A vacuum pump is then used to remove air, creating pressure of up to one atmosphere on the laminate for consolidation purposes.

-Pultrusion involves pulling carbon fibers through a thermoset resin bath and then through a heated die. This process aligns the carbon fibers axially and wets them with resin, creating a strong and lightweight product. Pultrusion is typically used for the production of long, straight parts such as beams, strips, or tubing. [36]

- Prepreg is carbon fiber wetted with resin and partially cured, so it has the consistency of tar paper. It is cured under heat and pressure. Parts made from prepreg are strong and lightweight with higher stiffness and strength and are well suited for use in a variety of high-end applications. Prepreg lay-up is normally used for the production of flat parts such as panels or sheets, or parts with cylindrical curvature because prepreg material will not drape well over compound curvatures. There are two kinds of Prepreg methods: Autoclave and out of autoclave.

In the Prepreg-autoclave method, fiber materials are pre-impregnated by manufacturers with pre-catalyzed resin. The catalyst remains latent at room temperature, providing the prepreg with an extended useful life. Typically stored in a frozen state for prolonged shelf life, during the composite forming process, the prepregs are laid up on a mold surface, covered with bleeder and breather materials, sealed with a vacuum bag, and then heated to temperatures typically ranging from 120 to 180 degrees Celsius [37,38]. This process results in the melting and reflow of resin within the prepreg, followed by curing. The autoclave, by creating an enclosed space, can exert high pressure, up to 5 atmospheres, on the laminate. Autoclave curing is widely utilized in the aerospace industry for producing high-quality laminates. [39]

For Prepreg out of autoclave, Fiber Reinforced Plastic products with a fiber volume fraction ranging from 50% to 60%, extremely high pressure is not necessarily required in the forming process. Instead of using the costly autoclave, the vacuum bagging technique can be employed to provide the required pressure as an economical alternative [38]. The prepreg-out-of-autoclave method combines the use of prepregs with the vacuum bagging technique. In this process, a specific type of prepreg that cures at lower temperatures, typically between 60 to 120 degrees Celsius, is utilized. Heating to the curing temperature can be achieved using simple hot-air circulated ovens [37].

- Filament winding, this process is generally used for hollow components with circular sections, such as pipes and tanks. In the filament winding process continuous impregnated fibers are wounded on a rotating mandrel according to the design pattern, and cure either at room temperature or elevated temperature in an oven. [36]

1.3. The importance of recycling of Carbon fiber reinforced thermoset polymers

As shown in **Figure 4**, the global CFRPs demand has tripled from 2010 to 2020 and is expected to exceed 190 kt by the year 2035. [40-44]

Analyzing global demand statistics categorized by resin types reveals that in 2020, the thermosetting segment emerged as the leading source of revenue. This segment is projected to undergo growth at a Compound Annual Growth Rate (CAGR) of 8.2% within the period spanning from 2020 to 2030. Thermosetting resins, encompassing epoxy, polyester, and acrylics, play a pivotal role in the manufacturing of CFRPs due to their associated advantages. These benefits encompass enhanced fiber-matrix adhesion, adaptability, robust strength, and minimal shrinkage. As a result, the demand for these resins has surged within the global market.[45] Nevertheless, it is essential to acknowledge the counterbalancing challenge posed by the irreversible cross-linked structure inherent in cured thermoset polymers. This unique feature engenders significant obstacles in the recycling of both the fibers and the polymer. Once these materials are cured, they lose the

capacity for processes like melting, remolding, reprocessing, or re-crosslinking into solid polymers.[46] Out of all the manufacturing processes available for CFRPs, the conventional prepreg processing method remains the predominant technique adopted for producing a diverse range of products across various applications, as was mentioned before. This method accounts for 40% of the overall processes, translating to a consumption of 57 kilotons in the year 2020. [47,48]

With these prospects, the development of recycling techniques and methodologies for CFRPs constructed from prepreg and cured with epoxy thermoset resin holds significant interest and importance from both a sustainable and economic standpoint.[49]

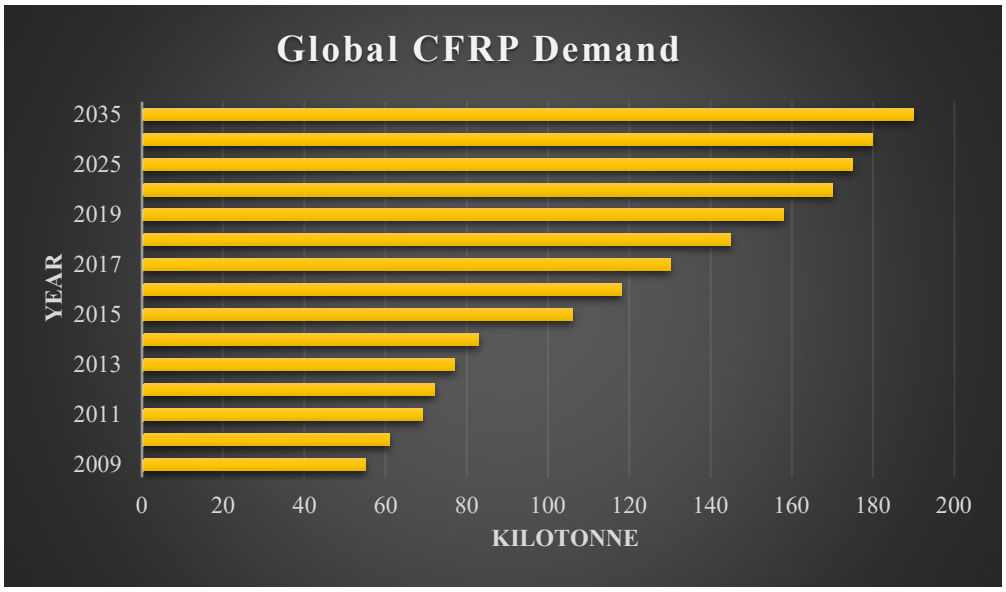

Figure 4. The global demand of CFRPs [40-44]

Chapter 2 Review for recycling of CFRPs

According to the high demand of CFRPs in a variety of applications, especially light weight design engineering, recycling methods are of great importance. On the other hand, energy consumption, environment and economic aspects should be taken into account.

There are a variety of published methods of recycling CFRPs under different conditions.

2.1. Review (recycling methods and processes)

Existing research on recycling carbon fiber composites is primarily focused on three main subjects: mechanical, thermal, and chemical processes. Mechanical methods involve physically disassembling the composites to generate filler materials for the creation of other composite materials. Thermal and chemical methods, on the other hand, are geared towards breaking down the epoxy matrix to recover clean carbon fibers for reuse. In thermal methods, the epoxy matrix is decomposed by the application of heat, which can be carried out in air, inert gas, or a specialized packed bed reactor. On the other hand, chemical methods employ solvolysis to break down the epoxy matrix, substituting heat with a chemical process for decomposition. Both thermal and chemical approaches aim to facilitate the recovery of pristine carbon fibers from recycled composites.

2.1.1. Thermal processes

In terms of thermal processes, Carbon Fiber Reinforced Polymer can undergo various procedures for recycling, including incineration for energy generation or more specialized techniques such as pyrolysis, fluidized bed pyrolysis, and microwave-assisted pyrolysis. [50-53] Incineration, while yielding electricity, produces ash that needs to be disposed of in landfills and is not concluded in reusable materials.

In the pyrolysis process, CFRP is exposed to temperatures ranging between 450°C and 700°C, depending on the type of resin used. These elevated temperatures lead to the decomposition of epoxy, separating the carbon fibers from the composite structure. However, the resulting fibers often require additional treatment for further purification. Prolonged exposure to high temperatures during pyrolysis can potentially degrade the fiber, especially if it is susceptible to oxidation. To mitigate this, controlling the atmospheric conditions in the oven, typically using nitrogen or superheated steam, can reduce char residue and enhance fiber strength.

Fluidized Bed: This method typically involves utilizing a stream of hot air or gas through a bed of particles, such as silica sand, creating a fluid-like mixture where the particulates blend with the air. The fundamental principle behind this process is similar to pyrolysis, as the material is heated to degrade the resin, facilitating the recovery of fibers. Temperatures around 550°C led to the full reclamation of fibers, which could potentially be reintegrated into a resin matrix, albeit with a 25% degradation in strength. Nevertheless, the high temperatures and intricate process flow necessitate sophisticated equipment, rendering this approach economically challenging for industrial implementation. [54]

Microwave-Assisted Pyrolysis: this process takes advantage of microwave radiation for accelerated heating and recycling of CFRPs; However, this method also experiences substantial fiber degradation unless atmospheric conditions are meticulously controlled. It was reported that the use of an argon flow atmosphere, for instance, resulted in the removal of all resin with only a minimal 0.7% loss in strength [26]. While pyrolysis methods offer the potential for reclaiming reusable carbon fibers, the reliance on very high temperatures can incur significant energy and costs. This is particularly true when specialized and sophisticated equipment is required for controlled atmospheres, fluidized beds, and microwave-assisted pyrolysis. [55]

2.1.2. Chemical processes

Researchers are attempting to continue recycling process methods of Carbon Fiber Reinforced Polymer (CFRP) through chemical solvolysis, a process involving the use of a chemical solution to break down the resin. Solvolysis research can be classified into high and low-temperature processes. High temperature solvolysis utilizes supercritical fluids, primarily alcohols or water. [56,57] In this method, the solution is heated and pressurized past its critical point, creating a system with the dissolution properties of a liquid and the effusive properties of a gas.

It was reported that by utilizing supercritical water the epoxy can be decomposed. [58] requiring operating conditions of above 10 MPa and 300°C and removed upwards of 48 wt. % epoxy. They noted the maximum percentage removed was 79.3 wt. % at 28 MPa and 400°C, though with an

alkali catalyst added 95.4 wt. % could be achieved. However, these conditions, reaching 28 MPa and 400°C for optimal results, would be challenging and expensive to maintain in industrial operations. Supercritical alcohols, such as methanol, ethanol, 1-propanol, and acetone, have also been investigated. Studies showed that with an alkali catalyst, these solvents could decompose 95% of the resin, retaining 85%–99% of the fiber strength. Piñero-Hernanz, García-Serna et al. discovered that utilizing methanol, ethanol, 1-propanol, and acetone at temperatures ranging from 250°C to 400°C, along with an alkali catalyst, could decompose 95% of the resin within 15 minutes, while retaining 85%–99% of the fiber strength [59]. In contrast, Okajima et al. found that supercritical methanol led to a 9% reduction in tensile strength [60]. They also observed that acetone exhibited superior performance in removing amine-cured epoxy compared to methanol, 1-propanol, 2-propanol, 1-butanol, 2-butanol, tert-butanol, and methyl ethyl ketone. On the other hand, Cheng et al. reported that n-butanol resulted in the most effective resin removal while retaining 98% of the original tensile strength. [61]

Liu et al. employed nitric acid for epoxy decomposition, achieving complete fiber recovery after 12 hours at 90°C. The measured strength loss was only 1.1%. These findings indicated better results compared to the use of sulfuric or hydrochloric acid. While the resulting rates of fiber recovery and fiber strength retention are remarkably high, the prolonged duration and safety considerations associated with using concentrated sulfuric acid could potentially render the process impractical. [62]

Beyond the use of unconventional methods and acids, another approach involves the application of hydrogen peroxide mixed in various solutions. Notably, Li et al. conducted experiments where a hydrogen peroxide solution (30% in water) reacted with acetone in an autoclave chamber to decompose cured CFRP samples [63]. In this process, CFRP samples were expanded using acetic acid and then placed in the solution at elevated temperatures. The thermal decomposition of hydrogen peroxide formed hydroxyl radicals, powerful oxidizers that reacted with both acetone and epoxy resin. Acetone was believed to aid in dissolving resin. The study found that 90% of the epoxy was successfully dissolved, and the fibers retained most of their strength.

N, N-dimethylformamide in a 1:1 volumetric ratio for the successful removal of epoxy has been used, resulting in a 5% decrease in tensile strength. [64] However, it's important to note that N,N-dimethylformamide is a known toxic substance, and its use in CFRP recycling could pose significant safety hazards. Given that the primary mechanism of this reaction involves the decomposition of hydrogen peroxide to form hydroxyl radicals, finding an alternative chemical solvent to acetone or N, N-dimethylformamide would be ideal to address safety concerns in the recycling process.

Aluminum chloride in acetic acid has been employed to selectively cleavage the chemical bonds in cured epoxy matrix (**Figure5**). Under the optimal degradation conditions (15 wt %, 180 °C, 6 h), the recovery yield of Cured epoxy reaches up to 97.43 wt %, and the clean CFs recovered conserved about 97.77% of their tensile strength compared with that of virgin CFs. [65]

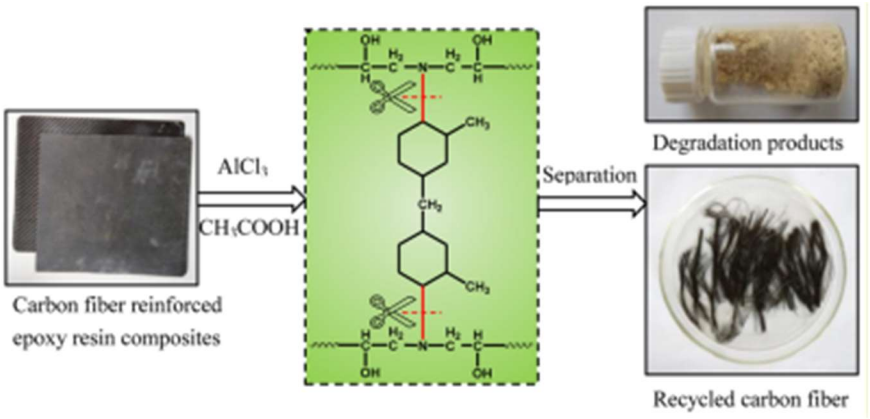

Figure 5. The recycling process with $AlCl_3$ in acetic acid solvent [65]

Also, Carbon fiber reinforced polymers (CFRPs) with high Tg (>200 °C) was successfully reclaimed Ethanol solvent and zinc chloride catalyst at 190°C (**Figure 6**). The high efficiency of $ZnCl_2$/ethanol was attributed to the strong coordination effect of ZnCl2 with the C-N bonds and the strong swelling ability of ethanol, which worked together to break down the chemical bonds of the cross-linked polymer. [66]

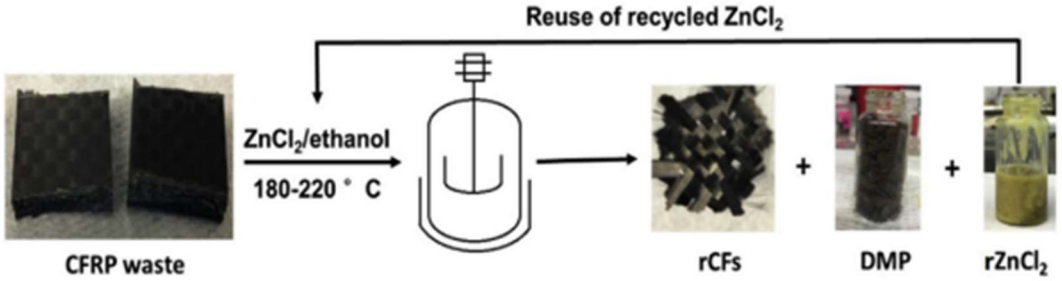

Figure 6. the recycling process with $ZnCl_2$ in ethanol solvent [66]

Another catalytic decomposition of CFRPs was investigated by using concentrated $ZnCl_2$ aqueous solutions. utilizing 60%w $ZnCl_2$ solution at 250°C has led to 100% degradation ratio of epoxy resin. [67]

2.1.3. Mechanical Processes

Mechanical process involves size reduction of Carbon Fiber Reinforced Polymer (CFRP) by crushing or shredding. Subsequently, these small pieces can serve either filler or reinforcement in new composite. The recovered fiber portions can be integrated as reinforcement in new composite products, but the mechanical properties of these composites are compromised due to inadequate bonding between the resin and recycled products.
On the other hand, diminishing fiber length is also directed toward lower-value applications compared to virgin carbon fibers. [68]

Chapter 3 Results and Discussion

It was an assumption that for the breaking down the chemical bonds of the cured resin in CFRPs composite, a Lewis acid in combination with the suitable solvent that can penetrate to the dense structure of the composite and coordinate with the electron pair of the nitrogen of the cured system. Thus, some catalysts with Lewis acid-function properties and also containing oxidizing anion were selected to be experimentally tested.

Dimethylacetamide demonstrated a remarkable swelling impact on CFRPs and also good compatibility with the catalyst, and it significantly aided the recycling process. subjecting the cured epoxy polymer to a mixture of DMAc resulted in an expansion of the polymer size and dimensions. This expansion is attributed to the capability of the solvent to penetrate within the epoxy dense structure, thereby facilitating the recycling process. [69]

On the other hand, ball milling was an effective way to produce active sites mostly at the edge of the graphene sheets of the graphite. Furfurylamine was attached to the graphene edges and consequently, deattached by increasing the temperature.

3.1. Catalytic recycling of CFRPs made out of Prepreg

This approach outlines a catalytic recycling method for Carbon Fiber Reinforced Polymers (CFRPs) produced from prepreg, which consists of epoxy resin cured by an amine-based hardener. The recycling process utilizes dimethylacetamide (DMAc) and catalyst at a temperature of 160°C in an oil bath. The recycled carbon fibers and epoxy polymer were characterized by different analytical and mechanical measurements.

3.1.1. Experimental section (recycling of CFRPs process)

First, 6 piles of the pure prepreg (unidirectional) were laminated manually and then cured under the pressure of 0.5 MPa at 150°c for 20 min. to obtain cured CFRP with a thickness of 1mm. In each experiment, a section of cured CFRP, crafted from prepreg, weighing approximately 0.3 g and shaped as a cuboid with dimensions 2cm by 1cm by 1mm, was employed. The experiment setup involved placing this CFRP strip, along with 0.5 g of $Al(NO_3)_3.9H_2O$ and 2 g of dimethylacetamide (at an aluminum nitrate-concentration of 20%), within a round flask at a temperature of 160°C using an oil bath with a condenser-equipped arrangement, and allowed to proceed for 5 h. After the decomposition process concluded and the system cooled to room temperature, the liberated carbon fibers were meticulously separated. These fibers underwent thorough washing with water and then acetone, followed by drying in a 50°C oven for a duration of 2 h.

After the removal of carbon fibers, the epoxy resin resulting from the degradation was dissolved in acetone, but the catalyst not According to the IR of catalyst (Figure 11), the catalyst changed to another chemical after the recycling process in the case of all used catalysts. So after completing the reaction, precipitated catalyst could be observed at the reaction container which proved insoluble in Acetone, thus, around 10ml acetone was used to separate the catalysts through a paper filter. Subsequently, the acetone was evaporated utilizing rotavapor. This process led to the

precipitation of a light-yellow degraded epoxy matrix by adding around 15 ml water (due to the insolubility of cleaved epoxy in water). It was perceived that the cleaved epoxy in DMAc could be more efficiently settled down by adding water at the PH around 6-7, thus the PH was raised from around 3 for the solvent to 6-7 by using potassium hydroxide (1M). The isolated matrix underwent several rounds of washing with water, followed by drying in a freeze-dryer. This degraded epoxy matrix served as a degradation product for subsequent measurements in relation to this recycling procedure. This outlined procedure was replicated for alternative catalysts, involving variations in catalyst concentrations, temperatures, and durations. Reference carbon fiber was obtained by the same reaction process on the uncured prepreg, but without any catalyst. On the other hand, this recycling process was repeated on the lab-prepared cured epoxy resin with the mixing of the exact ratio of the known commercially available epoxy resin (Epikote 05475) and curing agent (Epikure 05443) for further experiments. 100 parts by weight of Epikote resin in combination with 24 parts by weight Epikure hardener were mixed very slowly to prevent creating bubbles. Bubbles creation was so common in this process, and it can have a huge impact on the tensile properties of the cured epoxy. So, to get rid of the bubbles some measures were taken to prepare the curing process. For the first step preheating at around 60°c of the Epikote resin was necessary, consequently, the hardener should add and mix slowly, during the mixing we can remove surface bubbles with the help of heat gun for a very short time. Thereafter, the mixture was transferred slowly to the silicone mold and covered with another silicone sheet equipped with screw to have same load. The curing temperature was fixed at 120°c for 5 min. in the oven. Afterwards, the amin-cured epoxy (CEP) was removed carefully from the mold and was used for further experiments.

The experimental phase involved the use of two distinct catalysts, and the degradation process for both resulted in an approximate degradation ratio (DR) of 100% after 5 hours at 160°C (**Scheme 1**). However, in-depth analytical data revealed that when utilizing aluminum nitrate nonahydrate, the morphology, chemical composition, and mechanical properties of the resulting carbon fiber remained nearly indistinguishable from the reference carbon fiber obtained by dissolving prepreg in DMAc at 160°C (**Figure 7**). Subsequently, a series of characterization techniques were applied to the recycled carbon fiber as well as the degradation products resulting from the application of

these two catalysts. These outcomes were then subjected to a comparative analysis, both with each other and with the reference carbon fiber. The sample codes are listed in **Table 2**.

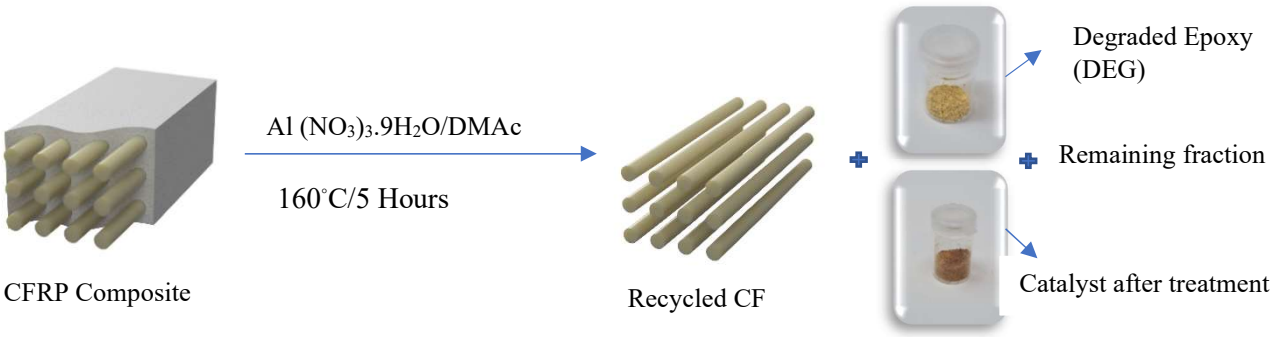

Scheme 1. The schematic of Recycling process

Sample codes	Definition
V-CF	Virgin Carbon Fiber
RI-CF	Recycled carbon fiber treated by Iron nitrate
RA-CF	Recycled carbon fiber treated by Aluminum nitrate
CEP	Amine-Cured Epoxy prepared in the lab without carbon fiber (Epikote and Epikure)
DEG	Degraded epoxy resulted from prepreg recycling process

Table 2. The definitions of the sample's code

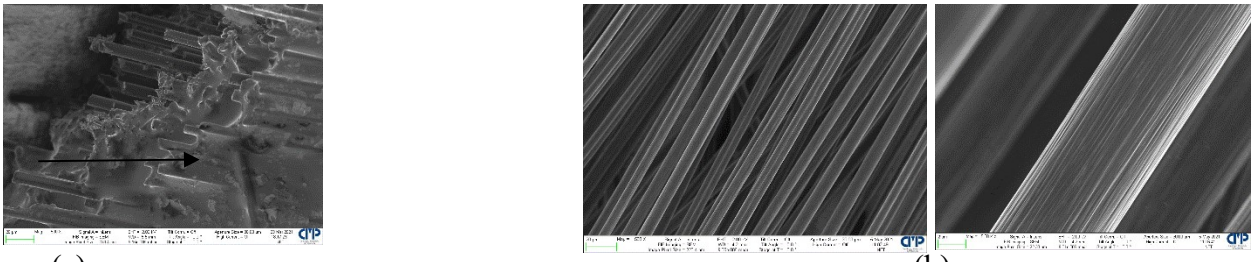

(a) (b)

Figure 7. SEM image of a) uncured prepreg b) CF after dissolving of other component in DMAc without any catalyst (Virgin CF)

Dimethylacetamide demonstrated a remarkable swelling impact on CFRPs and also good compatibility with the catalyst, and it significantly aided the recycling process. As depicted in **Figure 8**, subjecting the cured epoxy polymer to a 5-hour duration at 160°C resulted in an expansion of the polymer size and dimensions. This expansion is attributed to the capability of the solvent to penetrate within the epoxy dense structure, thereby facilitating the recycling process.

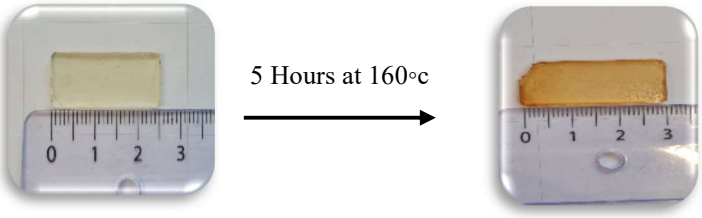

Figure 8. The impact of solvent on the dimension of cured epoxy

Various catalysts were explored within the recycling study, and among the assortment, aluminum nitrate and iron nitrate emerged as the most active catalysts, effectively facilitating the recycling approach. Zinc nitrate also exhibited some capability in recycling the fibers, albeit not to the same degree of efficiency as the aluminum nitrate and iron nitrate catalysts. This comparison provides insight into the varying effectiveness of these catalysts in the recycling process (**Table 3)** according to the degradation ratio (DR) of carbon fiber that was calculated based on the equation:

$$\text{DR } (\%) = \frac{W_2 - W_1}{W_2 \times 0.6} \times 100$$

W_2 is the weight of CFRP composite before recycling, W_1 is the weight of carbon fibers after separating, washing and drying from recycling process and 60% is the carbon fiber content into the prepreg.

Catalyst (20% C); 5 h at 160˚c	DR % (Degradation Ratio)
$MgCl_2$	Swollen
$AlCl_3$	Swollen
$Zn(NO_3)_2$	55
$FeCl_3$	Swollen
$Fe(NO_3)_3$	100
$Al(NO_3)_3$	100

Table 3. The comparison of the degradation ratios (DR) for selected catalysts

It can be interpreted that aluminum was considered as stronger lewis acid than Iron to coordinate with the electron pair of nitrogen.

3.1.2. Characterization analysis (the comparison of the efficiency of two Catalysts)

Recycled carbon fiber resulting from the catalytic chemical process were analyzed chemically and mechanically. Also regraded epoxy resin was analyzed.
According to the first results, Aluminum nitrate and Iron nitrate displayed 100% degradation ration of carbon fiber, Thus, the next experiments were conducted on these two catalysts.

3.1.2.1. Recycled carbon fiber analysis

Recycled carbon fiber after the recycling steps (**Figure 9**) were washed and dried and went through different analysis.

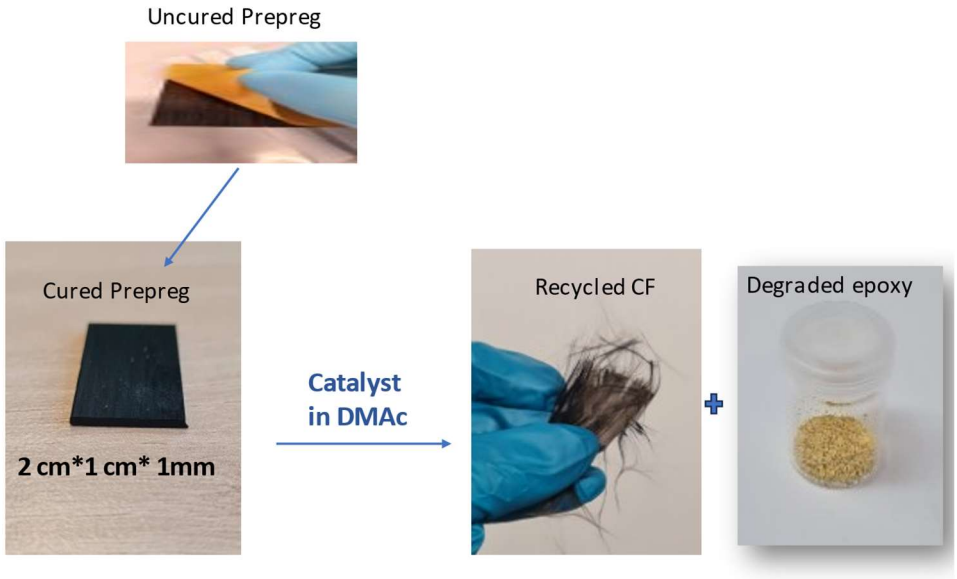

Figure 9. Recycling steps photos

3.1.2.1.1. TGA

Thermogravimetric analysis (TGA) was employed to examine the thermal characteristics of various carbon fiber samples (**Figure 10**): virgin carbon fiber (V-CF), carbon fiber treated with Iron nitrate nonahydrate (RI-CF), carbon fiber treated with aluminum nitrate (RA-CF), and a commercially available carbon fiber-containing binder, this is the commercially available carbon fiber that is containing low amount of epoxy resin as a binder (epoxy) to protect the alignment of fibers and make it much more workable. It was just used to compare the TGA curve of the recycled fiber obtained by this approach, and to be sure that there is no remaining epoxy on the surface of the recycled fibers.

TGA is a robust method for assessing a material's thermal stability and determining the fraction of volatile components by observing weight changes as the sample undergoes heating at a consistent rate. Results, shown in **Figure 10**, reveal distinct thermal behaviors. The virgin carbon fiber demonstrates exceptional thermal stability, maintaining its weight until 700°C, with only a minor 0.9% weight loss at 800°C, a characteristic shared with RA-CF. In contrast, the weight loss for RI-CF commences at approximately 580°C, ultimately reaching 12.8% at 800°C.

When examining the weight loss of carbon fiber combined with the binder, it is evident that there is no epoxy impurity on the surface of the RI-CF. This absence is corroborated by the absence of weight loss around 370°C, which would be indicative of epoxy presence. This observation provides assumption that the utilization of iron nitrate inflicted chemical damage on the carbon fiber surface, and the weight loss at around 580°c can be interpreted to be carboxylic functional group on the surface of the fibers, due to observing higher oxygen content in XPS. It can be possible that hydroxy functional group attached to the fibers were oxidized to carboxylic acid groups because of the nitrate anion of the catalyst.

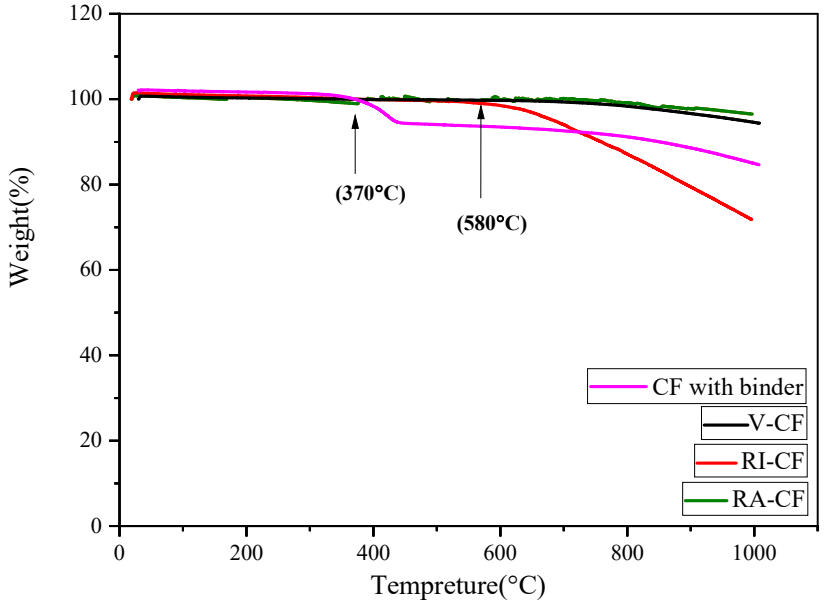

Figure 10. TGA of recycled carbon fibers and virgin fibers (With and without binder)

3.1.2.1.2. Raman Spectroscopy

Raman spectroscopy was utilized to investigate the surface structure and extent of structural disorder within the materials [70]. The spectra, as shown in **Figure 11**, indicates the existence of two significant peaks. The "G-band" corresponds to the vibration of the graphite structure's carbon-carbon (C–C) bonds, while the "D-band" signifies the vibration of structures with lower orientation and crystalline defects. The ratio of intensities between the "D-band" and the "G-band" (I_D/I_G),

referred to as the R-value, serves as an indicator of the relative proportion of structurally ordered graphite crystallites [71] Notably, a smaller R-value implies a higher degree of graphitization in the carbon fibers. Additionally, after undergoing peak fitting, a novel peak emerges around 1500–1550 cm^{-1} (A peak). This peak is linked to amorphous carbonaceous structures, hetero atoms present on the carbon fiber surface, or certain functional groups. The intensity ratio between the A and G peaks (I_A/I_G) provides insights into the proportion of amorphous carbonaceous structures. [72]

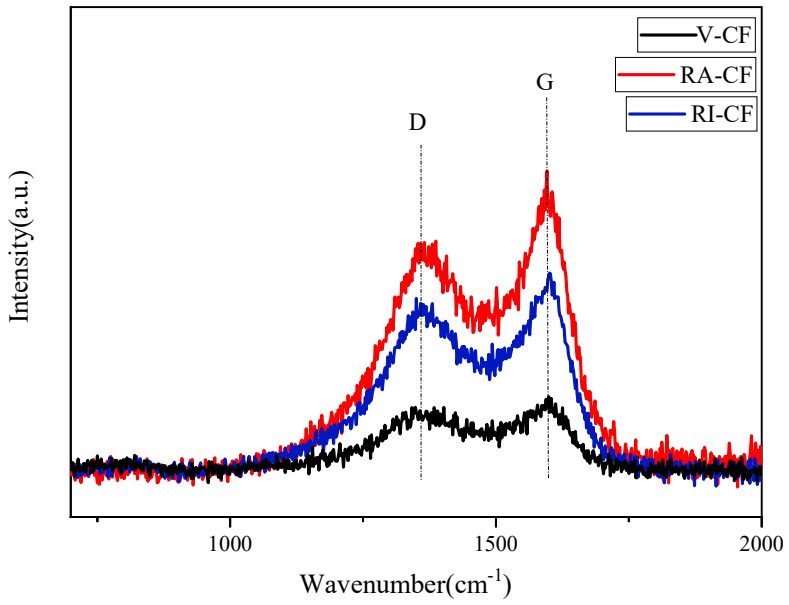

Figure 11. Raman spectra of virgin carbon fiber and recycled ones

Table 4 and **Figure 12-14**, indicate that the R-value for recycled carbon fiber, following the use of an aluminum nitrate catalyst, exhibited a slight increase when compared to virgin carbon fiber. Conversely, in the case of iron nitrate, this value underwent a more pronounced increase from 2.051 for virgin fiber to 2.398. This shift provides confirmation of the greater surface damage sustained by carbon fibers after the application of iron nitrate as the catalyst.

W(cm^{-1})				$R=I_D/I_G$	I_A/I_G
Sample	D	G	A		
V-CF	1362.01389	1601.64495	1527.84038	2.051	0.801
RA-CF	1364.89967	1600.49934	1525.71757	2.164	0.537
RI-CF	1363.14053	1603.24919	1532.29221	2.398	0.624

Table 4. Raman results of virgin carbon fiber and recycled CF

Lorentzian peak fitting of each carbon fiber:

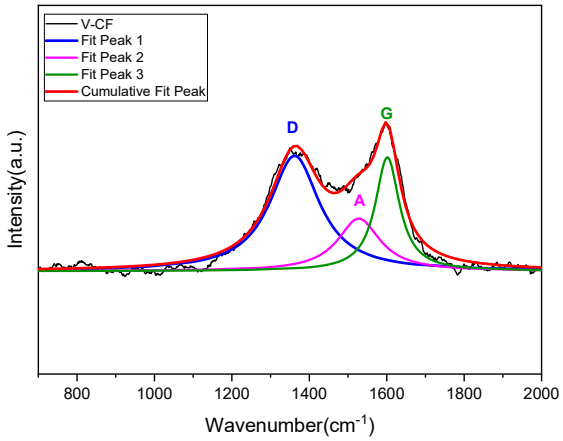

Figure 12. Lorentzian peak fitting of virgin Carbon fiber

Peak Index	Peak Type	Area Fit	Area FitT	Area FitTP	Center Max	Center Grvty	Max Height	FWHM
1	Lorentz	53777.22913	51988.8762	53.25458	1362.01389	1362.01389	218.83922	156.44201
2	Lorentz	20871.11735	20296.88711	20.79103	1527.84038	1527.84038	99.71476	133.24974
3	Lorentz	25738.70386	25337.52362	25.95438	1601.64495	1601.64495	216.02611	75.85087

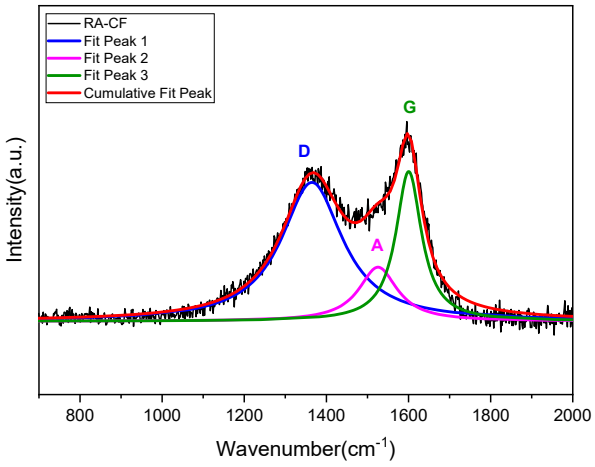

Figure 13. Lorentzian peak fitting of RA-CF

Peak Index	Peak Type	Area Fit	Area FitT	Area FitTP	Center Max	Center Grvty	Max Height	FWHM
1	Lorentz	253958.60606	244190.69437	58.45938	1364.89967	1364.89967	892.57611	181.13309
2	Lorentz	62155.51275	60694.29219	14.53024	1525.71757	1525.71757	347.67235	113.81241
3	Lorentz	114610.29278	112825.06989	27.01038	1600.49934	1600.49934	962.34755	75.81791

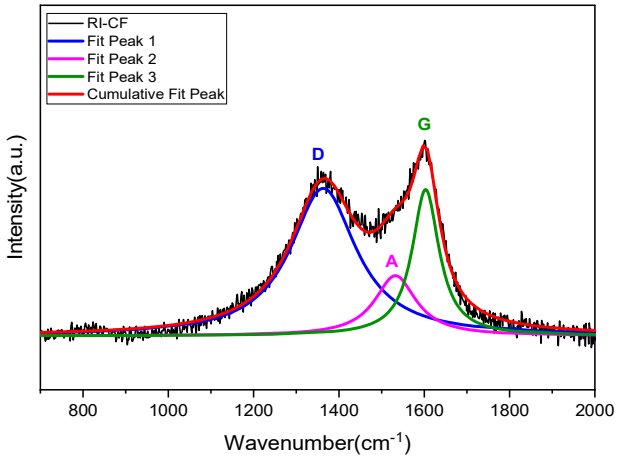

Figure 14. Lorentzian peak fitting of RI-CF

Peak Index	Peak Type	Area Fit	Area FitT	Area FitTP	Center Max	Center Grvty	Max Height	FWHM
1	Lorentz	197107.87842	189278.90196	59.62116	1363.14053	1363.14053	671.08178	186.98581
2	Lorentz	50502.83582	49279.06586	15.52246	1532.29221	1532.29221	273.87194	117.39466
3	Lorentz	80174.17983	78911.38796	24.85638	1603.24919	1603.24919	665.67262	76.67503

3.1.2.1.3. XPS

X-ray photoelectron spectroscopy (XPS) was carried out to discern the chemical composition of the fibers, encompassing the quantity of chemical functional groups and the elemental percentages present. As depicted in **Figure 15**, the spectra unveiled the presence of carbon (C1s), oxygen (O1s), and nitrogen (N1s) elements. These elements exhibited binding energies approximately located at 284.5 eV, 532.6 eV, and 399.9 eV, respectively, in the case of virgin carbon fiber. **Table 5** illustrates the atomic percentages for these elements on the fibers. Notably, the introduction of Iron nitrate as a catalyst resulted in an increase in the oxygen content, elevating it from 11.36% for virgin carbon fiber to 17.26%. Conversely, this percentage amounted to 13.24% for Aluminum nitrate. Consequently, the utilization of Iron nitrate prompted a heightened production of oxygen on the fiber surface. This outcome provides valuable insight into the observed weight loss in the TGA pattern around 580°C.

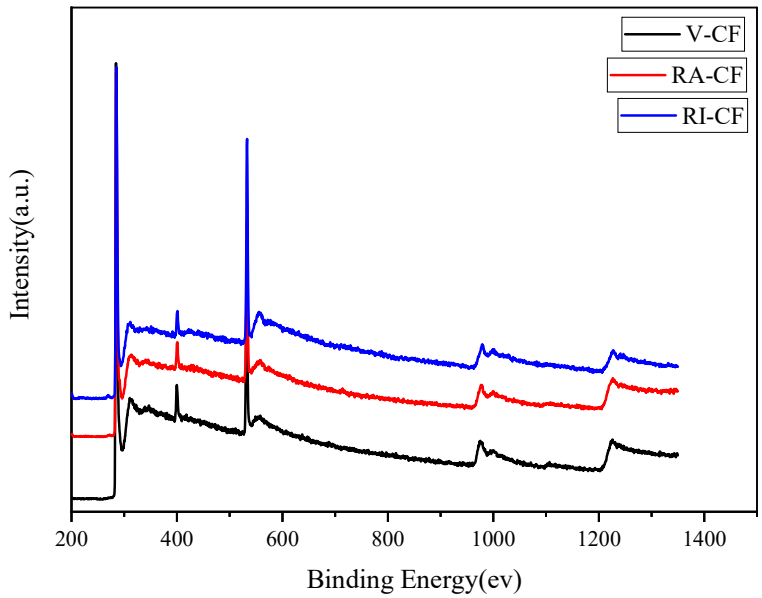

Figure 15. XPS survey spectra for virgin CF and recycled CF

	V-CF			RA-CF			RI-CF		
Peak name	C1s	O1s	N1s	C1s	O1s	N1s	C1s	O1s	N1s
Peak position	284.5	532.6	399.9	284.5	532.9	400.4	284.7	532.7	400.3
Area	27.4	10.8	2.37	24.9	11.6	1.78	21.31	13.6	1.74
Atom%	84.57	11.36	4.071	83.44	13.24	3.315	79.13	17.26	3.61

Table 5. The comparison of atomic% according to XPS spectra for virgin and recycled CF

High-resolution XPS C1s spectra obtained for CFs are shown below. The XPS C1s peak of the virgin fibers can be split into six components by Gaussian peak fitting, which corresponded to the following functional groups: C=C, 284.4 eV (sp^2 hybridized carbon), C-C, 265.1 eV (sp^3 hybridized carbon), C-N, C-O-(C, H, C=O), 286 eV, carbonyl and carboxyl group at 287.7 and 289 eV, respectively. a shake-up satellite peak ($\pi \rightarrow \pi^*$) located at 290 eV, related to the aromatic carbon structures [73]. The data clearly indicates that the percentage of C=C functional groups, which initially stood at 46.43% for virgin carbon fiber, experienced a decrease to 45.98% with the application of the Aluminum catalyst, and further dropped to 43.16% with the Iron catalyst. This reduction aligns with the trends observed in the Raman spectrum. Conversely, the percentage of C-C functional groups witnessed an increase, rising from 12.47% for virgin fiber to 13.48% and 16.73% for the Aluminum and Iron catalysts, respectively. This shift in the balance between sp^2 and sp^3 hybridized carbon is attributed to the incorporation of oxygen onto the fiber surface during the recycling process. However, it's notable that the amount of oxygen introduced is significantly lower when the Aluminum catalyst is employed, as opposed to the Iron catalyst. This distinction underscores the varying degrees of surface modification resulting from the use of these different catalysts. (**Figure 16-18**)

C-XPS for every carbon fiber after Gaussian peak fitting:

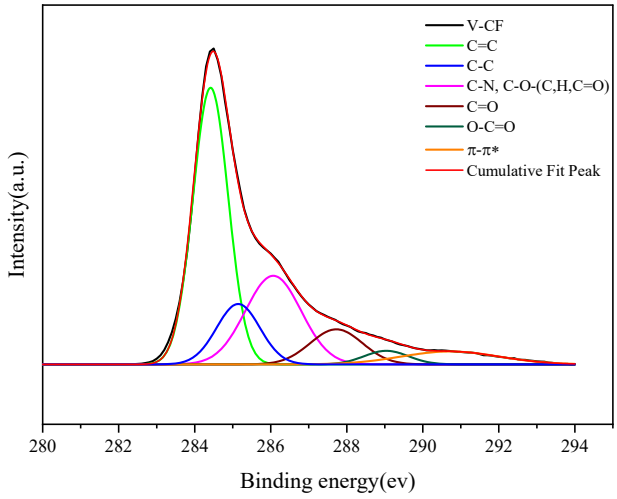

Figure 16. Gaussian peak fitting of V-CF

Peak Index	Peak Type	Area Fit	Area FitT	Area FitTP	Center Max	Center Grvty	Max Height	FWHM
1	Gaussian	26801.59747	26801.59747	**46.43636**	**284.41796**	284.41796	23093.38556	1.09029
2	Gaussian	7200.72791	7200.72791	**12.47596**	**285.14469**	285.14469	5039.7659	1.34225
2	Gaussian	13559.73238	13559.73238	**23.49355**	**286.06658**	286.06658	7395.47481	1.72247
3	Gaussian	5042.05977	5042.05977	**8.73586**	**287.72599**	287.72599	2927.62658	1.61793
4	Gaussian	1648.93859	1648.93859	**2.85695**	**289.03969**	289.03969	1132.32233	1.36805
5	Gaussian	3482.75075	3463.78305	**6.00134**	**290.72215**	290.72215	1079.25639	3.03156

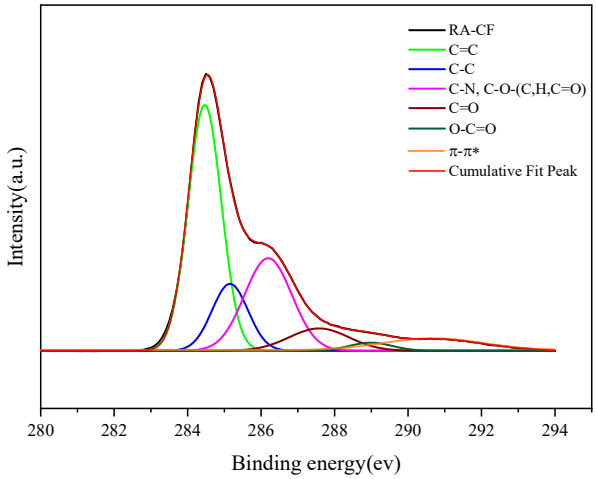

Figure 17. Gaussian peak fitting of RA-CF

Peak Index	Peak Type	Area Fit	Area FitT	Area FitTP	Center Max	Center Grvty	Max Height	FWHM
1	Gaussian	24200.8352	24200.8352	**45.98083**	**284.46497**	284.46497	21321.56746	1.0663
2	Gaussian	7100.09401	7100.09401	**13.48996**	**285.15385**	285.15385	5808.72917	1.14829
3	Gaussian	12935.53004	12935.53004	**24.5771**	**286.19231**	286.19231	8031.31625	1.51309
4	Gaussian	3944.2179	3944.2179	**7.49389**	**287.57692**	287.57692	1941.64061	1.90836
5	Gaussian	1022.91829	1022.91829	**1.94351**	**288.98462**	288.98462	705.63478	1.36185
6	Gaussian	3452.9571	3428.84548	**6.5147**	**290.69231**	290.69231	1023.72468	3.16866

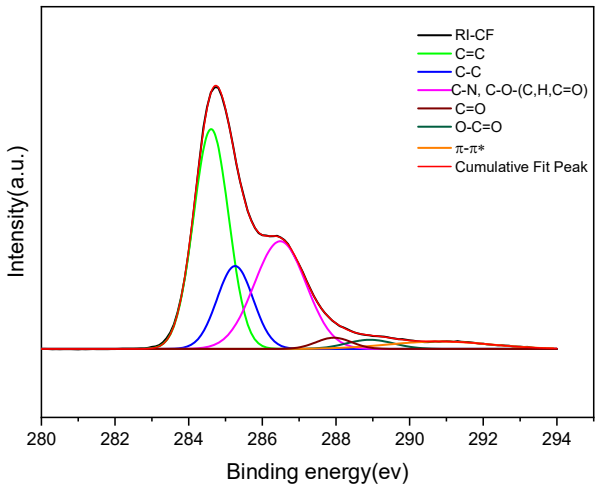

Figure 18. Gaussian peak fitting of RI-CF

Peak Index	Peak Type	Area Fit	Area FitT	Area FitTP	Center Max	Center Grvty	Max Height	FWHM
1	Gaussian	19100.0829	19100.0829	**43.16809**	**284.60934**	284.60934	16054.61082	1.11764
2	Gaussian	7404.24611	7404.24611	**16.73433**	**285.25992**	285.25992	6054.80336	1.14881
3	Gaussian	13830.99529	13830.99529	**31.25942**	**286.486**	286.486	7867.16598	1.65159
4	Gaussian	981.93454	981.93454	**2.21927**	**287.94317**	287.94317	820.06274	1.12487
5	Gaussian	1072.44216	1072.44216	**2.42383**	**288.92446**	288.92446	669.74598	1.50429
6	Gaussian	1875.24812	1856.14008	**4.19506**	**290.81434**	290.81434	544.65924	3.23446

3.1.2.1.4. XRD

The X-ray diffraction (XRD) technique was used to distinguish the crystalline structure of the materials, serving as a widely employed method for quantitative analysis. This method allows the determination of essential structural parameters like interplanar distance (d002) and crystallite sizes (Lc and La), thereby enabling the calculation of the graphitization degree of carbon materials

based on XRD results[74]. The interplanar distance is evaluated through the angles of diffraction peaks in line with the Bragg equation. Additionally, the crystallite sizes L_c (stack height) and L_a (stack diameter) are deduced from the angles and the full width at half maximum (FWHM) of diffraction peaks, employing the Scherrer equation[75].Based on the outcomes obtained from TGA and other analytical measurements, which indicated the superior efficiency of the aluminum catalyst, the decision was made to conduct XRD analysis specifically on the recycled fiber treated with the aluminum catalyst. This targeted XRD examination aims to further elucidate the structural changes and characteristics of the recycled fiber under the influence of the aluminum catalyst. **Figure 19** shows the XRD patterns of recycled and virgin carbon fibers. Notably, a strong peak corresponding to the (002) plane materializes at approximately 2θ = 25.44, 25.48 and 24.18 for virgin and RA-CF and RI-CF, respectively. It shows that the distance between the graphene layers in RA-CF is comparable with the virgin carbon fiber, but in RI-CF, this layer distances is slightly higher, that can be interpreted as slightly damage the crystallinity structure after using Iron nitrate catalyst for recycling process. The marginal reduction in the intensity of the (002) peak and the slight increase in the FWHM of the recycled fiber when contrasted with the virgin fibers suggest a minor impairment of fiber crystallinity resulting from the recycling process. On the other hand, XRD showed that the 002 peak for RI-CF was broader and of lower intensity than the reference and also RA-CF, and Lc decreased to 0.43 nm (vs. 1.368), so the crystallinity size of the fiber was damaged and drastically reduced after treatment with the iron catalyst. The degree of graphitization also decreased to 1.22 for the iron catalyst compared to 3.91 for V-CF. (**Table 6** and **Figure 20**)

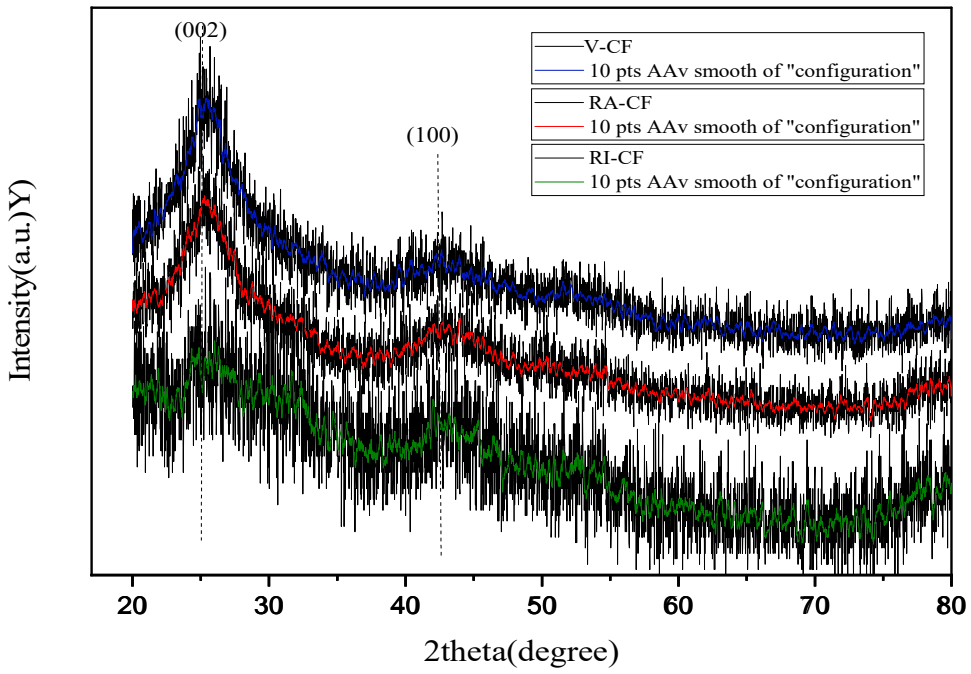

Figure 19. XRD spectra for virgin CF and recycled CFs

Parameters	V-CF	RA-CF	RI-CF
d_{002} (nm)	0.3491	0.3496	0.350
L_C (nm)	1.368	1.287	0.430
La (nm)	4.639	4.287	4.54
Graphitization degree (L_c/d_{002})	3.918	3.681	1.22

Table 6. Data resulted from XRD spectra

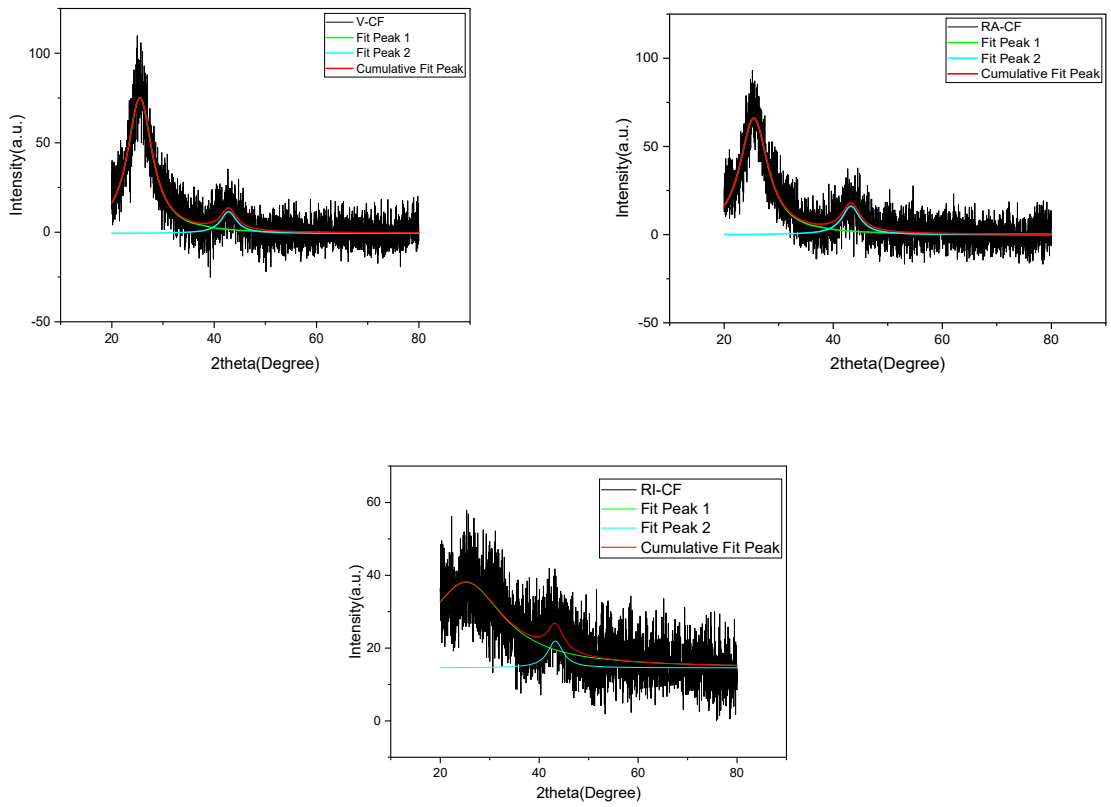

Figure 20. Lorentzian peak fitting data and pattern of XRD on the fibers

RA-CF:

Peak	Peak Type	Area Fit	Area FitT	Area FitTP	Center Max	Center Grvty	Max Height	FWHM
1	Lorentz	648.86321	529.37419	84.26751	25.44667	25.44667	66.03635	6.25533
2	Lorentz	103.54037	98.83254	15.73249	43.25487	43.25487	16.16906	4.07667

V-CF:

Peak	Peak Type	Area Fit	Area FitT	Area FitTP	Center Max	Center Grvty	Max Height	FWHM
1	Lorentz	700.64485	578.71614	89.33953	25.48278	25.48278	75.75641	5.88788
2	Lorentz	72.10106	69.05548	10.66047	42.82634	42.82634	12.20806	3.75989

RI-CF:

Peak	Peak Type	Area Fit	Area FitT	Area FitTP	Center Max	Center Grvty	Max Height	FWHM
1	Lorentz	691,30889	419,96345	90,83563	25,18881	25,18881	23,5353	18,69961
2	Lorentz	44,26257	42,36996	9,16437	43,2851	43,2851	7,34837	3,83465

$d002 = \lambda / 2\sin\theta$

$L = K\lambda / \beta\cos\theta$ (β in Radian)

The parameters used in the Scherrer equation are as follows: λ represents the wavelength of CuKα1 radiation, which amounts to 0.15405 nm. θ symbolizes the Bragg diffraction angle, while β corresponds to the full width at half maximum intensity (FWHM). The Scherrer shape factor K takes a value of 0.89 for the (002) peak and 1.84 for the (100) peak [76] Figure 3 shows XRD patterns for both recycled carbon fibers and their virgin counterparts, displaying a congruent pattern. After applying Lorentzian peak fitting to each peak, it becomes evident that the spacing between fiber layers experienced only minimal alteration following catalyst utilization. For instance, the values for V-CF and RA-CF were measured at 0.3491 and 0.3496, respectively.

However, treatment with the iron catalyst prompted changes in the 002 peak, rendering it broader and with lower intensity when juxtaposed with the reference and RA-CF. In this case, the L_c value collapsed to 0.43 nm, signifying a considerable disruption to crystallinity size (**Figure 19-20**). Conversely, the remaining three properties L_c, L_a, and graphitization degree, maintained comparability across the different fiber types. The XRD data, summarized in **Table 2**, corroborates that aluminum-based catalyst utilization preserved carbon fiber dimensions and maintained a high degree of graphitization akin to virgin carbon fiber. This conclusion is substantiated by the results from tensile strength tests of single carbon fibers, Raman spectroscopy, and scanning electron microscopy (SEM), which are elaborated upon in subsequent discussions.

3.1.2.1.5. Mechanical analysis

Single Carbon fiber Tensile strength:

For the tensile test, individual carbon monofilaments were carefully extracted from each fiber bundle and secured onto a paper holder using a mixture of epoxy resin and curing agent (Epikote and Epikure). The fibers were positioned to run straight along the central axis of the paper frame. Sufficient epoxy adhesive was applied to ensure that the fiber remains firmly attached during the stretching process, preventing it from dislodging due to applied force. The tensile tests were

conducted using an MTS machine equipped with a 10 N load cell and a gauge length of 10 mm. A crosshead speed of 0.5 mm/min was employed. The testing specimen was positioned within the grips of the tensile testing machine. Afterward, the paper frame was divided into two parts, as depicted in **Figure 21** All tests were carried out within the laboratory environment at room temperature. Over 50 specimens were subjected to testing to yield an average value for tensile stress. In order to calculate the cross-sectional area of each individual fiber, scanning electron microscopy (SEM) was utilized to measure the diameters of numerous fibers. The average diameter of carbon fibers, determined from measurements of approximately one hundred fibers, was established as 7.46 ± 0.7 microns.

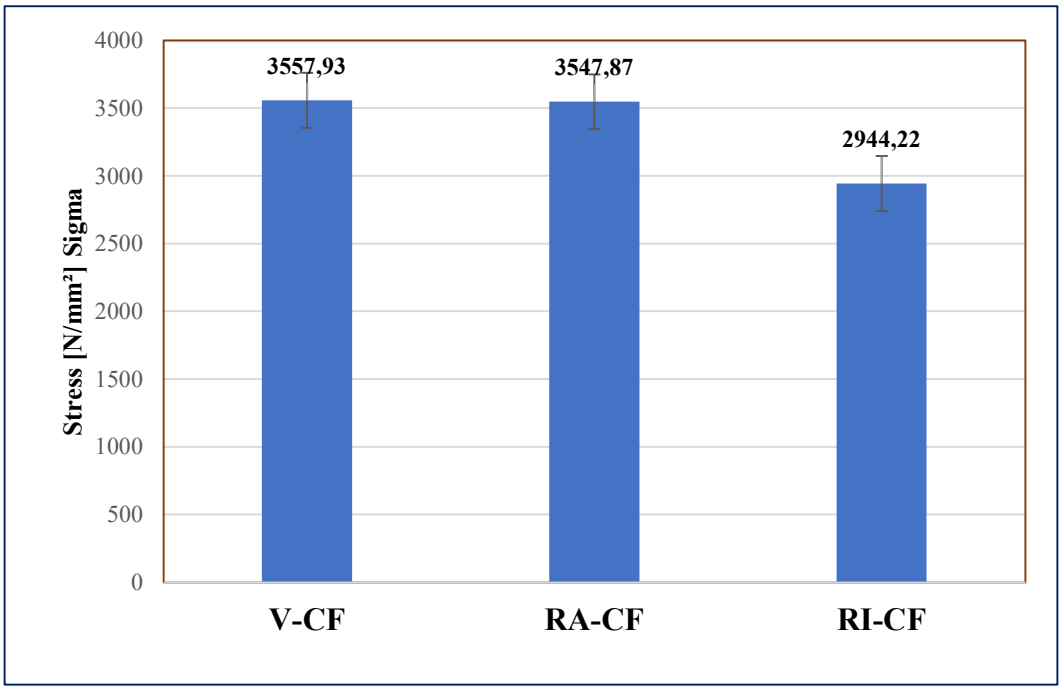

Figure 21. The comparison of the monofilament tensile strength for V-CF and recycled ones

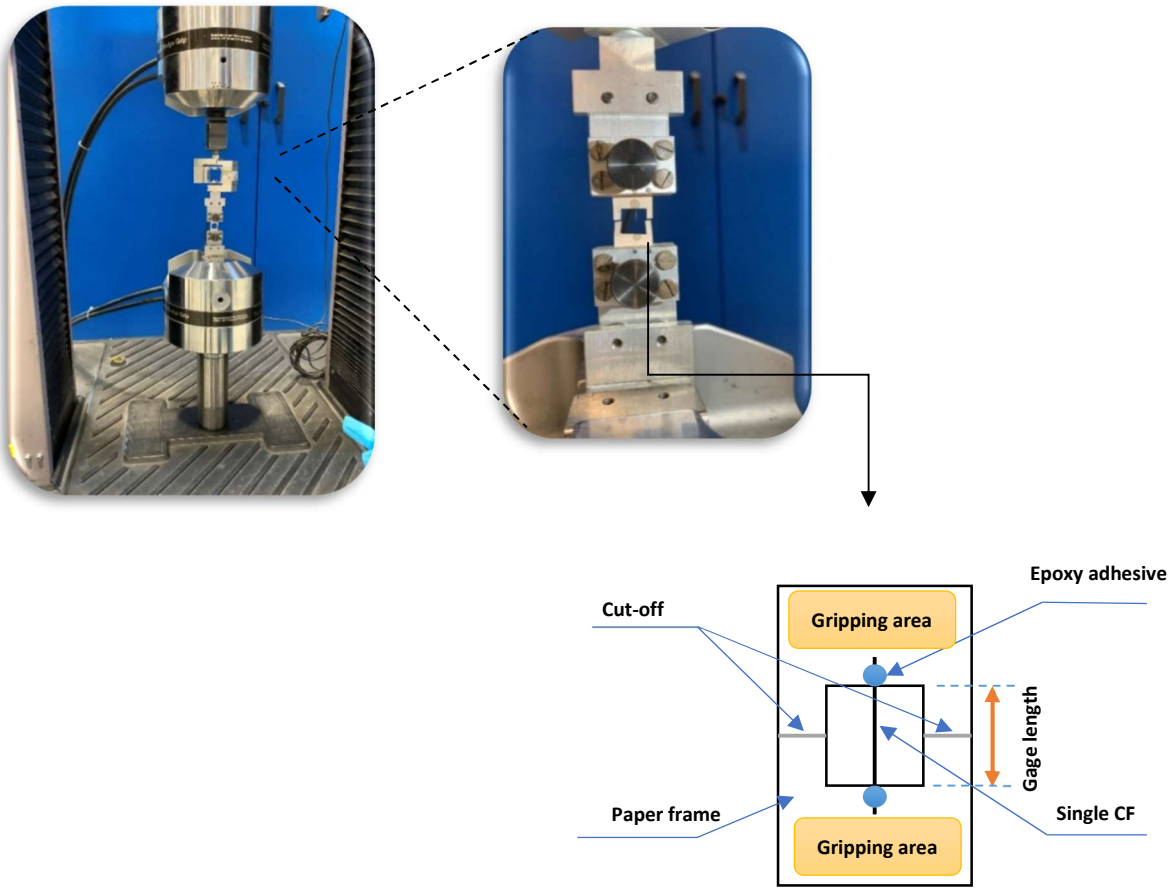

Figure 22. The schematic of the single CF tensile test specimen

The data presented in **Figure 21** clearly demonstrates the impact on tensile strength (σ) of the recycled carbon fibers. When aluminum catalyst was utilized, the recycled fibers retained an impressive 99.71% of the tensile strength exhibited by the virgin carbon fibers. On the other hand, with the application of the Iron catalyst, the recycled fibers managed to maintain only 82.75% of the original tensile strength. Also, **Figure 23** displays the stress-strain curve of the single carbon fiber and recycled ones. It is a comparison of the 3 single carbon fiber for each sample to get the better impression of the curve pattern (3 single fiber data was chosen out of around 20 specimen's data). This evidence suggests that the use of Iron nitrate had a more pronounced effect on the surface of the fibers, potentially inducing slight damage or oxidation. This interpretation aligns well with the observations from TGA, Raman spectroscopy, and XPS analyses. The schematic of the specimens in the tensile test and the photo of the machine were shown in **Figure 22**.

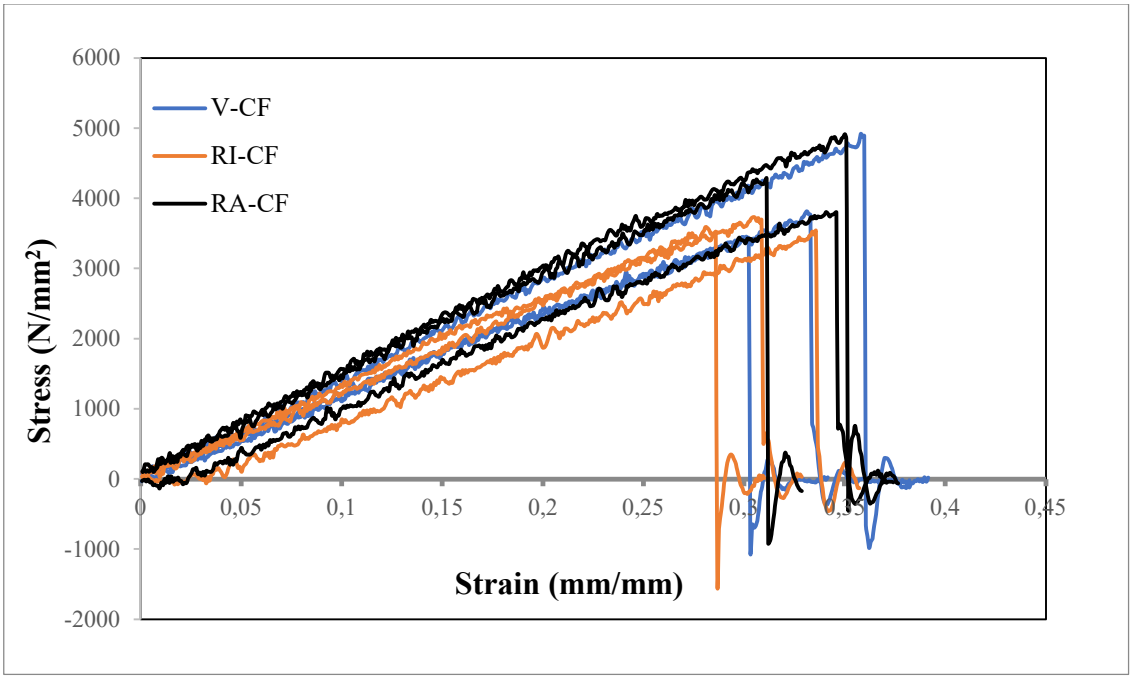

Figure 23. Stress-Strain curve comparison of 3 single virgin CF with 3 single recycled ones

3.1.2.1.6. SEM and EDX

Scanning Electron Microscopy (SEM) analysis was carried out to conduct an in-depth examination of the surface morphology of the recycled carbon fibers treated with two distinct catalysts (**Figure 24**), focusing on a comparison with virgin carbon fibers. In the case of virgin carbon fibers (V-CF), the surface appears entirely clean, free of any impurities or blemishes. Following treatment with an aluminum catalyst, the fiber surface maintains the same cleanliness as V-CF, showing no signs of epoxy matrix residues or other contaminants. However, challenges were encountered in eliminating complete iron impurities from the surface of the carbon fibers treated with the Iron catalyst. Subsequent EDX measurements revealed that the spots observed on the Iron-catalyzed recycled carbon fibers (RI-CF) were indicative of iron-containing impurities. To effectively eliminate these iron impurities from the fiber surface, an additional acid wash step involving 37% hydrochloric acid (HCl) was necessary. These observations underscore the distinction between the effects of the aluminum and iron catalysts on the fiber surface and provide valuable insights into the need for additional purification steps in certain cases.

V-CF:

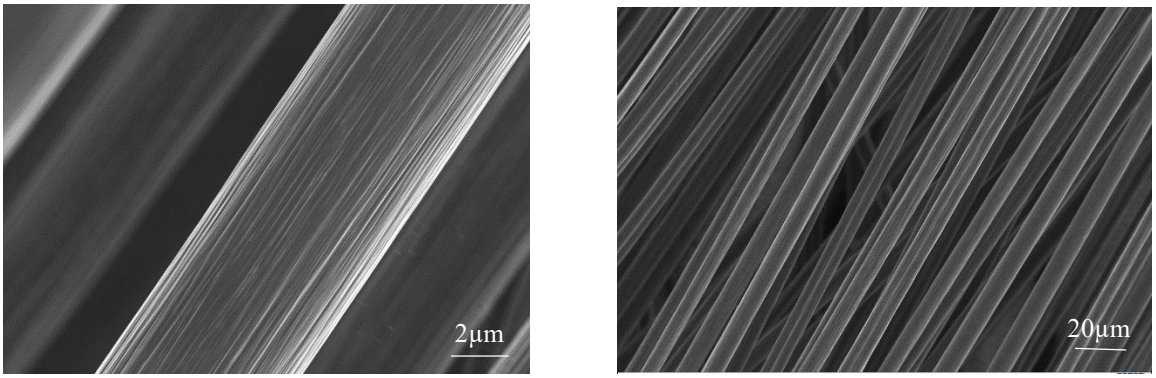

RA-CF:

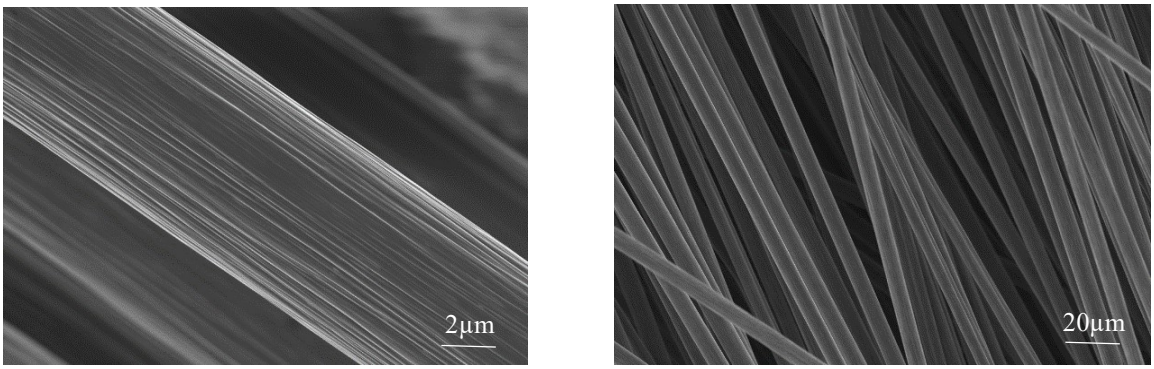

RI-CF:

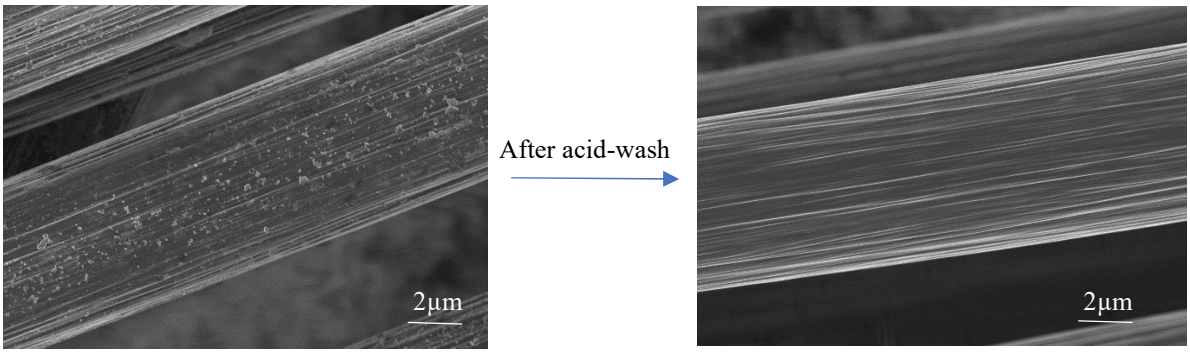

Figure 24. SEM images of the V-CF and recycled CF after using two different catalysts

Atom% examined by EDX:

The EDX data reveals significant insights regarding the oxygen content on the recycled carbon fibers (RA-CF and RI-CF) in comparison to the virgin carbon fibers (V-CF). Notably, the oxygen content of RA-CF closely resembles that of V-CF. However, even after the application of the Iron catalyst and subsequent acid wash, the RI-CF exhibited a higher oxygen content when compared to RA-CF (**Table 7**). The observed differences in oxygen content reinforce the distinctive effects of the catalysts and purification processes on the fiber surface. It further underscores the complex interplay between different catalysts and treatments in modifying the chemical composition of the carbon fibers during the recycling process.

	C-K	N-K	O-K	Fe-L
RI-CF before acid-wash	**85.42**	**7.01**	**4.19**	**3.38**
RI-CF after acid-wash	**94.23**	**3.65**	**2.12**	**-**
RA-CF	**96.44**	**2.61**	**0.95**	**-**
V-CF	**95.95**	**3.22**	**0.83**	**-**

Table 7. EDX results of V-CF and recycled CFs

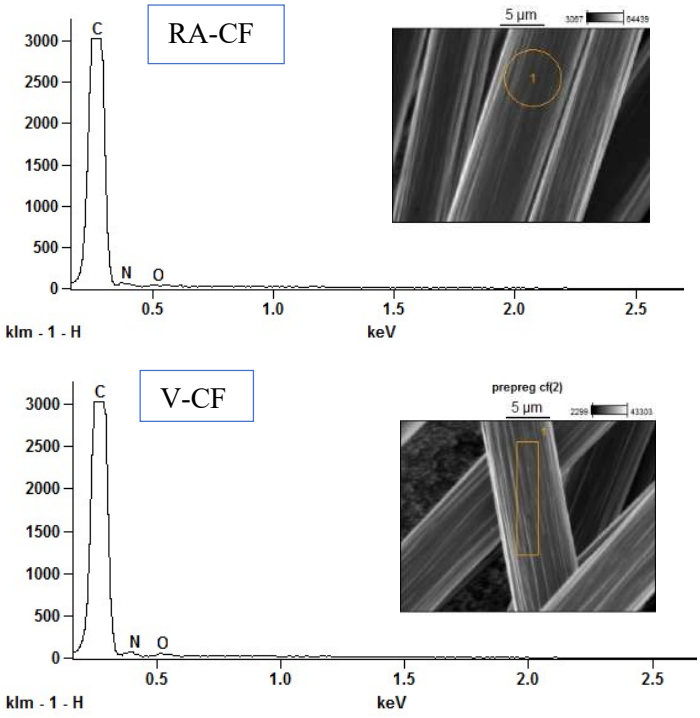

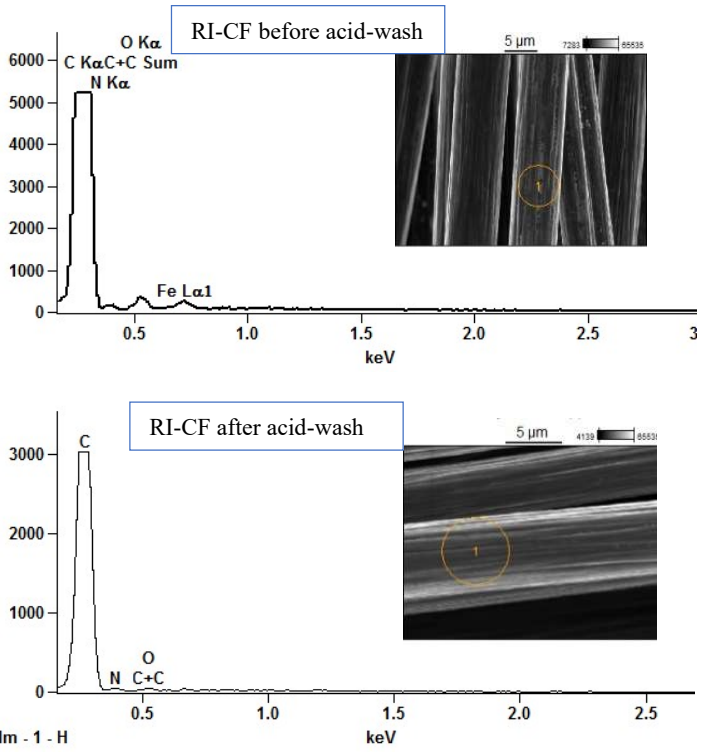

The steps of the recycling process followed by SEM:

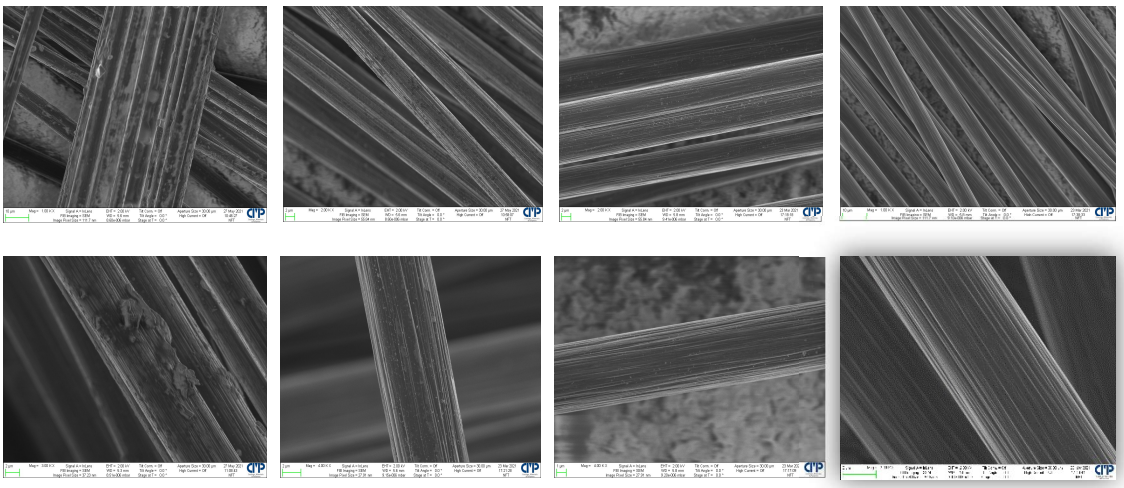

2 Hours (DR≤50%) 3 Hours (DR ≤70%) 4 Hours (DR ≤83%) 5 Hours (DR ~100%)

3.1.2.2. Degraded epoxy resulted from prepreg recycling (DEG) analysis

The degradation products arising from the recycling process with both aluminum and iron catalysts displayed identical Infrared (IR) spectra. As a result, the subsequent measurements concentrated on the degradation product derived from the recycling process using the aluminum catalyst on the cured prepreg, labeled as DEG-RA. Furthermore, the measurements were duplicated on the degradation product obtained after recycling the amine-cured epoxy (CEP) from commercially available networks, as well as lab-made networks (CEP-RA). During the prepreg recycling, the datasheet for the prepreg indicated that the epoxy matrix employed was BADGE (Bisphenol-A-Diglycidylether). However, the curing agent's identity remained unknown. The application of EDX analysis (**Table 8**) led to the deduction that the curing agent was of amine-based composition. This deduction was corroborated by the IR spectra, which exhibited a peak at around 3300 cm^{-1}, indicative of the presence of amine groups within the uncured prepreg. Despite this evidence, the precise structural details of the curing agent remained undisclosed.

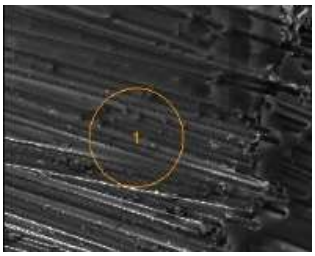

Atom %	C	N	O
Uncured Prepreg	69.99	5.14	24.88

Table 8. EDX result of uncured Prepreg

EPIKURE ™ Curing Agent 05443
3-Aminomethyl-3,5,5-trimethylcyclohexylamin (50-75%)

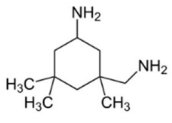

EPIKOTE™ Resin 05475
reaction product: bisphenol-A-(epichlorohydrin); epoxy resin
(number average molecular weight ≤700)

CEP

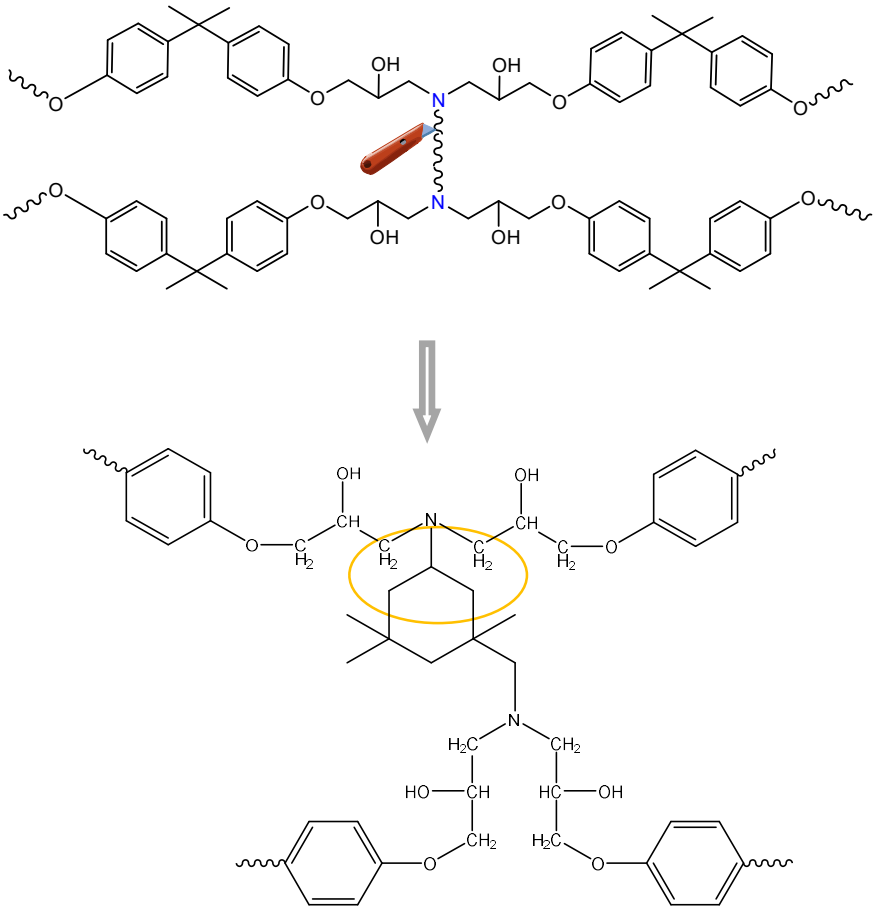

Scheme 2. The possible product structure of the reaction between BADGE and amine-based curing agent

As illustrated in **Scheme 2**, the creation of CEP involved a chemical reaction between amine-based Epikure 05443 and Epikote 05475. The percentage of the 3-aminomethyl-3,5,5-trimethylcyclohexylamin as curing agent is 50-75% according to the MSDS of Epikure 05443. 10-20% of the rest is triethylenetetramine. Therefore, it is clear that Epikure 05443 is an amine-based curing agent which is comparable with the curing agent of the prepreg.

3.1.2.2.1. Estimated structure of DEG

According to the data in ESI (**Figure 25**), an assumption regarding the structure of degradation product is the cleavage of C-N bond in the cured composite after utilizing the catalyst. The

intensive peak at 410.201 m/z clearly shows that the molecular weight of the degraded product is 387.2 m/z (after subtracting number 23 m/z for Sodium atom). The estimated structure (**Figure 26**) also was confirmed by IR and elemental analysis.

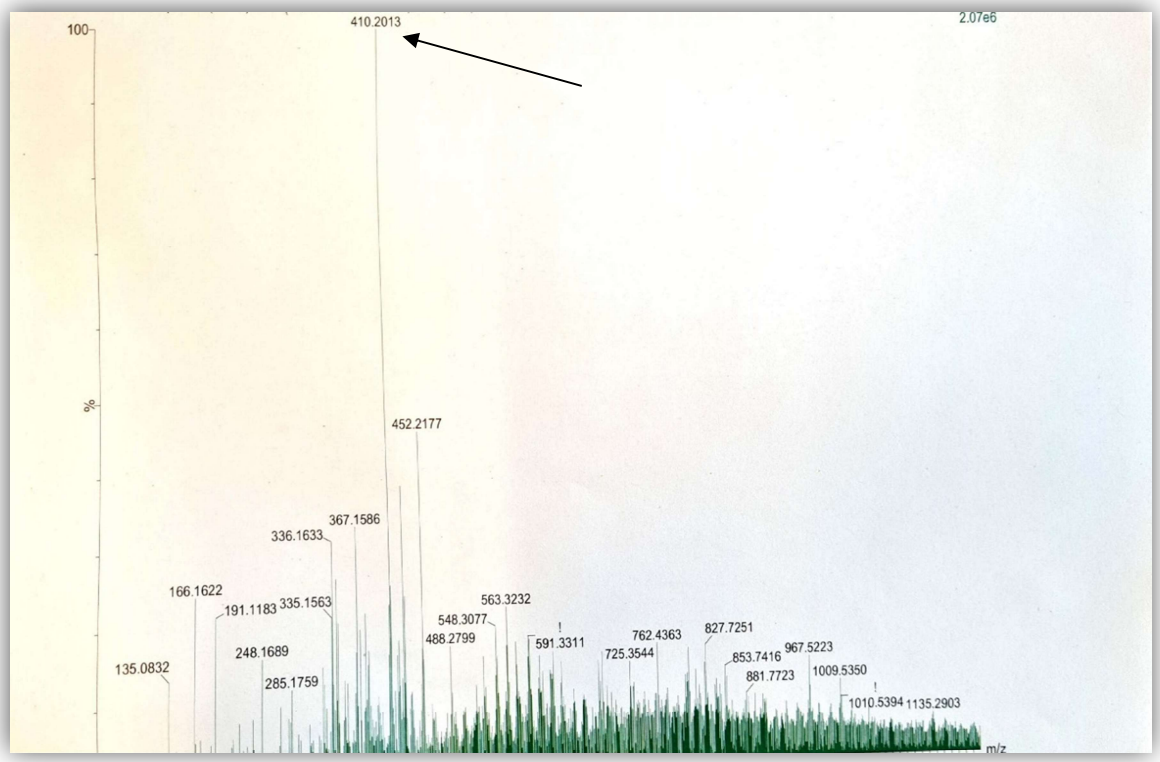

Figure 25. ESI of degradation product

Figure 26. The estimated structure of degradation product

Figure 27 presents the IR spectra, which was conducted to investigate the functional chemical groups present in the degradation products, namely DEG-RA and CEP-RA. Notably, these two spectra are nearly identical, aside from a distinct difference in the presence of a carbonyl group. In DEG-RA, the sharp and well-defined peak at 1732.7 cm^{-1} corresponds to a carbonyl group. This carbonyl group cannot be attributed to the solvent DMAc, as evidenced by the IR spectra of DMAc (**Figure 28**). Instead, its origin is likely related to the structure of the unknown curing agent in the prepreg. Correspondingly, a less intense peak at 1732 cm^{-1} is visible, further supporting the presence of a carbonyl group within one of the prepreg components. The appearance of an N-H functional group is evidenced by the peak around 3300 cm^{-1}. One another assumption is the impact of the nano structure of carbon fiber on oxidizing the hydroxy functional group of DEG to carboxylic group, thus the peak at 1732.7 cm^{-1} is visible just for the degradation products from the prepreg (DEG) not from the degradation product of the epoxy system without any carbon fibers (CEP). Notably, the peaks associated with NH_2 and OH overlap. Additionally, three peaks situated at 2968, 2928, and 2867 cm^{-1} are attributed to the C-H stretching vibrations of alkanes. The absorption bands centered at 1455, 1504, and 1599 cm^{-1}, displaying medium to strong intensity, signifies the C=C stretch vibration of aromatic rings, a characteristic feature present in all the products. Moreover, the presence of C–O–C and C–O stretching vibrations linked to ether bonding is confirmed by bands at 1235 and 1035 cm^{-1}. A peak located at 1180 cm^{-1} is indicative of the presence of a C-N bond within the structure of the degradation products. Specifically, the C–O stretching vibration mode of the oxirane ring at 910 cm^{-1} was exclusively observed in the uncured prepreg and BADGE.

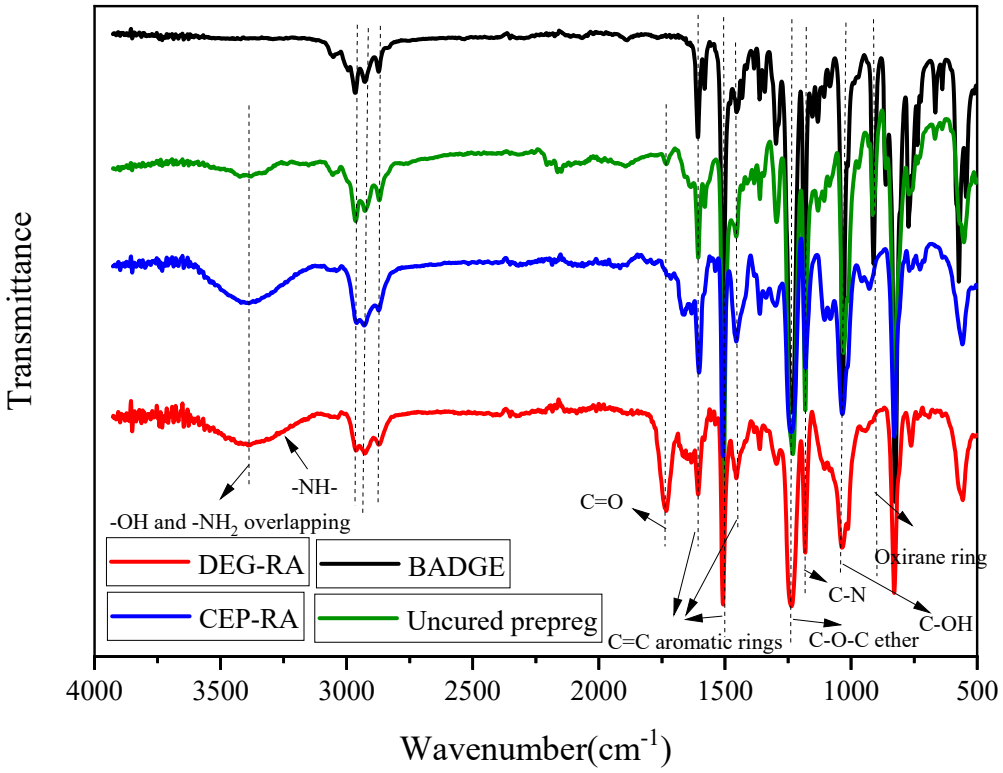

Figure 27. FT-IR spectra comparison of degradation products, uncured prepreg and BADGE

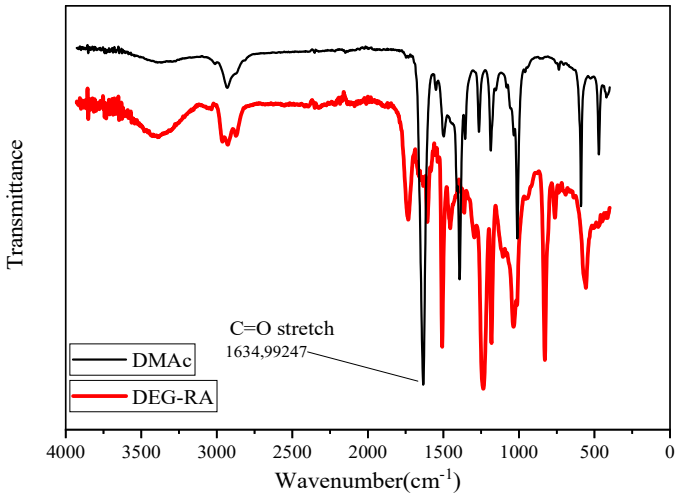

Figure 28. IR spectra of the DMAc and DEG-RA

The IR results unequivocally indicate that the degradation product encompasses C-N bonds, rendering it a valuable candidate for reuse in novel products. These C-N bonds possess potential utility in acting as co-hardeners or accelerators during the curing process. To streamline the reusability of the degradation product and to work with the readily available epoxy and curing agent network found in the lab, subsequent experiments were performed on the CEP. This involved the addition of the aluminum catalyst and DMAc, a process identical to that of prepreg recycling.

The elemental analysis of CEP-RA showcased a nitrogen content of 5.19%, as depicted in **Table 9**. The presence of nitrogen was further validated by EDX, which revealed nitrogen accounting for 10.09% in CEP-RA, along with 33.16% oxygen and 56.74% carbon (**Table 10**). Furthermore, the EDX outcomes suggest a transformation in the composition of the catalyst following the treatment, with the composition mainly composed of carbon, hydrogen, oxygen, and aluminum. The observed 17% carbon content may indicate a chemical reaction between the catalyst and the solvent or other components present within the recycling system. This fact was confirmed by IR spectra (**Figure 29**). These comprehensive analyses provide essential information about the elemental composition and structural changes within the recycled materials, contributing to a deeper understanding of the recycling process's intricacies and potential reusability prospects.

Elemental analysis	C (%)	N (%)	H (%)	O (%)
CEP-RA	65.14	5.19	7.30	22.37

Table 9. Elemental analysis of DEG-RA

EDX	**C (%)**	**N (%)**	**O (%)**	**Al (%)**
CEP-RA	56.74	10.09	33.16	-
Catalyst after the recycling process	17	3.43	63.26	17.11
Reference catalyst	0.00	10.30	77.37	12.33

Table 10. EDX results of CEP-RA, reference catalyst and catalyst after the treatment

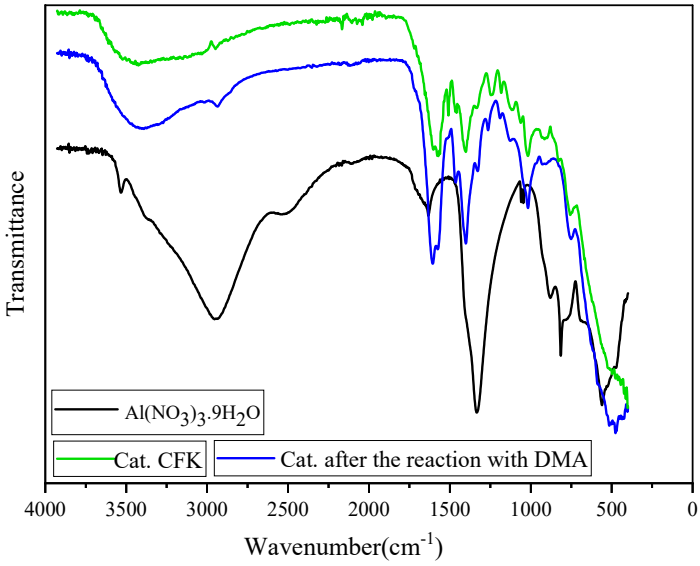

Figure 29. IR spectra comparison of reference catalyst, Catalyst after recycling process (Cat.CFK) and catalyst after the reaction with DMAc

The comparison between the carbon skeleton structures of BADGE and CEP-RA was carried out using ^{13}CNMR, shedding light on their structural characteristics. The results, depicted in **Figure 30**, reveal distinct peaks at 114, 128, 144, and 157 ppm that correspond to the aromatic rings, a feature shared by both the degradation product and the neat epoxy resin (C4, C5, C7, C6). This observation corroborates the IR findings, affirming the persistence of aromatic rings within the degradation product. Moreover, the remaining carbons in the BADGE structure were also present in the degradation product, with the exception of C1 and C2 associated with the oxirane ring. These carbons appear to have undergone reactions with the amine groups of the curing agent. A noteworthy development is the appearance of a novel peak around 30 ppm, attributed to the C-N bond of the amine. This finding serves as additional confirmation of the presence of nitrogen within the structure of the degradation product. Furthermore, two highlighted peaks located around 13 and 22 ppm point towards the presence of C-C bonds within alkanes, providing further insight into the structural characteristics of the degradation product. By employing ^{13}CNMR, a more comprehensive understanding of the carbon skeleton structures of BADGE and CEP-RA has been

achieved, solidifying the knowledge gained from other analytical techniques and enhancing our comprehension of the structural modifications resulting from the recycling process.

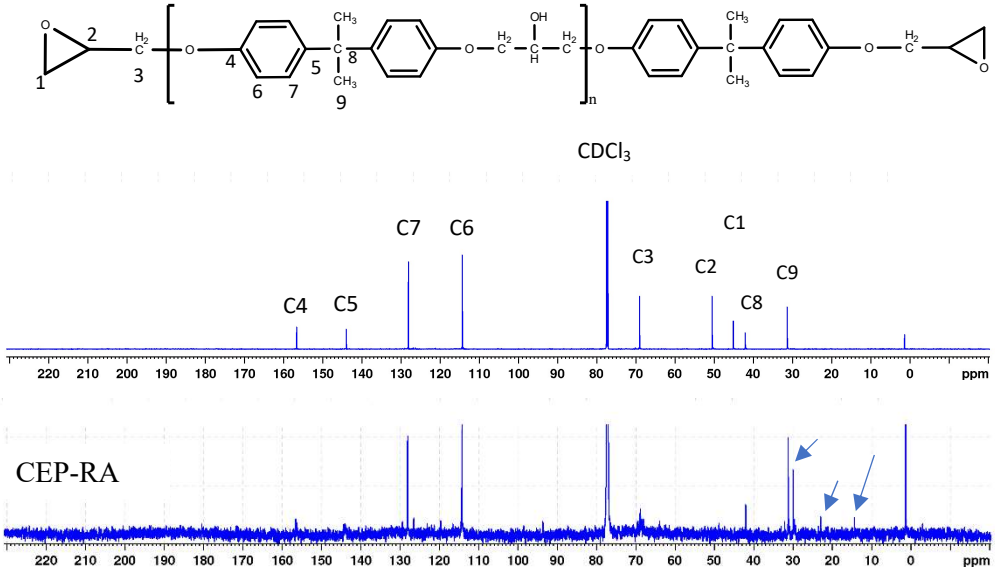

Figure 30. ^{13}CNMR spectra of BADGE and CEP-RA

3.1.3. The chemical mechanism of recycling process

Based on the above-mentioned results, we propose a possible catalytic mechanism of CEP treated by aluminum nitrate/DMAc (**Scheme 3**).

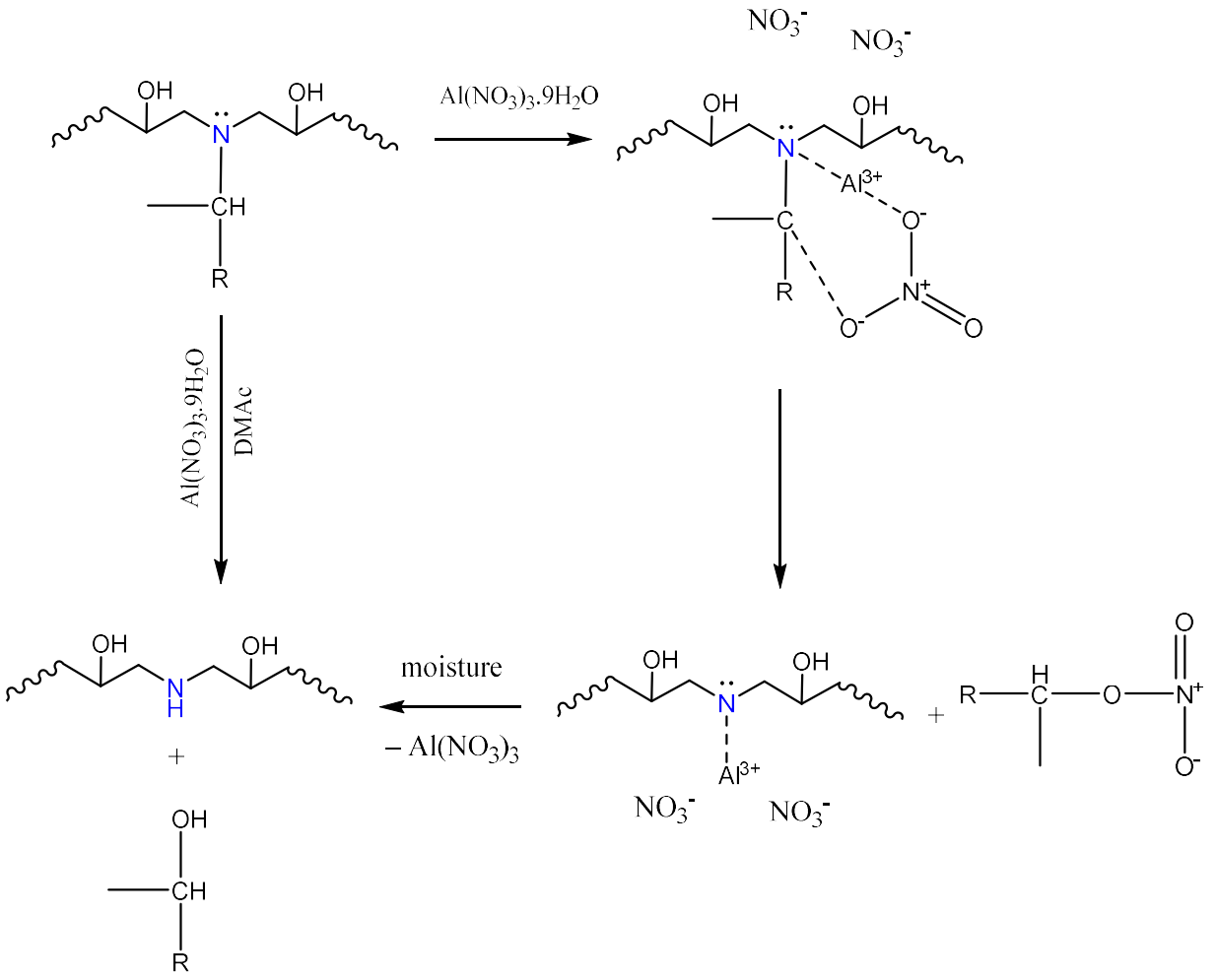

Scheme 3. The estimated mechanism of cleaving the bonds in cured epoxy system by the catalyst

3.1.4. Optimization of the recycling process

The optimization of the recycling process focused on determining the optimal conditions for achieving the highest degradation ratio, considering variables such as time, temperature, and catalyst concentration. The results, illustrated in **Figure 31**, reveal that the most favorable degradation ratio was attained when utilizing a 20% weight concentration of Aluminum catalyst at a temperature of 160°C over a period of 5 hours. This information helps establish the ideal

parameters for conducting the recycling process to achieve the most efficient and effective results in terms of degradation ratio.

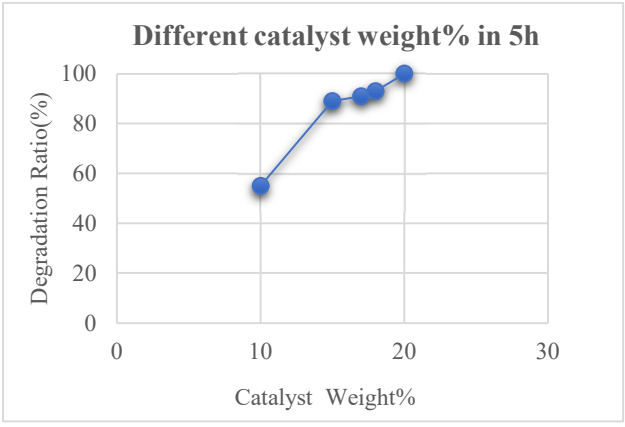

(a)

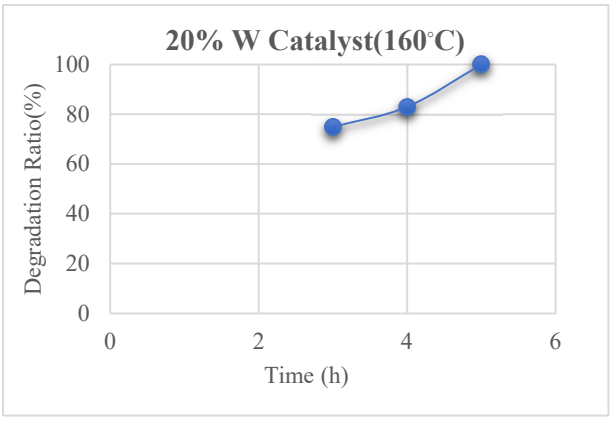

(b)

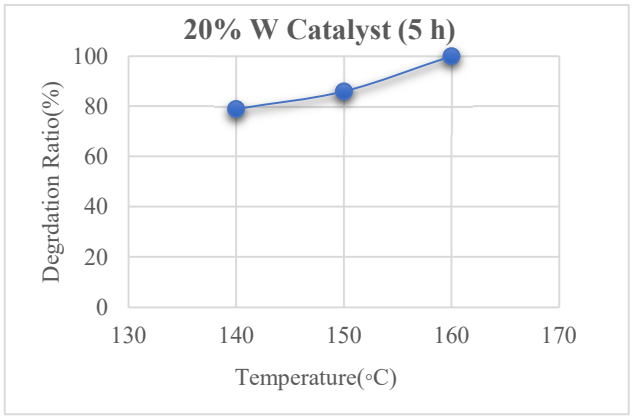

(c)

Figure 31. Optimization results based on a) catalyst concentration b) time and c) temperature

3.1.5. Recyclability of the solvent

Following the isolation of the degradation product, the remaining solvents encompassed water, DMAc, and remnants of the prepreg materials. Through the utilization of a Rotavapor, a successful separation and distillation process was carried out, initially removing water and subsequently

DMAc. Comparative analysis of the IR spectra of recycled DMAc against those of fresh DMAc was performed (**Figure 32**). The comparison illustrated no discernible differences between the IR spectra of the two, affirming the preservation of the structural integrity of the recycled solvent.

To ascertain the sustainability of the recycled solvent, it was employed twice in the recycling process, and the resulting degradation ratio was calculated. The outcome indicated an identical degradation ratio when compared to that achieved with fresh solvent.

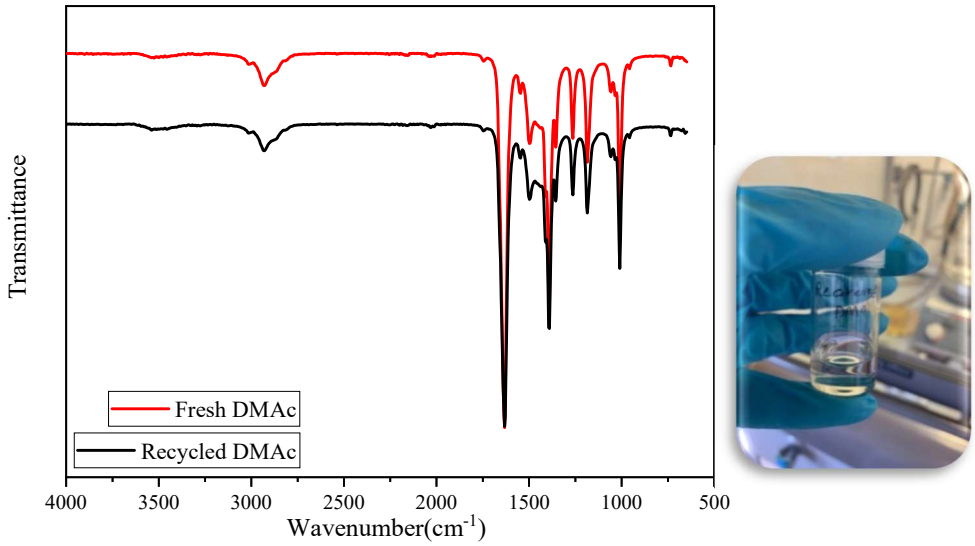

Figure 32. The comparison of the IR spectra of the recycled and fresh solvent

3.1.6. Reusing of degraded epoxy as co-hardener

The viability of reusing the degradation product obtained from the recycling of CEP was investigated by integrating it into a new epoxy system. The inclusion of nitrogen within the structure of CEP-RA indicated its potential utility as a co-hardener or catalyst in a freshly cured epoxy network. The objective was to evaluate its impact on the glass transition temperature (Tg) and tensile strength of the resulting cured epoxy. To achieve this, a mixture of Epikote and Epikure in a weight ratio of 100/24 was cured according to the protocols outlined in the datasheet, serving as the reference. Two distinct samples were examined: one containing 5% of CEP-RA as a

substitute for the curing agent, and another with 10% of the curing agent replaced by CEP-RA. The outcome of this experiment was shown in **Figure 36**, shedding light on the effects of incorporating CEP-RA on the glass transition temperature and tensile strength of the cured epoxy material.

Tensile tests were performed on carefully prepared specimens conforming to the DIN ISO 527-2 (1BA) standard, utilizing a silicone mold (**Scheme 4**). To ensure the absence of bubble formation during the curing process, meticulous attention was paid to specimen preparation. Over 30 specimens of each sample were cured and subjected to tensile testing using the MTS tensile machine. A gauge length of 25 mm and a crosshead speed of 0.5 mm/min were maintained throughout the testing procedure (**Figure 37**). The datasheet for the epoxy system specified a tensile strength of 85±2 MPa for the non-reinforced cured Epikote. The data presented in Table 10 demonstrated that the reference specimens exhibited an average tensile strength of 83.40 MPa, aligning closely with the datasheet specifications. Subsequent specimens were prepared and tested under the same conditions, adhering to the identical curing process (time and temperature) as the reference. Upon incorporating 5% CEP-RA as a replacement for the curing agent, the tensile strength was preserved at 96.5% of the reference value. However, when 10% CEP-RA was introduced in lieu of the curing agent, the tensile strength slightly decreased to 93.8%. The Glass Transition Temperature (Tg), representing the temperature at which a polymer transitions from a rigid, glassy state to a more flexible, rubbery state as molecular segments begin to exhibit increased mobility, was determined through Differential Scanning Calorimetry (DSC). In the context of these experiments, the Tg was slightly elevated from 123.8°C for the reference to 124.6°C for the sample containing 5% CEP-RA. This modest increase in Tg could be attributed to the presence of polar atoms and crosslinking chains, which restrict molecular mobility and thus contribute to an augmented Tg value (**Table 11** and **Figure 33-35**).

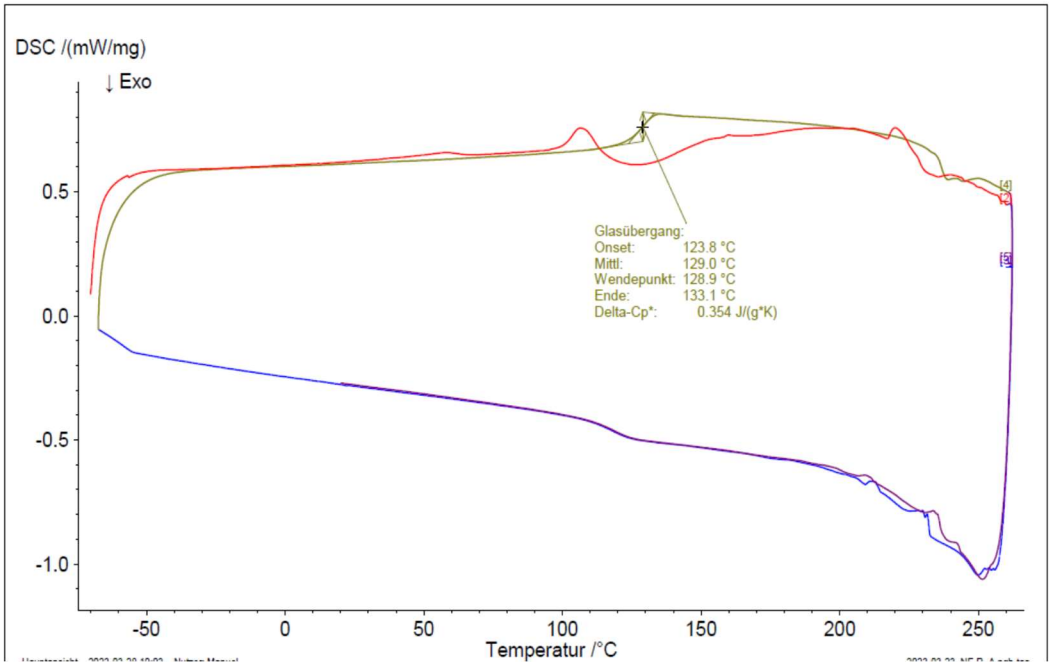

Figure 33. DSC of the reference (cured Epikote with Epikure)

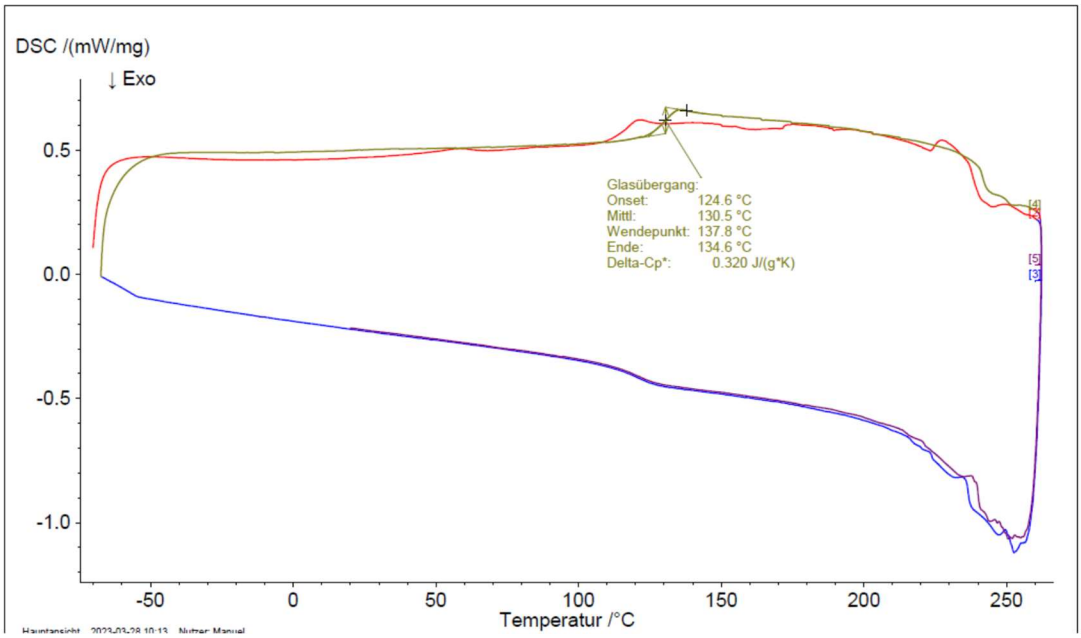

Figure 34. DSC of the cured Epikote containing 5% CEP-RA of Epikure

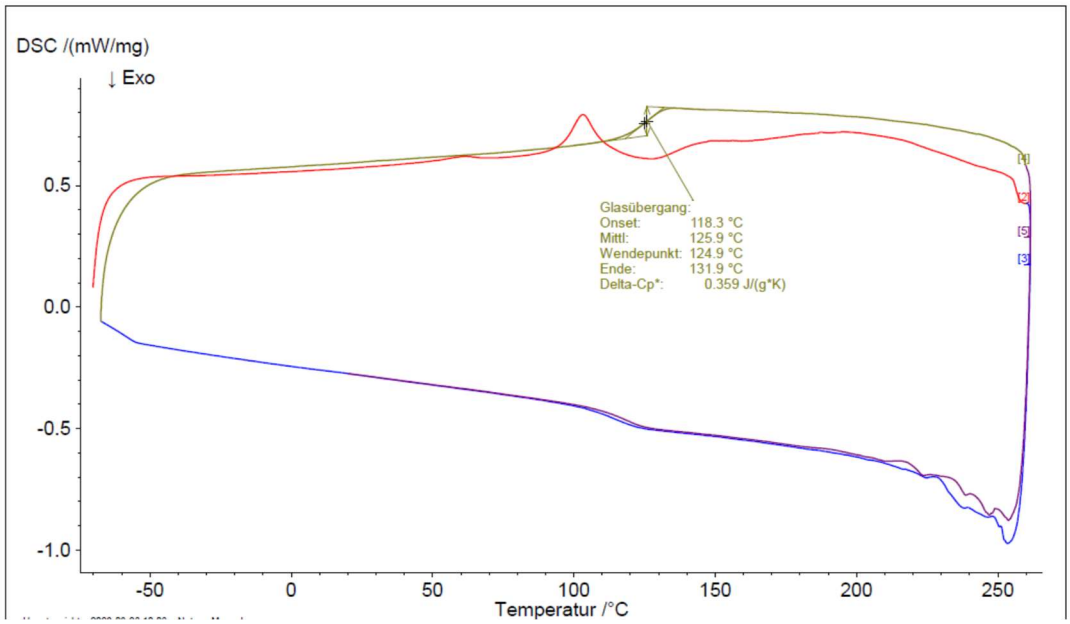

Figure 35. DSC of the Cured Epikote containing 10% CEP-RA of Epikure

Tensile strength test: specimens prepared according to DIN ISO 527-2:

- Reference: 100 parts Epikote+24 parts Epikure
- 5% DEG(CEP) of Epikure
- 10% DEG(CEP) of Epikure

The content of CEP-RA in curing agent: **10%**	**5%**	**0%**

Figure 36. The specimens of cured epoxy contain 5% and 10% CEP-RA of the curing agent.

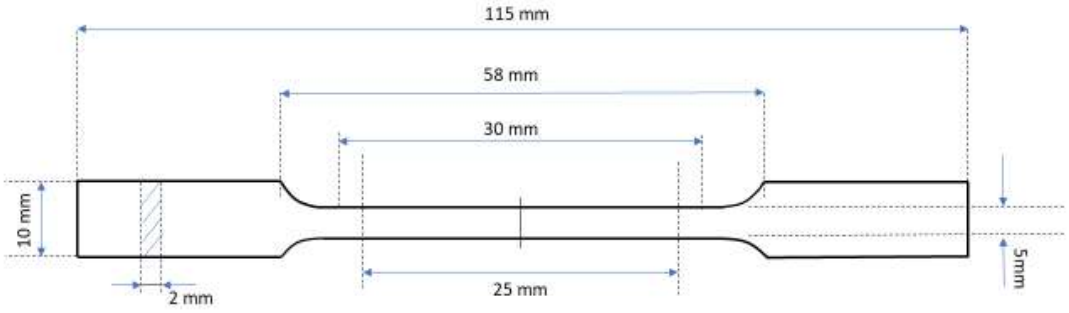

Scheme 4. Specimens according to DIN ISO 527-2 (1BA)

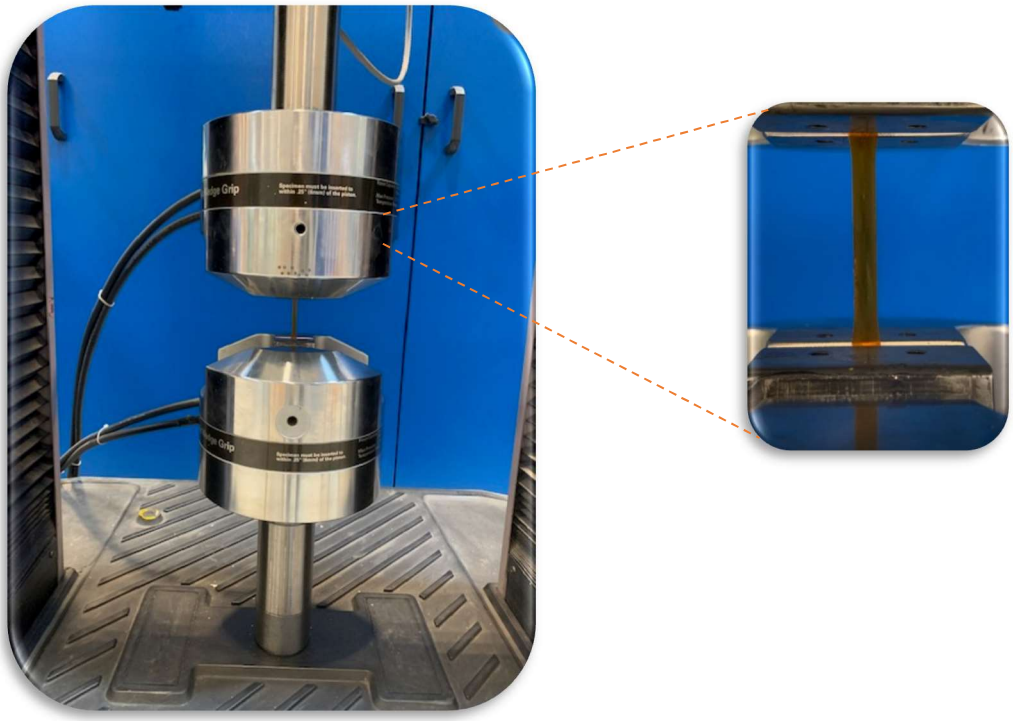

Figure 37. Tensile machine and gripped specimen

	Tensile strength (Mpa)	Tg (onset ˚c)
Reference (CEP)	83.40	123.8
Sample with 5% CEP-RA of curing agent	80.52	124.6
Sample with 10% CEP-RA of curing agent	78.28	118.3

Table 11. Tensile strength and DSC results of cured epoxy samples

Also **Figure 38**, shows the stress-strain curve of 4 specimens of each sample to compare the curve pattern of the sample with 5% and 10% CEP of the curing agent and reference one.

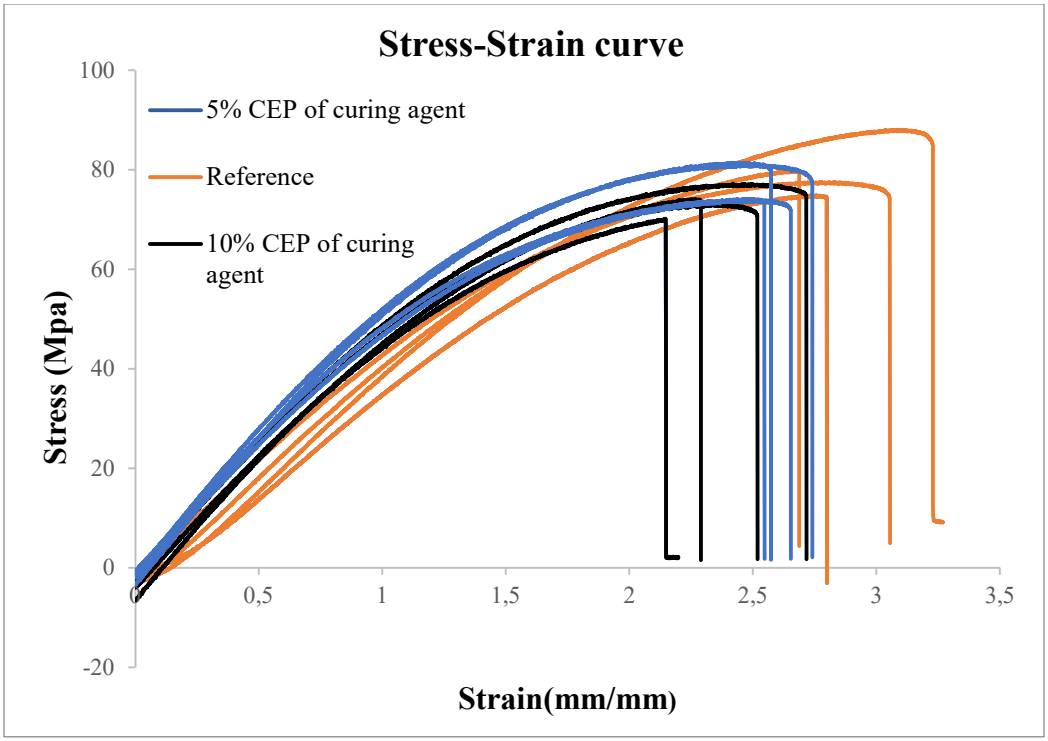

Figure 38. Stress-Strain curve comparison of 4 specimens, reference cured epoxy with 3 specimens of cured epoxy contain 5% and 10% CEP of the curing agent

3.1.7. Summary

In the scope of this study, a sustainable and straightforward process was successfully demonstrated for recycling carbon fibers from prepreg using aluminum nitrate nonahydrate and iron nitrate nonahydrate as catalysts. The application of Aluminum nitrate displayed superior efficiency compared to iron nitrate in recycling carbon fibers. The chemical and mechanical attributes of the fibers were effectively preserved after using aluminum nitrate as a catalyst. Achieving a degradation ratio of approximately 100%, the treatment with the catalyst at 160°C for 5 hours showcased remarkable efficacy in cleaving the chemical bonds within the crosslinked epoxy polymer matrix. This method emerges as a promising approach for recycling carbon fiber-reinforced epoxy polymers while maintaining their essential properties.

The empirical evidence derived from various analytical techniques, including TGA, Raman spectroscopy, XPS, XRD, and SEM (EDX), collectively verified that the chemical composition

and surface characteristics of the fibers remained unaltered. Notably, the tensile strength of the recycled fibers approached that of virgin fibers, signifying the successful preservation of mechanical properties. Moreover, the presence of amine and hydroxy groups within the degraded epoxy matrix unveiled the potential for reusing this product in new epoxy systems. Incorporating 5% of the degradation product as a curing agent yielded a cured epoxy with comparable tensile strength and even exhibited a higher glass transition temperature when contrasted with reference. This highlights the capacity of the degradation product to serve as a valuable component in epoxy formulations, contributing to improved mechanical and thermal properties.

Furthermore, the study successfully demonstrated the reusability of the solvent after distillation, attesting to the feasibility of recycling and reutilizing multiple elements within the carbon fiber-reinforced epoxy system. In sum, this research underscores a significant stride towards sustainable carbon fiber recycling, where the methodology's efficiency, effectiveness, and capacity for contributing to environmentally conscious practices were vividly demonstrated.

3.2. Reversible Edge-Functionalization of graphite by DA reaction

Another approach was the study of functionalization of graphite by the Diels-Alder reaction and investigation of reversibility of this reaction by applying external stimulus like raising the temperature. The aim was to find a way to utilize epoxy resin as a matix to make a thermoset graphene composite and then by Retro-DA, we will have a recyclable composite, but it was faced with some obstacles. Furfurylamine was successfully attached mostly to the edge of the graphene sheets with the help of ball milling. One assumption is that the equivalent amount of amine attached to the graphene sheets were not enough to react with the oxirane ring in the epoxy and was not able to cure the epoxy. So as the amine-functionalization was completely successful, it can be a good topic to make a recyclable composite or even another aim for the future

3.2.1. Introduction

Graphene is a 2D sheet of sp^2-hybridized, networked carbon. Its expansive honeycomb graphitic framework serves as the fundamental building block for various significant carbon allotropes. This versatile material can be stacked to form 3D graphite, rolled to create 1D nanotubes, and wrapped to generate 0D fullerenes. So, Graphite is the most stable allotrope of carbon with sp^2 (trigonal) hybridization that due to unique and exceptional properties is being widely used in many applications.

Chemical modification of Carbon-based materials has huge impact on their properties to be adapted to use in variety of applications. The chemical functionalization of graphene-based structures plays a significant role in various applications. It enables the creation of diverse graphene derivatives, manipulation of interfacial features, and the adjustment of the engineered energy band structure. Despite the strong chemical stability of graphite, designing and fabricating functionalized graphene without resorting to harsh reaction conditions remains a considerable challenge.

3.2.2. Graphite structure and properties

Graphene is the base structure of all graphitic forms; the structure of this wonderful material is a one-atom-thick planar sheet of sp^2-bonded carbon atoms that are firmly arranged in a honeycomb crystal lattice with carbon-carbon bond lengths of 0.142 nm. Numerous graphene sheets stack with an interplanar spacing of 0.335 nm to form graphite; a 1-mm thick graphite crystal contains approximately 3 million layers of graphene sheets which firmly are stacked together (**Figure 39)**.

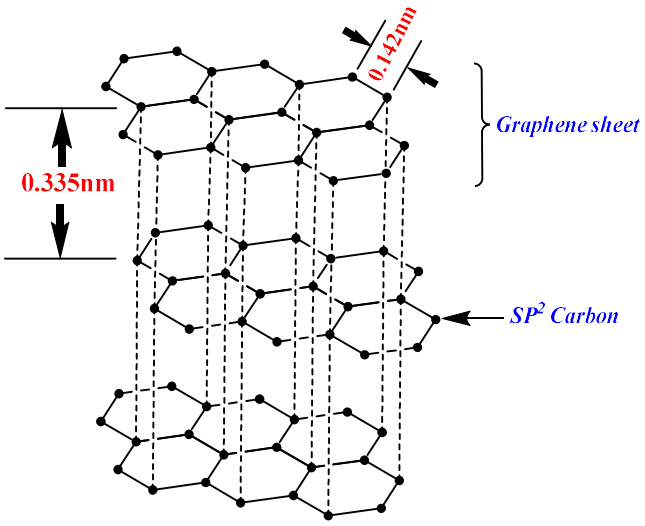

Figure 39. Layered structure of graphite contains sp^2 hybridized carbon

The fascinating properties of graphene have inspired scientists to further study this outstanding material. One of the most remarkable properties of graphene is that its charge carriers behave as massless relativistic particles or Dirac fermions, and under ambient conditions, they can move with little scattering. This unique behavior can create a number of remarkable phenomena in graphene [77]. First, graphene is a semimetallic or zero-band gap 2D semiconductor with a tiny overlap between the valence and conduction bands. Second, high Young's modulus [78] of 1.0 TPa. high optical transmittance [79] of 97.7% is considered as another superb property. Graphene has the ability to sustain extremely high electric current density around a million times more than copper [80]. It is also approximately 100 times stronger than steel 81. Graphene can be stretched up to 20% of its original length without breaking and is therefore used in making flexible and unbreakable displays that can be twisted easily. It exhibits a strong ambipolar electric field effect so that the charge carrier concentrations of up to 1013 cm^{-2} and room-temperature mobility of $\sim 10^4$ $cm^{-2}s^{-1}$ are

measured. An unusual half-integer quantum Hall effect (QHE) for both electron and hole carriers in graphene has been observed by adjusting the chemical potential using the electric field effect [82,83] High thermal conductivity due to covalent sp^2 bonding between carbon atoms with a value of ~ 5000 $Wm^{-1}K^{-1}$ for a single-layer sheet at room temperature can be mentioned too. [84]

The functionalization of graphene and its derivatives plays a crucial role in designing graphene-based conjugates with novel properties. Graphene can be covalently or non-covalently functionalized. In the first case, stable covalent bonds are formed, but in the second one, there is the formation of weak bonds like hydrogen bonds, π–π interactions and Van der Waals interactions. Covalent modification of graphene causes rehybridization of sp^2-carbon atoms of the aromatic structure, while in non-covalent functionalization the sp^2 structure is preserved. Due to the change of hybridization, the strictly constrained sp^2-carbon atoms have to move out of the plane in a tetrahedral sp^3 geometry and it is the reason that edge carbon atoms are more reactive in covalent addition reactions [85].

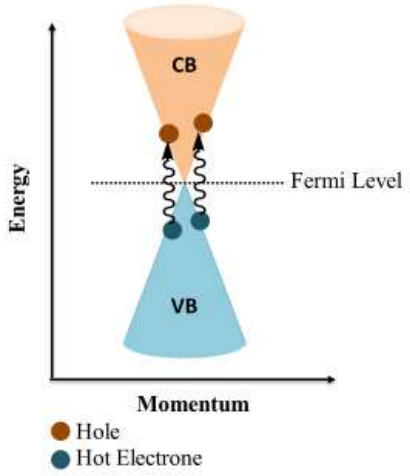

Scheme 5. Schematic diagram of energy band of graphene [77]

3.2.3. Diels-Alder reaction on graphite

The Diels-Alder (DA) cycloaddition reaction emerges as a highly desired method for graphene functionalization. This approach offers advantages such as mild reaction conditions, high effectiveness, and improved electrical conductivity of graphene. The use of Diels-Alder

cycloaddition presents a promising avenue for achieving functionalization goals while maintaining the integrity and desirable properties of graphene-based materials.

The covalent functionalization can be categorized into nucleophilic addition, atomic radical addition, free radical addition, electrophilic substitution, and cycloaddition reactions on the surface, at the edge and at the defect sites. One of the most basic and important reactions in synthetic organic chemistry is classical [4+2] cycloaddition (Diels-Alder) [86,87], between a diene and a dienophile to produce a stable cyclohexene derivative (adduct) [88-91]. This reaction shows a thermally reversible character especially with furan derivatives at relatively low temperatures that allow decoupling of the adduct to occur by increasing temperature as an external stimulus. Graphite and graphene have a similar carbon nanostructure, which has turned them into a research hotspot. In 2011, Haddon and co-workers demonstrated that graphite or graphene have dual functions in the D-A reaction due to the presence of p-conjugation and being gapless (the conduction and valence bands touch at the Fermi level (Dirac point) [86,92] (**Scheme 5**). Since then, a series of approaches have been reported, in which graphite or graphene acts either diene or dienophile under different conditions [93-96] (**Figure 40**).

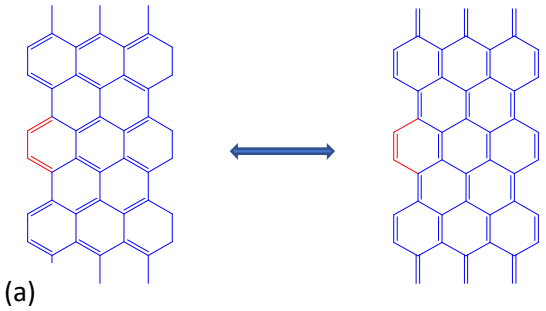

Figure 40. Two possible resonance forms of graphite [93-96]

Graphite in comparison with graphene is less prone to D-A reaction, because of its lower specific surface area [97,98], so a suitable method needs to facilitate the D-A reaction of graphite. For this purpose, we report here for the first time a solvent-free mechanochemical method driven by ball milling. In this efficient way, functional groups could be mostly introduced to the broken edges of graphene sheets. Rotating balls in the system can transfer their kinetic energy to the milled materials which included graphite as a dienophile and furfuryl amine as a diene and breaking

strong bonding interactions and creating new and chemically active edges and surfaces. The diene reacts well to produce D-A adducts mostly at the edges and to some extent on the surfaces.

The zero-band-gap electronic structure of graphene arises from the crossing of the valence and conduction bands at the Dirac point (K), which dictates that the highest occupied molecular orbital (HOMO) and lowest unoccupied molecular orbital (LUMO) energies are coincident with the work function (WF= 4.6 eV) figure 2b. Consequently, the HOMO and LUMO of graphene form a degenerate pair of orbitals at this point in momentum space with the same ionization potential (IP) and electron affinity (EA). These states determine reactivity. Pericyclic reactions are subject to the Woodward-Hoffmann rules, and inspection of the orbital symmetries of the degenerate pair of half-occupied HOMO and LUMO band orbitals at the Dirac point confirms that with the appropriate orbital occupancies, both diene and dienophile reaction partners should undergo Woodward-Hoffmann allowed, concerted D-A reactions with graphene. Thus, exceptionally low ionization potential (HOMO) and high electron affinity (LUMO), together with the orbital symmetries of the degenerate HOMO and LUMO bands at the Dirac point, enable graphene sheets to participate in the D-A reaction and to show dual reactivity as either diene or dienophile when paired with the appropriate reaction partner and make two new sigma and one new π bond. [86,87] (**Figure 41**).

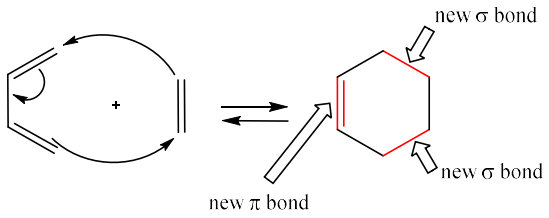

Figure 41. Schematic of Diels-Alder cycloaddition Reaction [86-87]

At the graphene sheets edges, which can be either zigzag or arm-chair structures (**Figure 42**), the achievement of aromatic sextets is frustrated in most of the rings where zig-zag edges are concerned and are therefore thermodynamically unstable and more reactive than arm-chair edges [99-101].

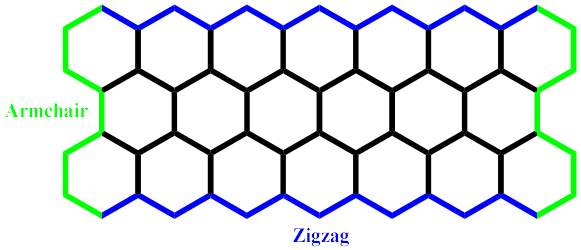

Figure 42. Zigzag and Armchair edges of graphene lattice [99-101]

3.2.4. Review of Diel-Alder reaction on carbon materials

There are several methods reported regarding Diels-Alder (DA) cycloaddition reaction on different carbon material under different conditions. Graphite, graphene and carbon nanotubes were functionalized through DA cycloaddition reaction.

Water-soluble graphene dispersion was produced by exfoliation of graphite functionalized with furfurylalcohol by DA reaction in two steps, first in NMP at 250°c and 2Mpa pressure for 8 hours, the interlayers distance of graphite was increased and then furfurylalcohol as a diene were attached to the exfoliated graphite at 130°c [102]. Also DA reaction was conducted on expanded graphite as diene and maleic anhydride as dienophile to produce MA-functionalized graphene nanosheet. The thickness of the resultant functionalized MAG measured by AFM was 3−4 nm with a yield of ∼64%. [103]

The Diels–Alder reaction has been successfully carried out with graphene oxide as a source of diene by using maleic anhydride as a dienophile. For the DA reaction, GO was heated in the presence of an excess of maleic anhydride at 60°C in anhydrous 1,4-dioxane under dry argon.[104]

(**Figure 43**)

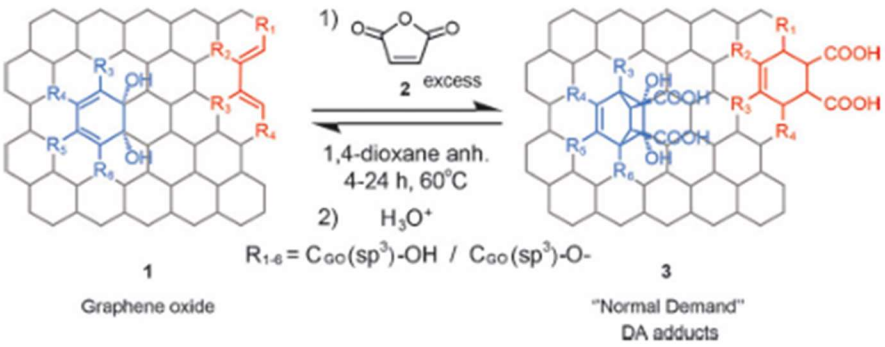

Figure 43. Diels-alder reaction on graphene oxide in the presence of maleic anhydride

A covalent functionalization of exfoliated few-layer graphene (FLG) with different arynes under microwave (MW) irradiation and solvent-free conditions was reported in 2018 year. The dispersibility of the DA- functionalized graphene in Ethanol after 15 days was confirmed. [105] (**Figure 44**)

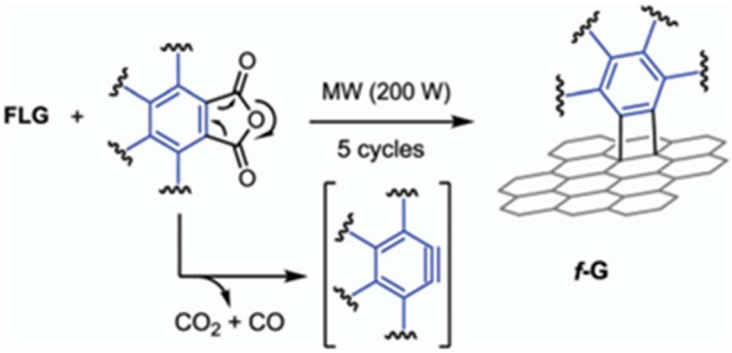

Figure 44. microwaved-assisted functionalization of FLG

Thermally healable graphene nanoplate-epoxy composite was investigated by DA reaction on the surface of graphene nanoplates. GNPs were utilized as reinforcement and crosslinking platforms for the diglycidyl ether of bisphenol A-based epoxy resin (DGEBA) through the Diels-Alder (DA) reaction with furfurylamine (FA). The GNPs and FA could then be used as a derivative of diene and dienophile in the DA reaction. [106] (**Figure 45**)

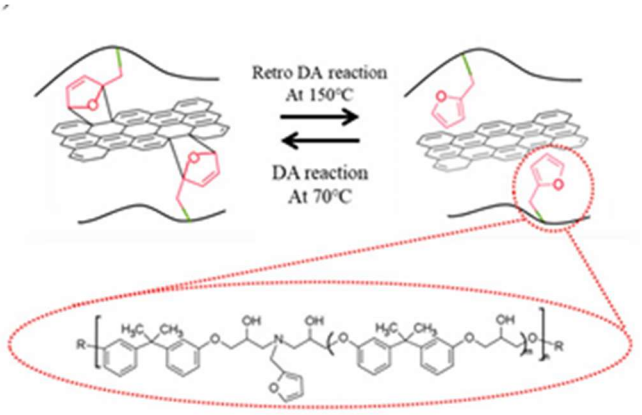

Figure 45. Functionalization of GNP through the Diels-alder reaction

Production of highly conductive graphene was reported by reversible DA reaction on graphite. graphite was mechanically exfoliated into graphene and then Diels–Alder reaction was used to bond TCNE (tetracyanoethylene) molecules onto the graphene layers of graphite to weaken the interlayer interactions and to improve the dispersibility of resulting graphene sheets. [107]

Reduced graphene oxide was modified by grafting maleimide group via DA reaction. [108]

Graphite was functionalized by DA reaction under solvent-free condition. Reported approach was carried out by heating a mixture of graphite and a typical dienophile, maleic anhydride (MA) or maleimide (MI), in a sealed glass ampoule of argon. [109](**Figure 46**)

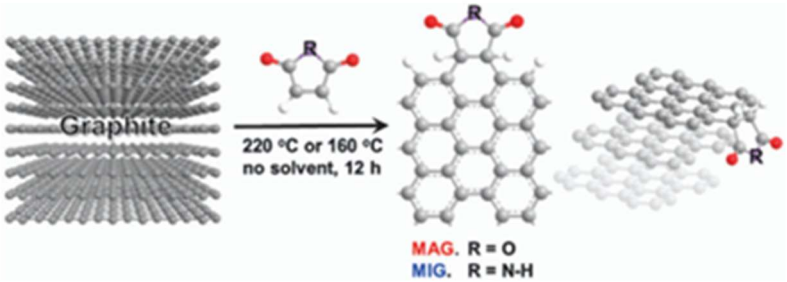

Figure 46. Solvent-free process of Diels-alder on graphite

Another study was under wet ball milling method to attach maleic anhydride to graphite by DA reaction. It was carried out in NMP solvent and under N_2. functionalized graphite displays an excellent dispersibility in polar solvents like water and ethanol. [110](**Figure 47**)

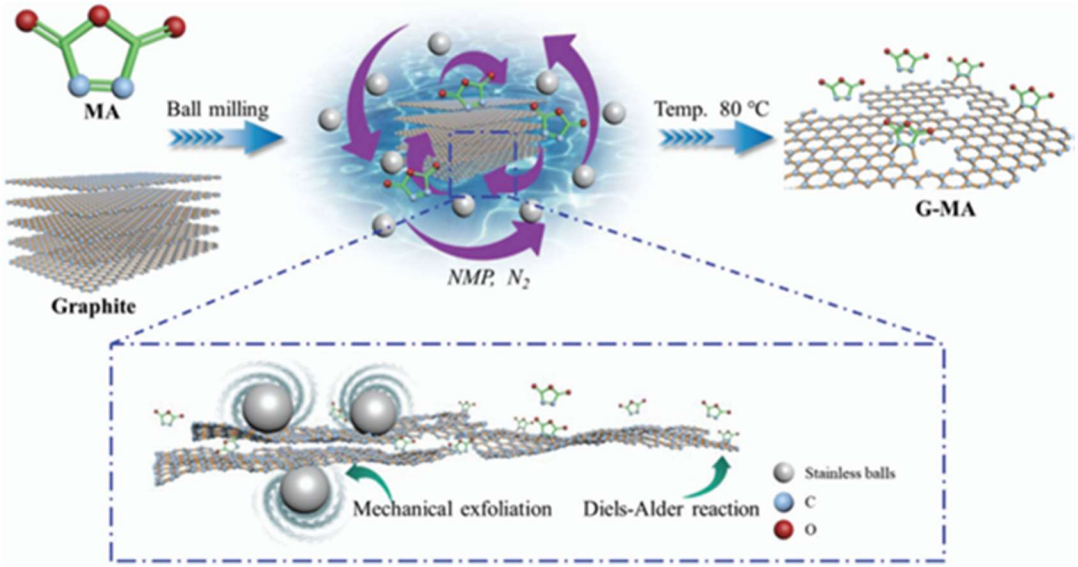

Figure 47. Ball milling process of Diels-alder on graphite in NMP

The CNTs (single and multiwall) also show a dual nature of reactivity in DA reaction, they behave both as dienophile and diene with furfuryl groups and maleic anhydride derivatives, respectively. Several kinds of functional groups, including alcohol, amine, epoxy, carboxylic and ester, were grafted on the carbon materials by DA reaction. It was investigated that single wall carbon nanotubes are more reactive than multiwall tubes, and in terms of reactivity, the CNTs show behavior reminiscent of small molecule chemistry. Other carbon materials like carbon nanofibers show relatively less reactivity, presumably due to the less available surface area.[111](**Figure 48**)

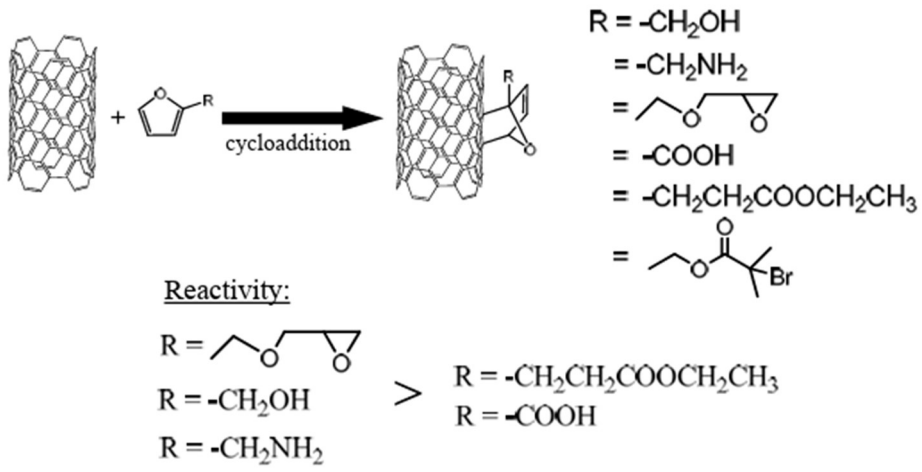

Figure 48. Diels-alder reaction on CNT

3.2.5. Experimental section (synthesis of edge-functionalized multilayered graphite by Diels-Alder reaction)

The facile route of dry ball milling is depicted in **scheme 6**, and the thermal reversibility is studied via a reverse D-A reaction in this work. Under mild strategy, graphite acts as a dienophile and furfuryl amine as a diene to produce the desired adduct. By applying two sizes of balls in the ball mill, the efficiency of creating active sites on the graphite was improved and the reaction rate between diene and dienophile effectively increased. First, reactants were exposed to the non-continuously ball milling in a sealed glass container under nitrogen gas and in an oil bath of 70˚C, respectively. The container was kept at 70˚C for 24 hours without milling to provide an efficient condition for the D-A reaction. Finally, the product displayed excellent dispersibility in polar solvents. The retro Diel-Alder happened simply by heat treatment of the functionalized graphite (150˚C for 2 hours).

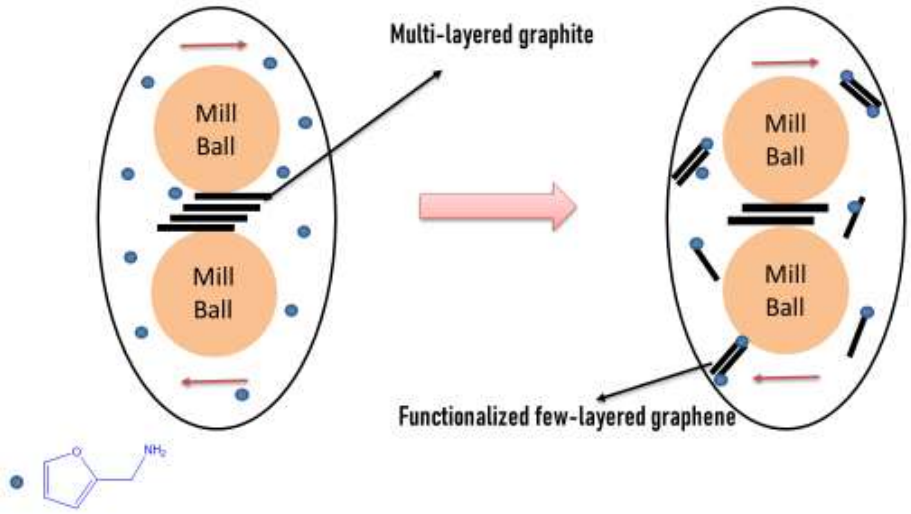

Scheme 6. Ball-milling schematic of graphite and furfuryl amine that leads to cycloaddition

Synthesis of G-FA:

Pristine graphite (2.5 g) and furfuryl amine (5 g) were added into a thick glass container which included small (0.5 mm) and bigger stainless-steel balls (2mm). The container was sealed and charged/discharged with nitrogen gas and placed in an oil bath of 80˚C (**Figure 49**). The ball milling step (medium speed) was carried out in a non-continuous process, after milling for 2 hours, the mixer was turned off for 1h and again milling for 2 hours. This cycle repeated 3 times resulting in an overall milling time of 6h and 3h without milling.

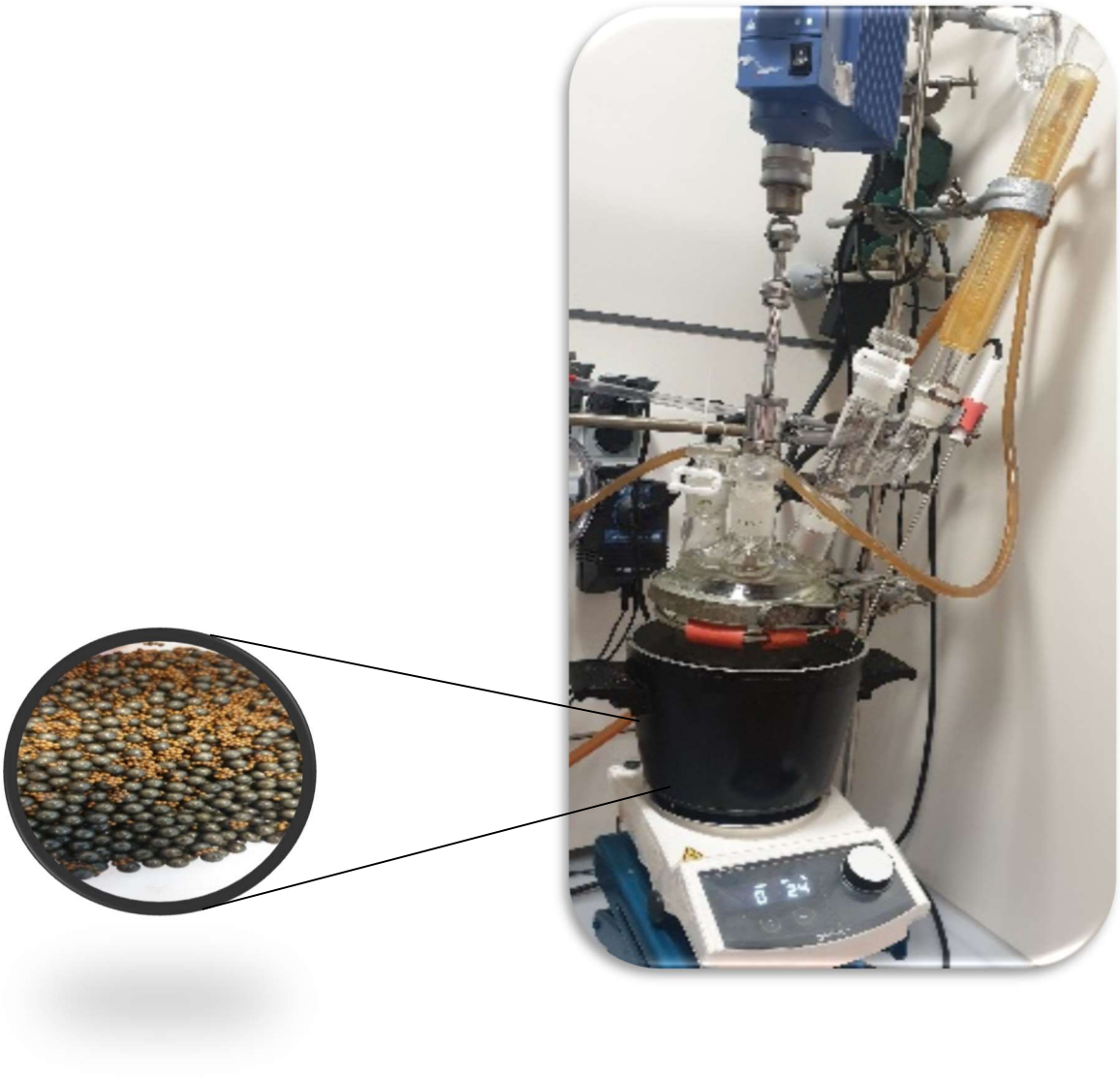

Figure 49. Experiment set up in the laboratory

Subsequently, the container was kept under 70˚C in the oil bath for 24h. Afterward, the product was treated with HCl (37%) in order to remove iron impurities from the milling process and the material was further washed with water until the pH value was close to 7. Thereafter the product was washed with THF to remove unreacted furfuryl amine. In the end, the product was left to dry in the oven at 70˚C. The G-FA was collected as powder and kept in a sealed glass container after freeze-drying to make it ready for further analytical measurements.

Control reactions:

G-BM: As a contrast, the control reaction was exposing graphite flakes to the ball mills under the same conditions as G-FA but without furfuryl amine. The powder of G-BM was obtained via the freeze dryer.

G-TFA: This control reaction was the reaction between pristine graphite and furfuryl amine, only in the presence of temperature (70˚C) and without any ball milling process. This reaction was kept for 2 days under 70˚C.

ReG-FA: Retro Diels-Alder reaction of G-FA: The reverse D-A reaction of G-FA was conducted under 150 ℃ for 2h.

3.2.6. Analysis of functionalized graphite

The collected functionalized graphite was investigated by analytical measurements to prove the DA and also retro-DA on graphite.

3.2.6.1. TGA

The thermal behavior of pristine graphite, G-BM, G-TFA and G-FA were analyzed by thermogravimetric analysis (TGA). This technique is a powerful technique used to determine material's thermal stability and its fraction of volatile components by monitoring the weight change that occurs as a sample is heated at a constant rate. As shown in **Figure 50** the pristine graphite displayed high thermal stability until 700˚C due to the perfect conjugated structure and the weight loss was only about 0.7% at 1000˚C. As it is clear in **Figure 51**, G-TFA did not show any weight loss at the temperature less than 500˚C and it was the sign of no D-A functionalization. Thus, further analytical measurements weren't carried out for this sample. In another analytical measurement, we compared pristine graphite, G-BM and G-FA. The G-FA pattern displayed in the beginning a weight loss at low temperature in the range of 30 to 300˚C that could be attributed to the detachment of the furfuryl amine on graphene sheets, while as shown in **Figure 52** the ReG-FA had a very small amount of weight loss in the range of 30 to 250˚C which is comparable with the G-BM pattern. At 250˚C, the weight loss for ReG-FA is 0.7% and for G-BM is 0.6%. This

indicated that ReG-FA had better thermal stability than G-FA due to the detachment of the Furfuryl amine on the graphene and the repaired conjugated structure during the reverse D-A reaction. These results show that furfuryl amine had been grafted on graphene sheets successfully. Also, the solubility test confirms the existence of amine groups on the graphene sheet which facilitates the solubility property of graphene in polar solvents such as ethanol. The container on the right in the photo is a G-FA sample dispersed in ethanol after 10 minutes of sonication. The suspension was stable for 3 weeks at room temperature. Indeed, it was still stable after 1 year. The left picture is a sample of ReG-FA in ethanol under the same condition as G-FA. No suspension was formed.

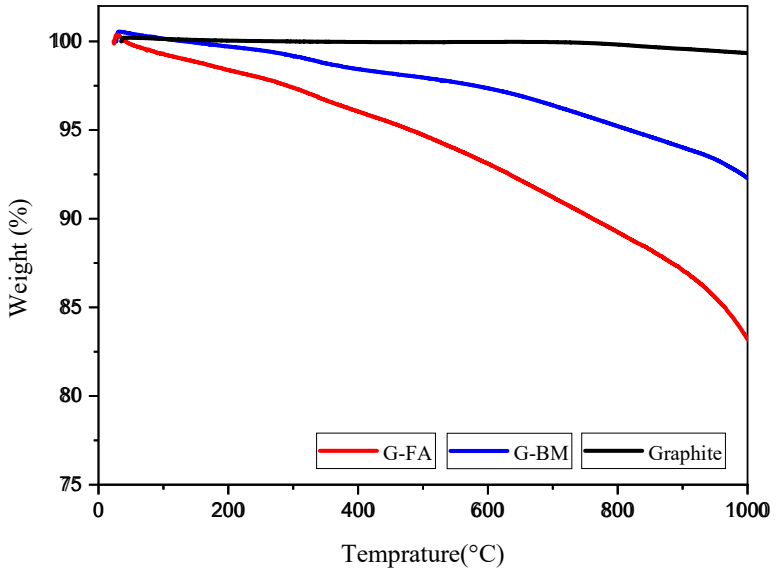

Figure 50. TGA curves of pristine graphite, G-BM and G-FA

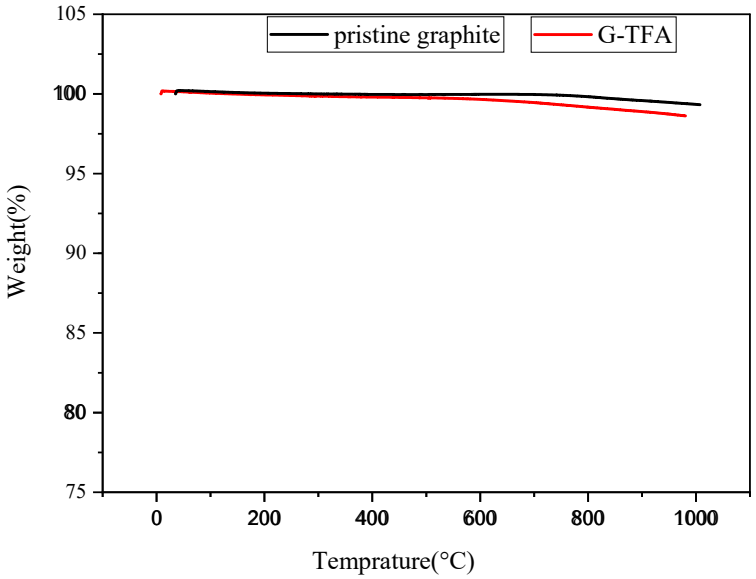

Figure 51. TGA curves of pristine graphite and G-TFA

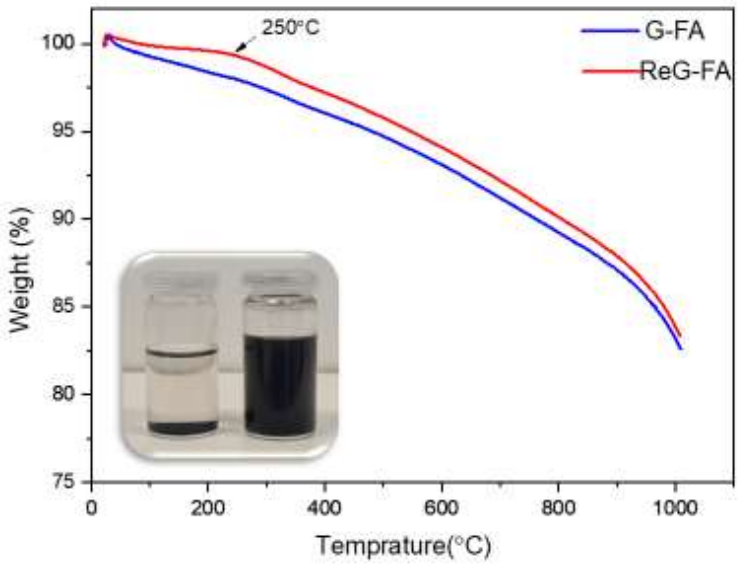

Figure 52. TGA curves of G-FA vs. ReG-FA confirmed by photographs of the solubility properties of G-FA (right) and ReG-FA (left) in Ethanol after 3 weeks standing at room

3.2.6.2. Raman Spectroscopy

Raman spectroscopy is a key technique to characterize various carbonaceous materials and analyze different types of sp^2 nanostructures in carbon nanotubes, graphite, graphene and it is capable of discerning any slight changes, defects and further functionalization in the structures.

Raman spectroscopy has been compared at the edge and also on the surface positions of each sample. As shown in **Figure 53**, the Raman spectra of the pristine graphite, G-BM and G-FA displayed two distinguishable peaks at 1340 and 1580 cm^{-1}, which correspond to the D band (the vibrations of the sp^3-hybridized carbons) and G band (in-plane vibration of sp^2 carbon atoms), respectively. Generally, the intensity ratio of the D-band to G-bands (I_D/I_G) is a good indicator of the level of defects, which are mainly sp^3 carbons on the graphene. These show the degree of functionalization introduced into graphene sheets [112,113]. For the pristine graphite, the D band intensity at the edge and also on the basal plane is remarkably small. Comparing the Raman spectra on the surface and at the edges of the product can clearly reveal that functionalization has occurred in both positions, due to the higher intensity ratio of I_D/I_G compared to the pristine graphite. Although the degree of functionalization in G-FA is significantly higher at the edges in comparison with surfaces. I_D/I_G ratio for pristine graphite, G-BM and G-FA at the edge, are 0.04, 0.30 and 0.65 respectively, while these ratios on the surface are 0.04, 0.06 and 0.20. This comparison clearly confirms that functionalization has occurred mostly at the edge of the graphene sheets and more sp^3 carbons were found in the G-FA structure owing to the characteristics of the D-A reaction, which involves C-C bond (sp^2) carbons in the reaction and generates a C–C bond (sp^3) in the products. Therefore, more sp^3-carbons were found in the G-FA structure. The results suggest that a small quantity of defects was introduced into the graphite flakes during the ball milling process (G-BM). The rise of the ratio of I_D/I_G in G-FA is due to the damage of the graphite lattice structure in the ball milling process and the other is contributed to the destruction of the π-conjugated structure of graphene by the D-A cycloaddition reaction that occurred between graphite and furfuryl amine, which lead to the increasing number of sp^3 carbon atoms mostly at the edges.

Another distinguished spectral feature of carbon-based materials is the appearance of a 2D band which is the result of a two-phonon lattice vibrational process. The shape, intensity and location (cm^{-1}) changes of the 2D peak reveal the evidence of the numbers of the layers of graphene sheets.

The 2D-band peak position is shifted to higher numbers, i.e., from 2702 cm^{-1} for 3-layer graphene to 2720 cm^{-1} for 10-layer graphene and 2725 cm^{-1} for a graphite thickness of 40 nm [114]. According to the Raman spectra of the samples at the edges, the 2D peak location of pristine graphite and G-FA are 2722 and 2708 cm^{-1}, respectively. These numbers for the surface of the samples are 2722 and 2715 cm^{-1}. It can be obviously confirmed that the ball milling process and the functionalization could decrease the number of layers from around 40nm thickness of pristine graphite to less than 10 layers at the edge of G-FA (estimation is between 6-8 layers).

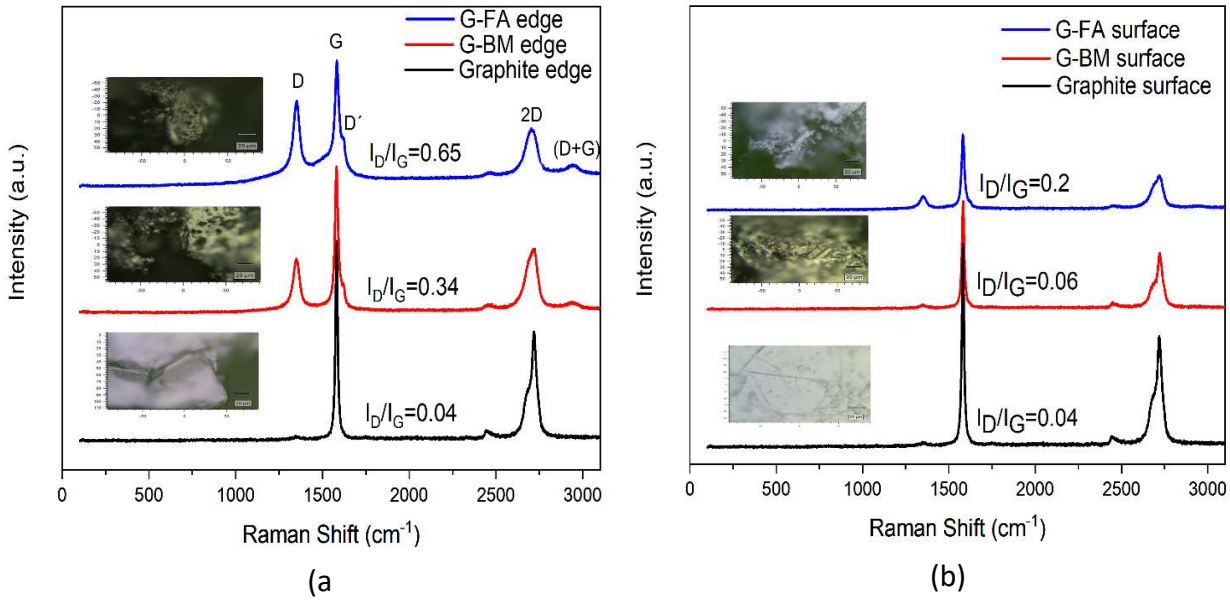

Figure 53. Raman spectrum a) at the edge and b) on the surface of pristine graphite, G-FA and G-BM

Another difference in the Raman spectrum of pristine graphite and G-FA is the shape of the 2D band which is formed from two Lorentzian peaks. The intense $2D_1$ band and a low-energy shoulder called the $2D_2$ band are present in **Figure 54**. The 2D band originates from a two-phonon double resonance process and it is interrelated to the band structure of graphene layers. According to the approach of A. C. Ferrari and coworkers in 2006 [115], a further decrease in layers leads to a significant increase of the relative intensity of the lower frequency $2D_1$ peaks. Also, Cancado et al. [116] have shown that as disorder increases, the $2D_2$ shoulder shift upwards and finally merges into the $2D_1$ band. As a result, the 2D band exhibits a single peak profile and the peak becomes

asymmetrical, to figure 5 shows, it can be a good confirmation that the thickness and the numbers of layers in the G-FA at the edge of the graphene sheets are less than in pristine graphite and due to high c-axis disorder, the two-peak profile of graphite is not maintained in the G-FA.

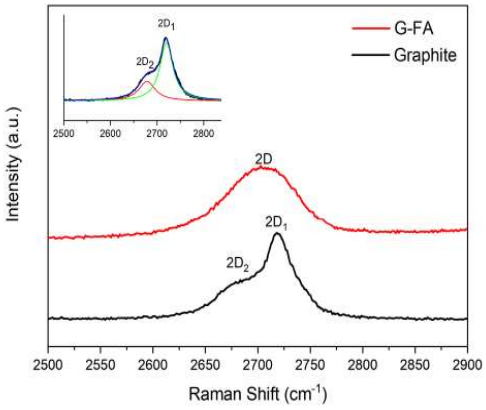

Figure 54. The expansion of the 2D peak of pristine graphite and G-FA

In addition, the D′ peak (1620 cm^{-1}) is also observed in the Raman spectra of G-BM and G-FA, which indicates the defects of the graphene because the defects will lead to an increase in the D′ intensity [117]. On the other hand, the appearance of the peak (D+G) strongly supports the higher disorder in the G-FA sample, although this peak is sharper at the edges of the graphene sheets in the G-FA compared with the surface, and it shows another evidence of the higher degree of disorders at the edge of the G-FA, figure 5b.

3.2.6.3. XRD

XRD diffraction is a widely used non-destructive method to analyze carbon materials. It is employed to study the phase composition of samples, to analyze the qualitative and quantitative composition and to assess the structural characteristics of crystalline carbon materials.

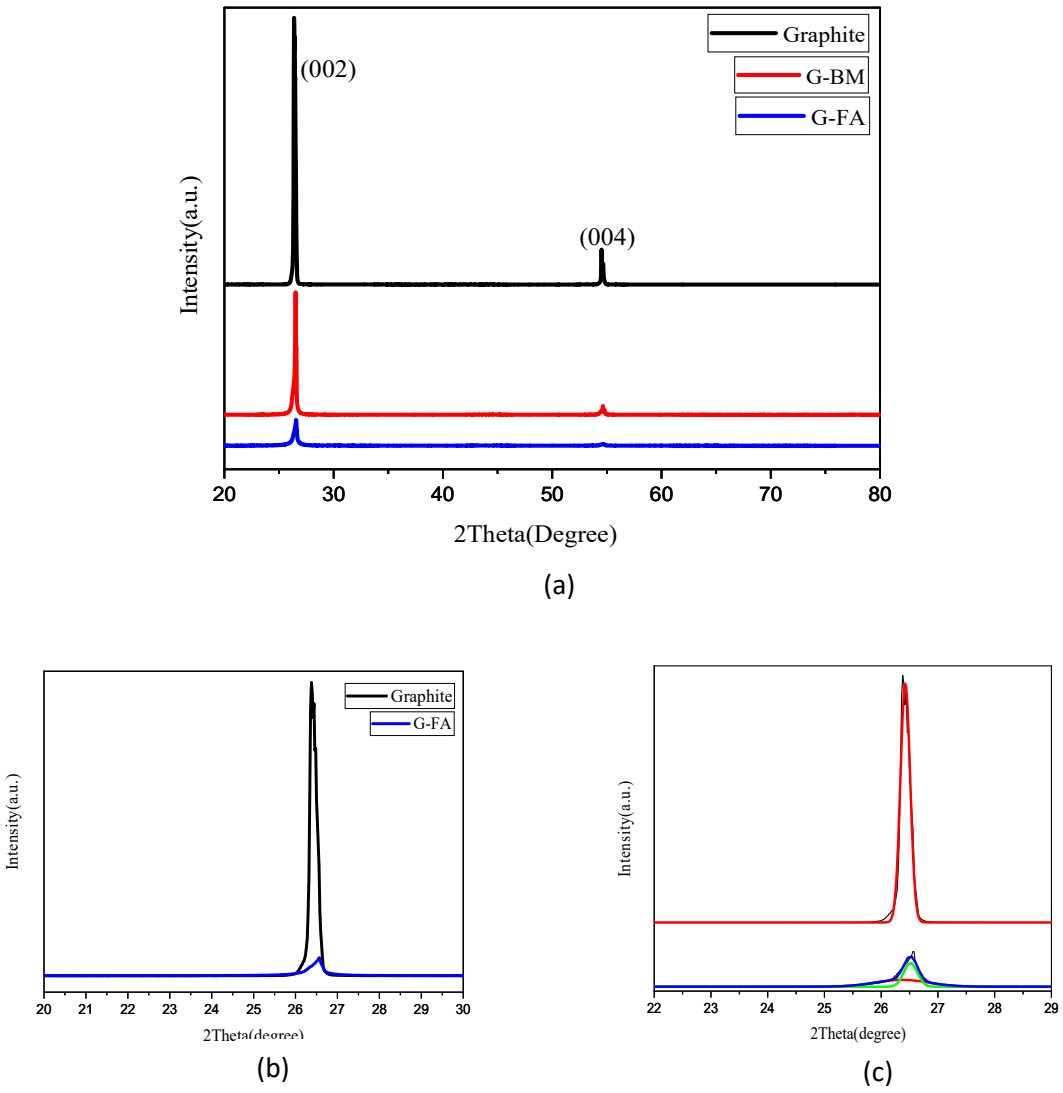

Figure 55. XRD patterns of a) pristine graphite, G-BM and G-FA b) Expansion of 002 peak of pristine graphite and G-FA c) Gaussian peak fitting of (b)

The XRD patterns of pristine graphite, G-BM and G-FA are shown in figure 9. As it is clear the obtained patterns from all samples exhibit two diffraction peaks at 26.40 and 54.5, which are attributed to (002) and (004) crystalline lamellae of the graphite [118,119]. For all of them the basal reflection peak is at 2θ=26.4 but different shape and broadness of the peaks, and with high difference in intensity. **Figure 55(a)** shows the intensity of graphite (002) is greater with a sharp and strong diffraction peak compared with that of graphene and it displays that the pristine graphite possessed a high quality and perfect crystalline structure. A dramatic decrease in the peak's

intensity of G-FA is caused by the decrease of the thickness of the graphite due to the breaking of inter-planar carbon within graphite structure during dry ball milling which has resulted in the exfoliation of the graphene sheets. The latter indicates that the D-A reaction does not change the characteristic crystalline structure of graphite considerably.

XRD results have been recently used to determine the thickness and layer numbers of graphene flakes [120]. The shape of the (002) reflection depends on the thickness of the graphite sample. Thinner graphite samples result in a broader peak with a maximum at lower diffraction angles due to the increased contribution of intercalated planes on the top/bottom of the graphitic flakes. [121,122] The application of the Scherrer equation [123] on the (002) diffraction line allows for an estimation of the average crystalline size (D) [122,124]:

$$D = \frac{K\lambda}{\beta \cos\theta}$$

where K is the Scherrer constant, λ is the wavelength of light used for the diffraction (0.15406 nm), β is the "full width at half maximum" of the sharp peaks (FWHM) in radians, and θ is Bragg diffraction angle. The Scherrer constant (K) in the above formula accounts for the shape of the particle and is generally taken to have the value 0.9 for spherical crystals with cubic unit cells.

Figure 55(b) indicates a symmetric 002 peak for pristine graphite but an asymmetric one for G-FA. After the gaussian peak fitting in **Figure 55(c)**, it is obviously clear that there are two distinguishable peaks in G-FA (002). In one peak, 2θ shifted to the left in comparison with the gaussian peak fitting of graphite. 2θ for the pristine graphite after the peak fitting is 26.42 degrees while this number for the G-FA sample is detected as 26.36 and 26.51 degrees. According to Bragg´s law, the distance between the graphene layers in the G-FA is higher than in the graphite flakes. Therefore, after calculating the thickness of the samples (D), the thickness of the lower 2θ in G-FA, has been turned from 40.57 nm to 7.45nm. This evidence can be interpreted as a good indicator for the exfoliation of graphite due to the ball milling process integrated with the functionalization of graphite. Referring also to other analytical measurements like Raman spectroscopy, it can determine that different locations on the graphene sheets have different functionalization degrees and thicknesses at the edge (7.45nm) which is much lower compared to the surface (29.5nm). **Table 12** shows the calculated FWHM and the crystalline size of the pristine graphite and functionalized graphene (G-FA). According to the data in table 1, the first fitted peak in the G-FA with 1.095 degree of FWHM can be interpreted as lower thickness at the edges of the

graphene sheets and the second fitted peak with 0.277 degree of FWHM indicated compressed layers mostly on the surfaces, although these data showed lower thicknesses on the surfaces after ball milling compared to the pristine graphite with 0.201 degree of FWHM and 40.57 nm thickness. On the other hand, due to further destruction of the crystal structure of G-FA due to the D-A reaction, the diffraction peak of G-FA was weaker and broader than that of G-BM.

	Pristine graphite	G-FA	
2θ (degree)	26.42	26.36	26.51
FWHM (degree)	0.201	1.095	0.277
D (nm)	40.57	7.45	29.5

Table 12. Parameters and calculation the thickness (D) of pristine graphite and G-FA according to Scherrer equation after the Gaussian peak fitting. K and λ are 0.9 and 0.15406 nm respectively

3.2.6.4. XPS

X-ray photoelectron spectroscopy (XPS) is the most widely used surface analysis technique to provide both quantitative atomic concentration and chemical state information of the detected elements. G-FA and pristine graphite were also examined by high-resolution XPS. As it is shown in **Figure 56(a)**, the pristine graphite flakes exhibit two prominent peaks for carbon and oxygen, while the G-FA shows a nitrogen peak too. This peak for nitrogen appears at 399.7 eV and displays the grafting of the primary amine to the graphene sheets and confirms a D-A functionalization of graphite. On the other hand, the amount of Oxygen increased in the G-FA sample from 1.5% to 6.4% due to attaching furfuryl amine function to the graphite. So, the sharp changes are mainly attributed to higher oxygen content and the appearance of nitrogen peak in the G-FA. Moreover, detailed information of C1s regions can be detected to confirm the change of the chemical structure.

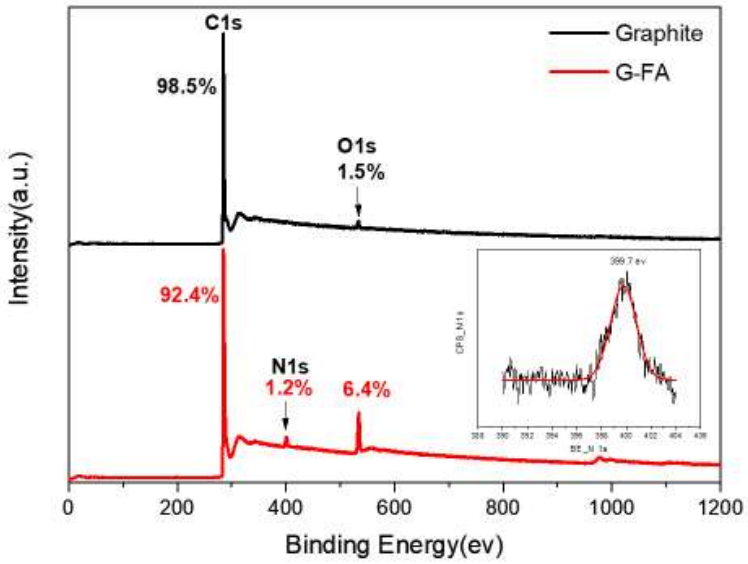

(a)

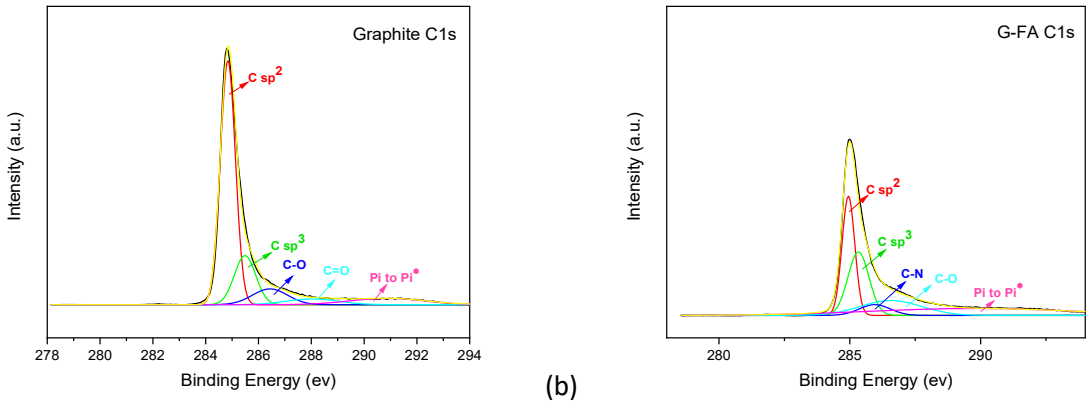

(b)

Figure 56, a) Survey of XPS of pristine graphite and G-FA

b) High resolution C1s after Gauss fitting

In **Figure 56(b)**, the black lines are raw data curves for the pristine graphite and the G-FA, while the other colored lines are gauss fitted ones analyzed by Origin, which is finalized in **Table 13**. As it is clearly seen, the ratio of the sp^3/sp^2 carbon in the G-FA is higher than in the pristine graphite, and a new peak assigned to a C-N bond appeared at 285.95 (eV), which confirms the existence of a carbon-nitrogen bond in the G-FA. Also, peaks at 286.43 (eV) in graphite and 286.57 (eV) in G-FA are attributed to C-O and C-O-C bonds which exhibit an increase from 5% in graphite to 16.47 in G-

FA. All these facts are in good agreement with other analytical data and confirm the successful D-A functionalization of graphene.

Pristine Graphite		G-FA	
Binding Energy (eV)	Area (%)	Binding Energy (eV)	Area (%)
284.84	61	284.94	27.56
285.49	17	285.33	24.27
286.43	9.3	285.95	6.0
288.05	5	286.57	16.47
290.86	7.7	289.73	25.70

Table 13. High resolution C1s, Gauss fitting by Origin. Colors in the table are attributes to the colors in the spectra (Figure 41b)

3.2.6.5. Contact angle

When an interface exists between a liquid and a solid, the angle between the surface of the liquid and the outline of the contact surface is described as the contact angle θ (lower case theta). The contact angle (wetting angle) is a measure of the wettability of a solid by a liquid. Samples were examined by investigation of the interactions between water and two samples (G-BM and G-FA) surface. Samples had been prepared by drop-casting on a silicon wafer. When the binding energies between water are less than the associated adsorption energies on the material surface, the water molecules tend to spread out on the material surface to form a thin liquid film, and the material surface displays hydrophilic properties and concludes a contact angle less than 90°. On the contrary, when the associated adsorption energies between water molecules and the material surface are less than the binding energies between water, the water molecules are inclined to agglomerate on the material surface to form spherical droplets, and the material surface displays a hydrophobic nature and yields a contact angle more than 90°. [125]

As shown in **Figure 57**, the contact angle for G-BM is around 105° compared to around 32° for G-FA. Based on these results, it can be determined that due to the attachment of amine functional groups to the graphene sheets, the interaction between water with G-FA is much higher than of graphite and G-FA exhibits a high wettability and higher hydrophilic properties than the pristine graphite.

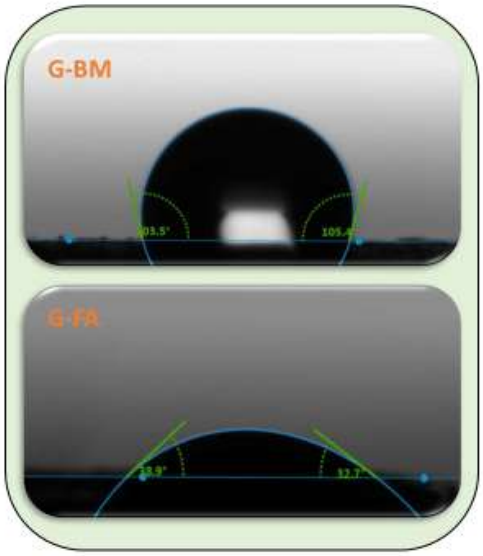

Figure 57. Contact angle of G-BM and G-FA with water on silicon wafer

3.2.6.6. SEM and EDX

The morphologies of graphite and G-MA were compared using SEM. As shown in **Figure 58(a)**, the pristine graphite, the left image, has smooth surfaces while G-FA displays a coarse surface (right image). The grain size is smaller in G-FA. SEM images from the edges of the two samples clearly show the layer-like morphology with little aggregation at the edge of the graphene sheets of G-FA **Figure 58(b)** right. On the contrary, the edges of the graphite obviously show firmly stacked layers figure12b left. On the other hand, as shown in **Figure 58(c)**, exfoliated edges of G-FA are coarser than the edges located in the pristine graphite. According to these distinguishable differences, effective functionalization onto the surface and mostly at the edges of the graphene sheets occurred in G-FA. The left and right images in **Figure 58(c)** are from G-FA samples but with different scales to show the edge location better.

Energy Dispersive X-Ray Analysis (EDX) was performed to identify the elemental composition of the samples. Spectra data of G-BM and G-FA were measured at a voltage of 5 KV. **Table 14** has been ordered by atom percentages for the two mentioned samples. As it is clear, due to the D-A reaction on G-FA, the nitrogen and oxygen content increased compared to G-BM.

Sample	Carbon	Nitrogen	Oxygen
G-FA	86.50	4.79	8.71
G-BM	97.45	0.00	2.55

Table 14. EDX data for G-BM and G-FA based on atom%

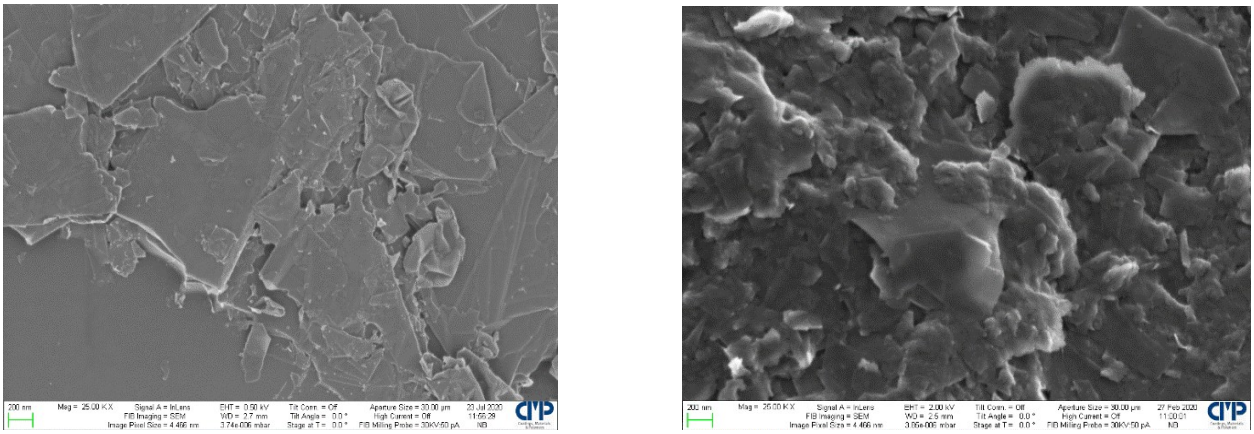

(a)

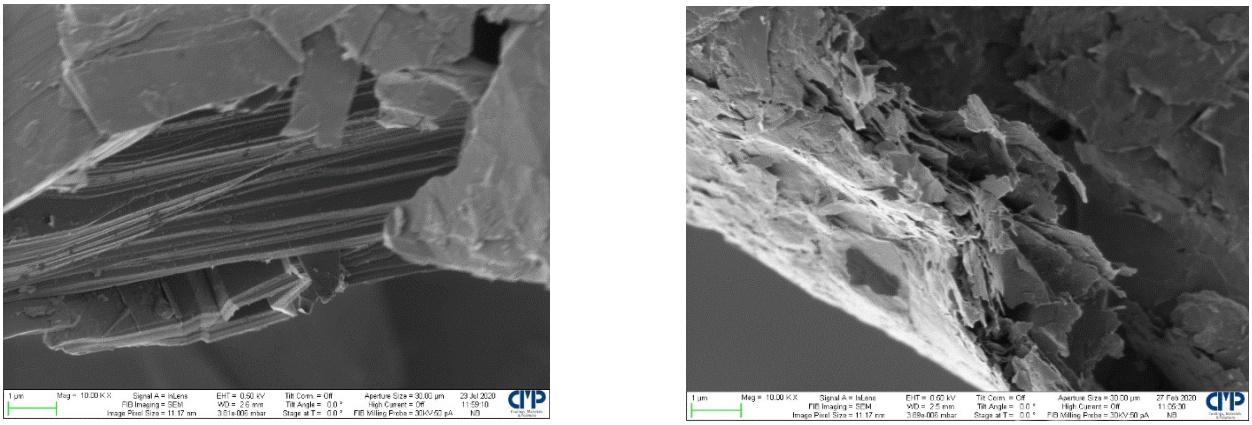

(b)

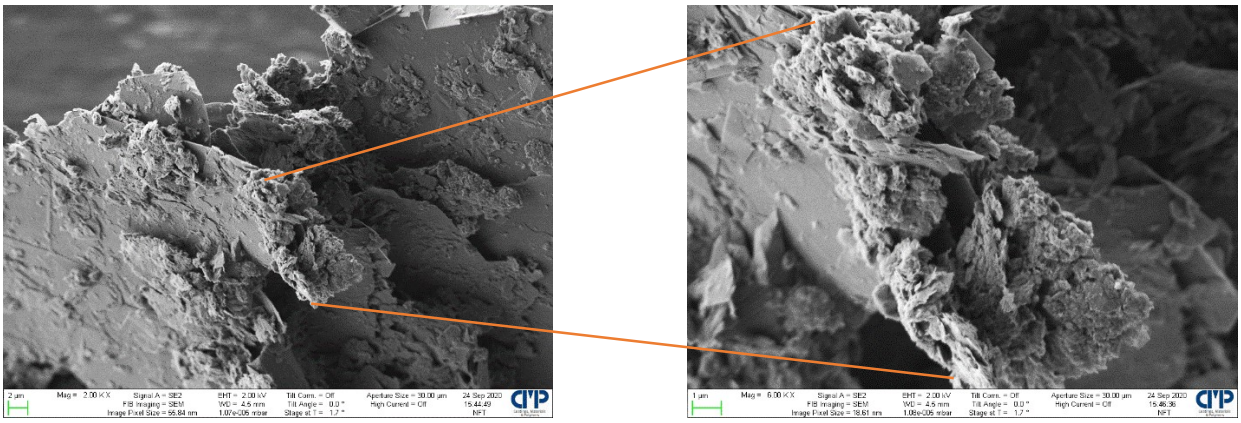

(c)

Figure 58. SEM images a) on the surface of pristine graphite(left) and G-FA (right) b) at the edge of graphite(left) and G-FA (right) c) scaling up the edge of G-FA sample

3.2.6.7. AFM

Atomic force microscopy (AFM) is one of the most powerful tools for the study of graphene film thickness and surface features. Single-layer graphene is ~0.34 nm thick and this value adds up accordingly for multilayer graphene. However, due to the surface roughness of graphene, changing cohesive forces between graphene and supporting substrates and variation introduced by AFM, graphene thickness and number of layers are difficult to determine the number of layers precisely. Sometimes the graphene surface absorbs water vapors, and a very thin layer of water is formed on graphene films. Sometimes different contamination stays on the surface of the graphene films. Hence, it is difficult to determine the actual thickness of the graphene films. Often, the single-layer graphene thickness is recorded between 0.4 nm and 1.0 nm, instead of 0.34 nm. Yao et al. demonstrated the use of histograms and found that the flake thicknesses of 1, 2, and 4-layer graphene were 1.5, 1.9, and 2.73 nm, respectively, by AFM. [126]

As shown in **Figure 59** the average thickness of particles in the G-FA sample is around 4 nm (**Figure 59(a, b)**), while this number is for graphite flakes around 40 nm (**Figure 59(c)**). It can be estimated that G-FA has less than 10 layers. These results are comparable with the results from the XRD to some extent. This is another suitable indicator for the low thickness and the low number of layers of G-FA due to the successful ball milling and functionalization process.

G-FA:

(a)

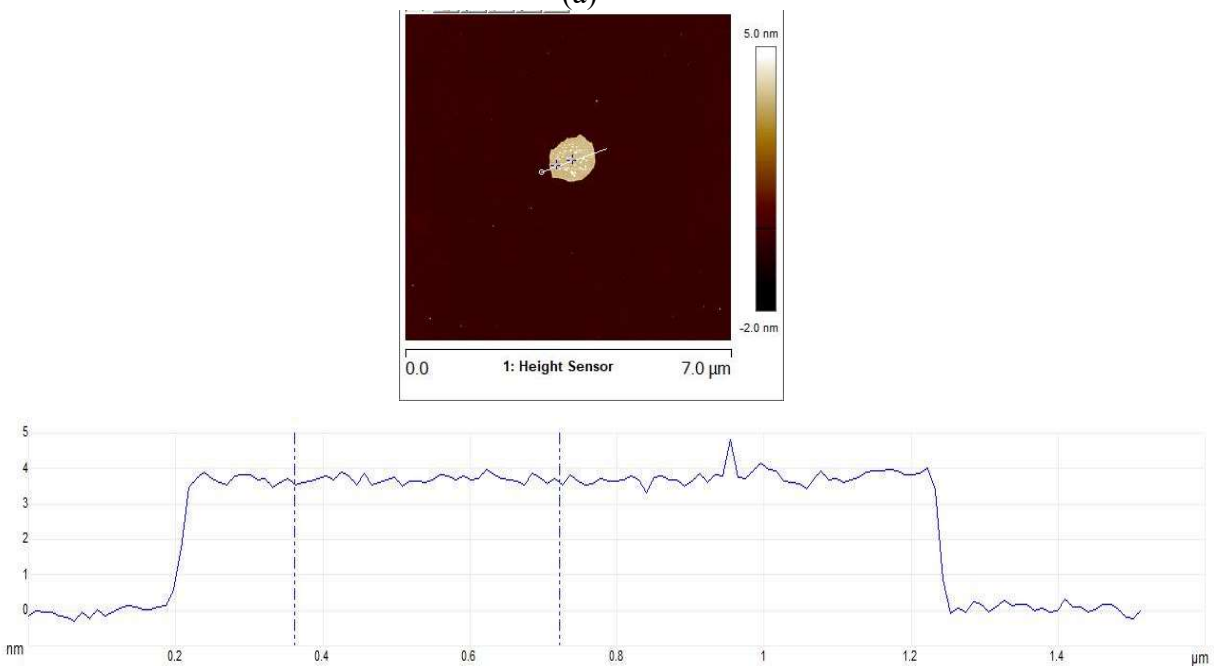
5.0 nm
-2.0 nm
0.0
1: Height Sensor
7.0 µm
nm
µm

(b)

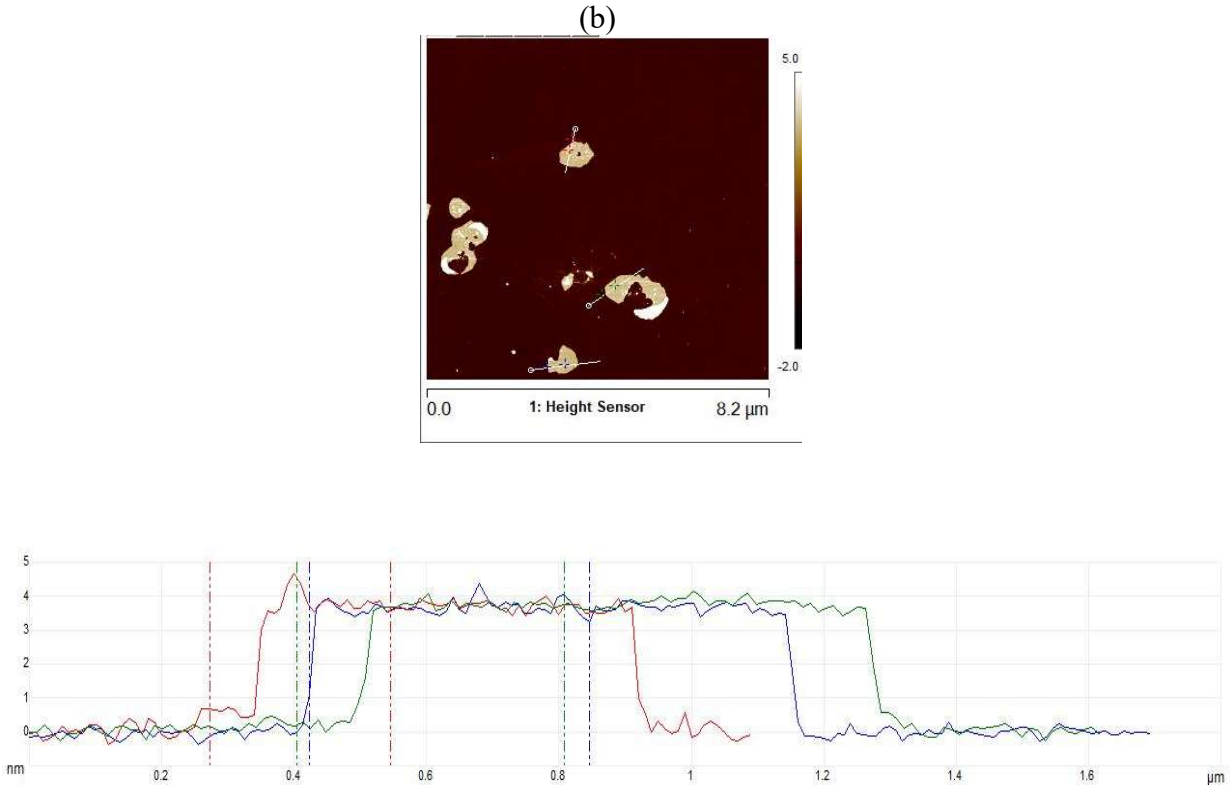
5.0
-2.0
0.0
1: Height Sensor
8.2 µm
nm
µm

Graphite:

(c)

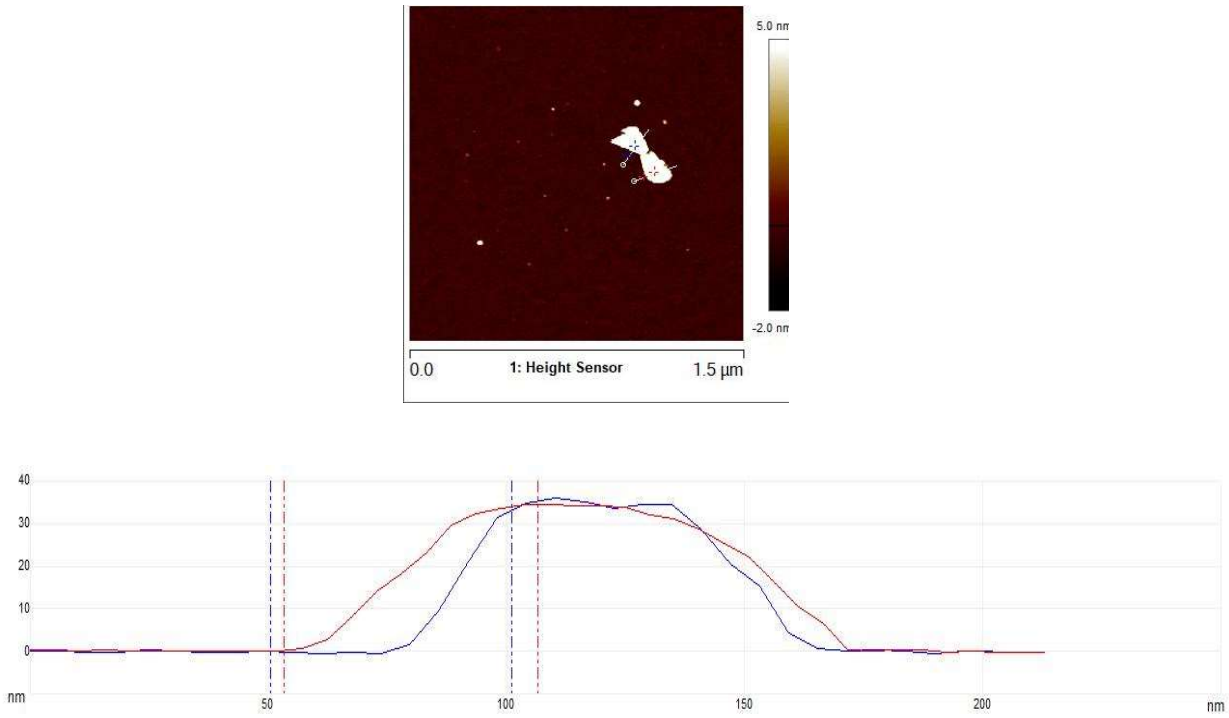

Figure 59. AFM images and graphs for a) G-FA, Scale: 7 micrometer b) G-FA, Scale: 8.2 micrometer c) Pristine graphite, Scale: 1.5 micrometer

3.2.7. Summary

Furfuryl amine-functionalized few-layered graphene was prepared successfully via a mechanochemical process by a [4+2] cycloaddition under solvent-free condition. By employing ball milling, active sites are merged mostly at the edge of the graphene sheets and make them prone to Diels-Alder click reaction (D-A) in the presence of a diene precursor. Consequently, one-pot grafting with furfuryl amine onto the graphene sheets, exfoliate pristine graphite resulting in functionalized few-layered graphene which is soluble in organic solvents. Thereafter, the cleavage of the bonds in the adduct can happen by exposure to an external stimulus like temperature, to initiate a retro Diel-Alder reaction. Various techniques were employed to reveal the confirmation of the functionalization, the location of the functional groups on the graphene sheets and also the thickness and layer numbers of the samples. According to all of the revealed evidence that reported here, furfuryl amine attached effectively mostly at the edges of the graphene sheets and caused the edges of the sample to lower the thickness compared to pristine graphite. The preparation of the presented material with this discussed approach will be beneficial for the synthesis of thermoreversible composite in the future by utilizing the presented retro-DA reaction.

Chapter 4 Inter and trans-disciplinary concepts

The quest for innovation in the scientific understanding of complex problems, marked by escalating levels of uncertainty, has led to a growing emphasis on addressing societal challenges and promoting sustainable solutions. The demands of the knowledge society further underscore the need for inter- and transdisciplinary research. [127]

Interdisciplinary and transdisciplinary research and teachings are influential approaches to solve complicated problems which require exchanging knowledge and experience among a diversity of disciplines with stakeholders, such as big societal challenges.[128] Therefore, this approach intends to create more socially robust knowledge and to make a bridge between society and science.[129]

4.1. Transdisciplinary research

The model of an Idealtypical transdisciplinary research (ISOE), reveals the idea of a transdiciplinary research strategy and addresses the problems in the society employing interdiciplinary collaboration between society and science.[130] To make a strong link between society and science, a diversity of knowledge and experiences has to be integrated due to obtain transdiciplinary results. This integration can be achieved by combining practical and scientific paths to solve the societal problems and producing new theoretical knowledge, respectively. (**Figure 60**)

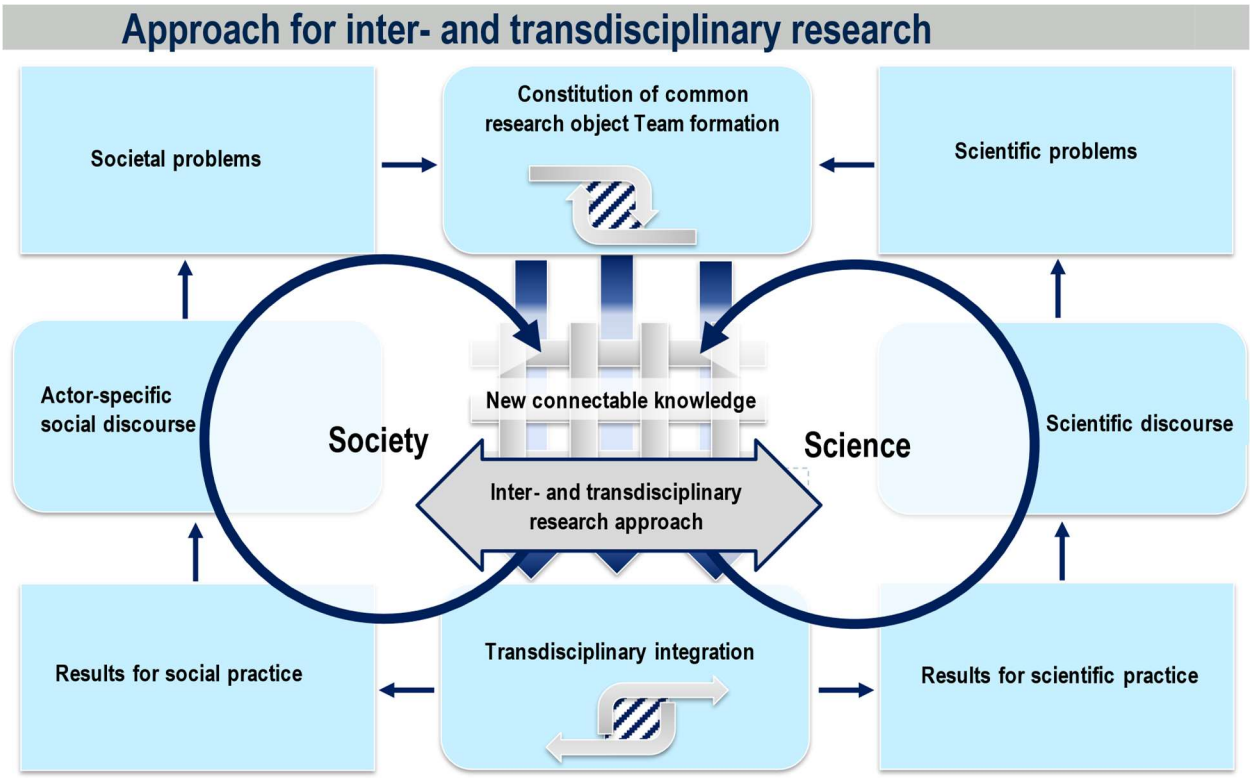

Figure 60. ISOE model of Transdisciplinary research [130]

4.2. FK-LEM

FKLEM is a research network of the Forschungskoleg" Light-Efficient-Mobile (FK-LEM) found in 2014 that was funded by the Ministry of Culture and Science of the State North Rhine-

Westphalia. FK LEM is a research initiative that tackles significant societal challenges, including resource efficiency, environmentally friendly mobility, climate protection, and applications in medical technology. The key strategy for addressing these challenges is the implementation of lightweight construction for mobile masses across various applications. Lightweight design plays a crucial role in reducing resource and energy consumption, and hybrid lightweight design, utilizing two or more different materials, is particularly promising.[131]

Hybrid design often involves combining isotropic materials (e.g., steel) with anisotropic materials (e.g., unidirectional fiber-reinforced plastics) to maximize the advantages of each material. Given economic considerations and the fact that stress exposures are typically inhomogeneous on components, cost-intensive high-strength materials are strategically used for localized, partial reinforcement. This approach optimizes both economic and technical aspects.

The FK LEM during the second research period 2019-2022 comprises 13 PhD candidate from diverse research areas such as mechanical engineering, chemistry, physics, and sociology to cooperated on the development of lightweight construction technology, with the focus on how light weight design can solve the problems of different areas in the society and technology users. This PhD approach as a chemistry part of FKLEM, was dealing with chemical recycling of CFRPs, the composite which is the most widely used material in light weight design engineering nowadays. Thus, in collaboration with other research groups of FKLEM, we could make a bridge between society and science based on sustainability point of view.

Through close collaboration in inter- and transdisciplinary projects, we addressed hybrid systems at various scales from macroscopic (sociology) to microscopic (engineering) and nanoscopic (chemistry, physics) problems. This holistic approach ensured the systematic development of sustainable solutions.

To maintain a continuous connection with society, the FK LEM engages in active discourse with partners from different societal fields. This interaction results in new research ideas and projects that stem from real social needs. The inclusion of society in the development process ensures that the research outcomes are applicable and specifically address social needs.

In addition to technological advancements, FKLEM emphasizes a broader perspective for graduate students. They learn to consider new technologies within the overall social context. The expansion of research activities at the intersection of social, gender, and technology-related questions acknowledges the interdependence of these factors. The reflection on social consequences is a central goal of FK LEM, aiming to establish a progressive think tank and prepare young PhD students for societal and industrial challenges in the development of social, economic, and ecological advancements.

Totally the goals of the FK-LEM were:

- Strengthening interdisciplinary and transdisciplinary research

- Training of specialists with a "focus on society

- Relevant social references of the developments

-The development and reinforcement of sustainable and responsible engineering (longer service life)

-Gender equality specific networks, in addition to gender, other diversity criteria such as ethnic origin, migration background, educational background, age, physical impairments or socio-economic status should be taken into account.

- The reflection of social consequences in society (to promote social acceptance of products.)

The structure of the case studies conducted at FK-LEM follows the model of a transdisciplinary research above, so that a brief clarification of the transdisciplinary profile serves to introduce the work of 3 research clusters, reuse and recycling, medical technology, and rescue cluster.[132]

In reuse and recycling cluster that this enclosed PhD topic (recycling of CFRPs composite) was one of the approaches in this cluster, we deal with the recycling and reuse potentials of different industrially used materials and products in an interdisciplinary way.[133]

4.2.1. Industry project

To establish the challenges of interdisciplinary and transdisciplinary work, we as reuse and recycle cluster, collaborated with an industrial partner.[134] For this purpose, the possible optimization potential from the sustainability point of view was shown on the basis of a bicycle stand (Turrix). The Turrix is already established on the market and is manufactured by injection moulding from a thermoplastic with glass fiber content. The material used is made from fossil raw materials that the disposal at the end of the life takes place via household waste, so it isnot reusable, just thermal recycling has been established. This project illustrates that by a small change in the choice of material content, a positive benefit for the environment can be obtained.

First, the actual properties of the material (glass fiber reinforced polypropylene) and the manufacturing process were recorded. Consequently, alternative materials were compared with each other in terms of sustainability and mechanical properties. Furthermore, the stress distribution and potential of light weight design were determined. Based on this information, suggestions for development and design optimization can be identified.

Hebie GmbH& Co. KGT was the industrial partner in this project. This company is a family-owned one with a long tradition and sustainability and responsibility are considered as the prerequisite for long-term success for them. The company is well-versed in steel, aluminum, and plastic processing. The product range includes accessories for bicycle operation. Bicycle stands are also one of their important products. Hebie addresses aspects of Corporate Social Responsibility (CSR).

In this company, the conventional version of the bicycle stand is made of a glass fiber-reinforced polypropylene with a fiber content of 30% and is consisting of three components: standing foot, stand and bracket (**Figure 61**)

Figure 61. Turrix (bicycle stand)

Innovation and sustainability are of great importance. Increasing mechanical properties along with increasing sustainable manufacturing and recycling process should be combined. So different kinds of materials have been suggested and tested. Composite materials were one of the material classes that has the potential to meet the requirements. Natural fibers and synthetic fibers in combination with different thermoplastic matrixes were considered and compared.

Among them, Wood-plastic composite (WPC), showed good results. WPC is the term that refers to any number of composites that contain wood (wood flour, wood fiber) and either thermoset or thermoplastic polymers. Fibers display higher mechanical properties such as strength and stiffness rather than flour. Also other additives like coupling agents, pigments, lubricants and etc. in small quantities are necessary for the processing and performance. Maleic anhydride grafted polypropylene is a common compatibilizer to improve the interfacial bonding of hydrophilic wood part and hydrophobic plastic part in wood-plastic composites.

The manufacturing was the task of mechanical engineers with the help of CAD calculation.

In the case of life cycle assessment (LCA), the variant of the Turrix and the original from Hebie were examined. Two materials that were used: PP GF30 original Turrix and PP WF30, WPC composite. Both materials use polypropylene as matrix. PP has good recycling properties, and it is suitable for recyclability issues. In WP, the glass fiber in original Turrix was replaced by wood

fibers which can be recycled. The CO_2 emissions that are used to produce the individual materials are shown in **Table 15**. (3)

Component	CO_2 (kg CO_2/kg m)
Wood fiber	1.8
Glass fiber	2.1
Polypropylene (PP)	1.9

Table 15. CO_2 emission of individual components [134]

Thus, CO_2 emissions caused by wood fibers are lower than glass fibers. The cooperation with Hebie has successfully indicated that previously used materials can be replaced by the counterpart that has a lower CO_2 balance. Polypropylene with 30% glass fiber-reinforced was replaced by a wood-plastic composite.

4.3. Sustainable and responsible engineering

The human population has experienced exponential growth, particularly intensifying over the last century, and surpassing planetary boundaries in recent decades. Beginning at 2 billion in 1927, the population has now exceeded 7.9 billion and is projected to reach approximately 9.7 billion by 2050, and 10.9 billion by 2100. [135]

As the global source and sink capacities are final, this type of evolution has increased pollution and reduced resource availability to critical values. The current state of sustainability is critical. Our civilization has breached four out of nine "planetary boundaries." The concentration of greenhouse gases (GHGs) is leading to climate change, along with issues such as species extinction, deforestation, and nitrogen and phosphorus pollution.[136] Additionally, the other four boundaries, including ocean acidification, freshwater use, atmospheric aerosol loading, and chemical pollution with radioactive and nanomaterials, are rapidly nearing their limits. These planetary boundaries serve as crucial references for environmental sustainability.[137]

Engineering has brought faster development across nations and most people, fostering more wealthy societies, and reducing existential problems. On the other hand, it has contributed to strong environmental impacts, climate change, species extinction, and increased pollution. We need technical solutions that will not cause long-term harm impacts on the environment, while enhancing human society's resilience and sustainability. New approaches are needed that require (among others) a new type of engineering—a sustainable engineering approach in the design and control of systems, processes, and products.[138]

Sustainable consumption and production aim, no waste, a circular economy, and resource efficiency are some concepts that we are faced with in this respect. besides the environmental pillar, we need to consider the social and economic pillars, equality, decent jobs, the engagement of all stakeholders, social responsibility, innovations, life cycle analysis, the cost–benefit approach, reporting to public and etc.

Sustainable engineering is the science of applying the principles of engineering and design in a manner that fosters positive social and economic development while minimizing environmental impact. Therefore, Engineers must consider 3 important pillars: environmental, economic and social issues in the design, production and operation of facilities. (**Figure 62**) [139]

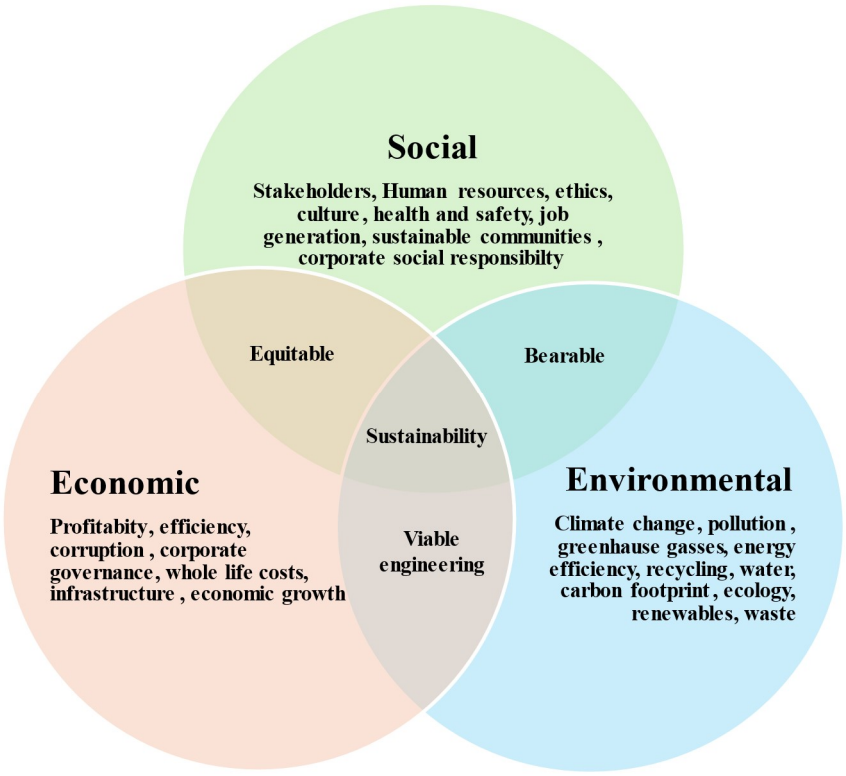

Figure 62. Sustainable engineering pillars [139]

• Economy: The creation of wealth and livelihoods

• Society: The elimination of poverty and improvement of quality of life

• Environment: The enhancement of natural resources for future generations

Consisting of these three interconnected pillars, sustainable development seeks to achieve economic development, social development, and environmental protection in a balanced manner.

Environmental protection, high economic performance and social accountability are inseparably connected, and recycling is one of the key actions we take in our aim to improve sustainability.

The abundant end-of-service-life carbon fiber reinforced plastic (CFRP) composites have become an increasingly significant environmental issue, making the key challenge to be how to increase the resource efficiency by turning waste into reusable materials.

These three interconnected pillars have driven the development of recycling routes for the increasing amount of carbon fiber reinforced polymer (CFRP) waste generated.

4.4. Survey analysis (Hyopt project)

At the Faculty of Mechanical Engineering, such as HyOpt – Optimierungsbasierte Entwicklung von Hybridwerkstoffen (NW-2-2-008a), a research team from the working group Technology and Diversity tried to consider light-weight design (Hybrid material) and also sustainable and responsible engineering into a survey and examine it from social environmental and economic aspects to find out which aspects and criteria and to some extant plays an important role for different groups in our society. So, a survey was prepared to assess these issues and to distinguish predominant criteria and properties which scientific or engineers, journalist, and most important group, customers, prefer (good design, CO_2 emission, sustainability issues or recyclable materials, price and etc. Which one has priority? To what extent and under what conditions do novel hybrid materials meet with acceptance or rejection? (Focus on the automotive industry) What role does "trust in nature" (bionics) and "trust in technology and engineering" play? What role do sustainability aspects play in the acceptance of materials? To some extent recyclability or sustainability is important in the customer's decision to buy an engineered product and on the other hand for engineers and scientist to meet the sustainable aspects of technology. what Scientifics predict regarding the use of CFRPs in different applications in the future. These assessments lead to make a close relationship between science and technology, society, and environment.

the Questionnaire was sent to two groups, experts and non-experts, in Dezember 2021 and the evaluation and analysis was performed in January and February 2022. (**Figure 63**)

QP6 Social acceptance:

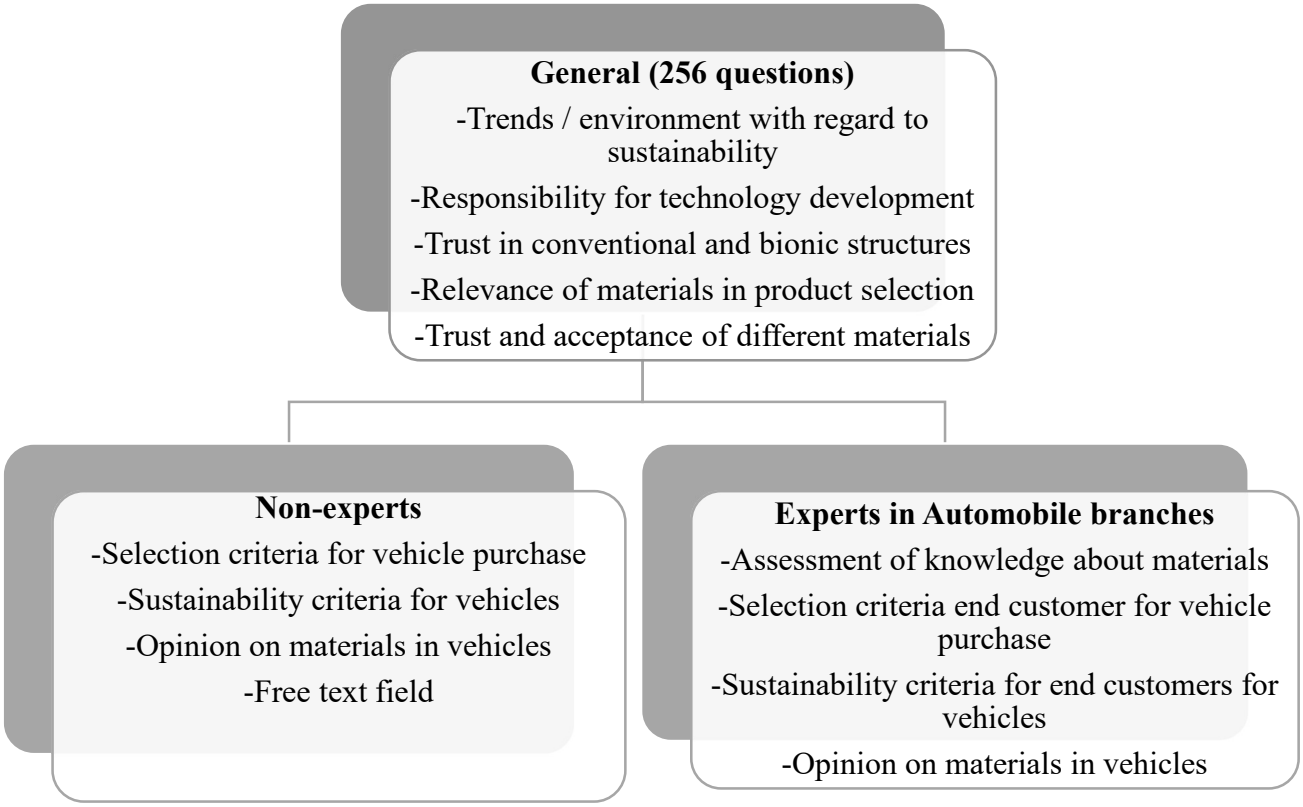

Figure 63. The Structure of the questionnaire

Trust and acceptance of materials:

Eight different materials were asked by these two groups, in terms of their safety and reliability in safety-relevant structures (bicycle frames, car doors, etc.):

-Steel

-Plastic

-Aluminum

-Magnesium

-Hybrid material

-Fiber reinforced

-Bio composites

-Wood

The following description of results is based on n=256 completed questionnaires of participants. In the case of safety and reliability, Steel was rated best (> 80 %). Fiber reinforced plastic and aluminum follow (74.2 % and 68.4 % respectively) Hybrid materials in 4th place (67.2 %), Plastics and wood were rated worst (39.1 % and 32.0 % respectively).

And in the case of sustainability, wood was rated the best (78.9%). This was followed by steel and bio composites (50.0% and 47.7% respectively). Hybrid materials (21.9%). Plastics and FRP were rated worst in terms of sustainability (16.4% and 12.5% respectively).

According to the responses to the question regarding the development of materials in the automobile industry over the next 10 years, it was evaluated that the development of hybrid materials, bio composites and fiber-reinforced plastics is rated very positively (> 60% at least increase in premium and sports vehicles) For hybrid materials, 50% of respondents forecast that their share in cars will increase in all vehicle classes For FRP, > 75% forecast at least increase in premium and sports vehicles.

Challenges for wider use of FRP and hybrid materials:

Increased costs and recyclability are seen as the biggest challenges and fiber reinforced plastic and hybrid materials were rated the same.

4.5. Summary

As a member of the Technology and Diversity research group, we developed inter- an transdisciplinary concepts to foster a strong link between our society and science to solve the problems by different activities, programs, and seminars. Sustainability and responsibility were the important concepts in this way that can be seen obviously in industrial cooperation. On the other hand, Hyopt project (optimization and development of hybrid materials) as part of Technik and diversity project, was dealing with the survey regarding the social acceptance of engineered materials and making this linkage between the academic and society stronger.

Chapter 5 Summary and conclusion

In the present doctoral thesis, two approaches have been developed. One is the recycling of CFRPs composite, and another one is functionalization of graphite by Diels-alder chemical reaction.

The first approach was recycling of Carbon Fiber Reinforced thermoset polymer made out of commercially available prepreg by utilizing two different catalysts. Evaluation of the efficiency of these two catalysts was determined and compared by different analytical and mechanical measurements. Loosing the dense structure of the cured system was the task of DMAc as a solvent to penetrate to the structure and pave the way for the catalyst to cleavage the chemical bonds. As the mentioned-results show, by using $Al(NO_3)_3.9H_2O$ as a lewis acid, the chemical bonds between C-N in the cured system were cleaved successfully at the mild condition without damaging the properties of the carbon fiber. The degradation degree was 100% which shows that recycled carbon fibers did not contain any residue of epoxy matrix. On the other degraded epoxy resulted from the recycling process was reused in a new curing system and the results show that by adding 5% of the degraded epoxy instead of the curing agent, the properties of the cured system stay relatively steady. This fact confirms that the cleavage of the bonds was between C-N and the degraded epoxy contains nitrogen in the structure which can act as a co-hardener in the system. Some other measurements confirmed this statement.

The used solvent was recycled several times and reused for the recycling process.

Another study was on graphite to gain the furfuryamine-functionalized multilayered graphene with the outlook of producing recyclable composite. This approach was facilitated by applying two different ball sizes to increase the interaction of the reactant and to create active sites on graphite. Thus, furfurylamine was successfully attached mostly at the edge of the graphite sheets. The results

from different measurements obviously demonstrated that the layers after the reaction are less than 10 layers and the thickness of the particle of functionalized graphite is around 4nm instead of 40nm for reference graphite. After the Diels-Alder reaction, the product was exposed to 150°C to make retro Diels-Alder. Solubility test and also TGA revealed that retro DA was accrued successfully.

Beside all the chemical approaches, being a member of Technik and diversity research group, opened a new horizon in terms of society, environmental and economic which are the three main pillars of sustainability. By conducting a survey, a linkage between society and science was built. Also FKLEM cooperation helped engineers effectively to experience new challenges. Every PhD from different research groups was gathering to implement new projects which create again a bridge between society and science. Recycle and reuse cluster as one of the clusters of FKLEM was in cooperating with industry to develop sustainable and responsible engineering by producing bicycle stand from WPC composite that shows positive impact on environment regarding recyclability.

Summing up, with the prospect of wide range application of CFRPs and increasing the amount of waste produced after the end of life of CFRPs, the author hopes that this proposed work may be useful for the future development of the recycling process.

Parts of this thesis were published in:

-Reversible functionalization and exfoliation of graphite by a Diels–Alder reaction with furfuryl amine, **Najmeh Filvan Torkaman**, Marina Kley, Wolfgang Bremser and Rene Wilhelm

RSC Adv., 2022, 12, 17249–17256, DOI: 10.1039/d2ra02566c

-Climate protection, resource efficiency, and sustainable engineering book (Transdisciplinary approaches to design and manufacturing technology)- Ilona Horwath, Swetlana Schweizer (eds.) (2023)

- Catalytic recycling of thermoset Carbon Fiber-Reinforced Polymers, ACS Sustainable Chem. Eng. 2024, 12, 7668−7682, **Najmeh Filvan Torkaman**, Wolfgang Bremser and Rene Wilhelm

References

(1) Composites Manufacturing: Materials, Product, and Process Engineering, CRC Press Taylor & Francis Group, DOI:10.1007/978-3-030-39062-4_20

(2) Davis, S.C., Diegel, S.W., Boundy, R.G., Moore, S., 2014. Vehicle Technologies Market Report

(3) Wu, J.W.; Posen, I.D.; MacLean, H.L. Trade-offs between vehicle fuel economy and performance: Evidence from heterogeneous firms in China. Energy Policy 2021, 156, 112445.

(4) Malick, P.K., Fiber-Reinforced Composites, Marcel Dekker, Inc., 1988, https://doi.org/10.3390/polym14214768),

(5) Ahmad, H., et al. A review of carbon fiber materials in automotive industry, *Materials Science and Engineering*, 971 (2020) 032011), doi:10.1088/1757- 899X/971/3/032011,

(6) Maier,A.; et al. Non-Destructive Thermography Analysis of Impact Damage on Large-Scale CFRP Automotive Parts, *Materials* 2014, 7, 413-429; doi:10.3390/ma7010413.

(7) Chalot, A.; Michel, L.; Ferrier, E. Experimental Study of External Bonded CFRP-Concrete Interface under Low Cycle Fatigue Loading. *Compos. Part B Eng.* 2019, 177, 107255.

(8) Lee, T.; Jeong, S.; Woo, U.; Choi, H.; Jung, D. Experimental Evaluation of Shape Memory Alloy Retrofitting Effect for Circular Concrete Column Using Ultrasonic Pulse Velocity. *Int. J. Concr. Struct. Mater.* 2023, 17, 13.

(9) Obaidat, Y.T.; Barham, W.; Obaidat, A.T.; Abuzakham, H. Improving the Shear Capacity of Recycled Aggregate Concrete Beams with NSM-CFRP Strip. *Pract. Period. Struct. Des. Constr.* 2023, *28*, 04023016.

(10) Yang, J.; Lu, S.; Zeng, J.J.; Wang, J.; Wang, Z. Durability of CFRP-Confined Seawater Sea-Sand Concrete (SSC) Columns under Wet-Dry Cycles in Seawater Environment. *Eng. Struct.* 2023, *282*, 115774.

(11) IOP Conf. Series: *Materials Science and Engineering* 971 (2020) 032011 IOP Publishing doi:10.1088/1757-899X/971/3/032011

(12) Jeong-Min L.; et al., Design of Lightweight CFRP Automotive Part as an Alternative for Steel Part by Thickness and Lay-Up Optimization, Materials 2019, 12, 2309; doi:10.3390/ma12142309

(13) Felice R.; et al. Marine Application of Fiber Reinforced Composites: A Review. *J. Mar. Sci. Eng.* 2020, 8, 26; doi:10.3390/jmse8010026

(14) Fratzl, P.; Weinkamer, R.; Nature's hierarchical materials, *Prog. Mater. Sci*. 52, 1263 (2007) https://doi.org/10.1016/j.ast.2018.06.020

(15) Mansour, A. et al. Investigating the compressive strength of CFRP prepreg scrap from aerospace industries, conference paper, March 2019 , doi:10.1109/ICASET.2019.8714519

(16) Corrine Ying Xuan C.; et al. Carbon fiber reinforced polymers for implantable medical devices, *Biomaterials* 271 (2021) 120719, https://doi.org/10.1016/

(17) Saringer, W.; bauer-Huhmann and Knosp, E.; Cranioplasty with Individual Carbon Fibre Reinforced Polymer (CFRP) Medical Grade Implants Based on CAD/CAM Technique; *Acta Neurochir* (2002) 144: 1193–1203 DOI 10.1007/s00701-002-0995-5

(18) Kim, W., Manufacture of antibacterial carbon fiber-reinforced composites (CFRP) using imine-based epoxy vitrimer for medical application); *Heliyon* 9 (2023) e16945.

(19) Carbon Fiber Composites in Wind Turbines | Nordex Energy GmbH | Dresden | July 15th, 2015),

(20) Ennis, B. Optimized Carbon Fiber for Wind Energy; Project and Market Overview, 2017, Composite world

(21) Jinho L. et al. Implicit force and position control to improve drilling quality in CFRP flexible robotic machining, *Journal of Manufacturing Processes* 68 (2021) 1123–1133.

(22) Slamani, M. et al. Issues and Challenges in Robotic Trimming of CFRP, 2015 12th *International Conference on Informatics in Control, Automation and Robotics (ICINCO)*, Colmar, France, 2015, pp. 400-405.

(23) Li Na, S. et al. The carbon fiber composites materials application in sport equipment, Advanced Materials Research, ISSN: 1662-8985, Vols. 341-342, pp 173-176 doi: 10.4028/www.scientific.net/AMR.341-342.173.

(24) Qi, S. the black revolution of sports equipment, Applied Mechanics and Matedoi: 10.4028/www.scientific.net0, pp 69-73 doi: 10.4028/www.scientific.net/AMM.440.69

(25) Himayat U., Dynamic bending behaviour of woven composites for sports products: Experiments and damage analysis *Materials and Design* 88 (2015) 149–156, http://dx.doi.org/10.1016/j.matdes.2015.08.147)

(26) Cruz, R.; Correia, L.; Cabral-Fonseca, S.; Sena-Cruz, J. Durability of Bond of EBR CFRP Laminates to Concrete under Real-Time Field Exposure and Laboratory Accelerated Ageing. *Constr. Build. Mater.* 2023, *377*, 131047.

(27) Bahl, O.P. et al., Carbon Fibers, ed. J.B. Donnet et al. (New York, Marcel Dekker, 1998), pp. 1-84

(28) Chung, D.L. Carbon Fiber Composites; Butterworth-Heinemann: Boston, MA, USA, 1994; pp. 3–65.

(29) Donnet, J.B.; Bansal, R.C. Carbon Fibers, 2nd ed.; Marcel Dekker: New York, NY, USA, 1990; pp. 1–145

(30) Observation of Distribution of π-Orbital-Oriented Domains in PAN- and Pitch-Based Carbon Fibers Using Scanning Transmission X-ray Microscopy, *Appl. Sci*. 2020, 10, 4836; doi:10.3390/app10144836

(31) Baker, A., Dutton, S. and Kelly, D., 2004, 'Composite Materials for Aerospace Structures', Second Edition, American Institute of Aeronautics and Astronautics, Inc., Reston, Virginia.

(32) Brent Strong, A. "Thermoplastic Composites", *Fundamentals of Composites Manufacturing: Materials, Methods, and Applications*, Society of Manufacturing Engineers, 2008.

(33) Jin, Z. Current status of carbon fibre and carbon fibre composites recycling, *Composites Part B: Engineering* Volume 193, 15 July 2020, 108053, DOI: https://doi.org/10.1016/j.compositesb.2020.108053

(34) Vita A, Castorani V, Germani M, Marconi M. Comparative life cycle assessment of lowpressure RTM, compression RTM and high-pressure RTM manufacturing processes to produce CFRP car hoods. Procedia CIRP. 2019; 80:352-7.

(35) Sozer, E. M., Simacek, P. and Advani, S. G. "Manufacturing Techniques for Polymer Matrix Composites (PMCs)," in Manufacturing Techniques for Polymer Matrix Composites (PMCs), Elsevier, 2012, pp. 245–309.

(36) Cantwell, W. "Composite Forming Techniques." [Online]. Available: https://www.flickr.com/photos/core-materials/albums/72157627122081332. [Accessed: 06-Aug-2015].

(37) Gurit, "Gurit's Guide to Composites.

(38) Creasy, T. "Manufacturing Techniques for Polymer Matrix Composites (PMCs)," in Manufacturing Techniques for Polymer Matrix Composites (PMCs), Elsevier, 2012, pp. 123–138.

(39) Campbell, F. C. Structural Composite Materials. ASM International, 2010.

(40) Lin G. 2016 Global Carbon Fibre Composites Market Report. ATA Carbon Fiber Tech. Guangzhou Co., Ltd.; 2016.

(41) Melendi-Espina S., Morris C., Turner T., Pickering S. Recycling of carbon fibre composites. In: Proceedings of Carbon 2016. Penn State University, State College, United States, Conference, Conference 2016.

(42) Pickering SJ., Turner TA. Research and development in support of carbon fibre recycling in: Proceedings of CAMX2014-Composites and Advanced Materials Expo: Combined Strength Unsurpassed Innovation. Orlando, FL, USA, Conference, Conference 2014.

(43) Lin G. Global Carbon Fiber Composite Market Report. Guangzhou Saiao Carbon Fibre Technology Pty Ltd.; 2016.

(44) Melendi-Espina S., Morris C., Turner T., Pickering S. Recycling of carbon fibre composites. In: Proceedings of Carbon Penn State University, Conference, Conference 2016

(45) Carbon Fiber Reinforced Plastic (CFRP) Market, Global Opportunity Analysis and Industry Forecast, 2021–2030, 2022, Pages: 380.

(46) Wang, S.; Xing, X.; Zhang, X.; Wang, X.; Jing, X. Room-temperature fully recyclable carbon fiber reinforced phenolic composites through dynamic covalent boronic ester bonds. *J. Mater. Chem. A.* 2018, 6(23), 10868-78.

(47) Markets and Markets. Carbon fiber market by raw material (PAN, Pitch, Rayon), fibre type (virgin, recycled), product type, modulus, application (composite, non-composite), end-use industry (A & D, automotive, wind energy), and region - global forecast to 2029. Research and Markets; 2019.

(48) Lin, G. Global Carbon Fibre Composites Market Report. ATA Carbon Fiber Tech. Guangzhou Co., Ltd.; 2016.

(49) Zhang, J.; Chevali, V.; Wang, H.; Wang, C. Current status of carbon fibre and carbon fibre composites recycling, *Compos. B: Eng*. 2020, 193, 108053.

(50) Gopalraj, Sankar K., Karki, Timo. A review on the recycling of waste carbon fbre/glass fibre-reinforced composites: fiber recovery, properties and life-cycle analysis, *Applied Sciences*, 2020, 2, 433 101.

(51) Pickering, S.J. Recycling technologies for thermoset composite materials—current status, Composites Part A, 2006, 37(8), 1206 – 1215

(52) Pimenta, Soraia, Pinho, Silvestre T. Recycling carbon fiber reinforced polymer s for structural applications, Waste Management, 2011, 31, 378 – 392

(53) Meyer et al. CFRP-Recycling Following a Pyrolysis Route: Process Optimization and Potentials, *Journal of Composite Materials*, 2009, 43(9). 1121 – 1132

(54) Yip et al., Characterisation of carbon fibres recycled from scrap composites using fluidised bed process, *Plastics Rubber and Composites*, 2002, 31(6), 278 – 282

(55) Obunai, K. et al., Carbon fiber extraction from waste CFRP by microwave irradiation, *Composites Part A*, 2015, 78, 160 - 165

(56) Pickering, S.J. Recycling technologies for thermoset composites materials, *Composites Part A*, 2006, 37(8), 1206 – 1215.

(57) Meyer et al. CFRP-Recycling Following a Pyrolysis Route: Process Optimization and Potentials, *Journal of Composite Materials*, 2009, 43(9). 1121 – 1132.

(58) Hernanz et al., Chemical recycling of carbon fibre reinforced composites in nearcritical and supercritical water, *Composites Part A*, 2008, 39(3), 454 – 461

(59) Pinero-Hernanz et al., Chemical recycling of carbon fibre composites using alcohols under subcritical and supercritical conditions, *Journal of Supercritical Fluids*, 2008, 46, 83 – 92

(60) Okajima et al., Chemical recycling of carbon fiber reinforced plastic using supercritical methanol, *Journal of Supercritical Fluids*, 2014, 68 – 76

(61) Cheng et al., Degradation of carbon fiber-reinforced polymer using supercritical fluids, Fibers and Polymers, 2017, 18, 795 – 805

(62) Liu et al., Recycling of carbon/epoxy composites, *Journal of Applied Polymer Science*, 2004, 94(5), 1912 – 1916

(63) Li et al., A promising strategy for chemical recycling of carbon fiber/thermoset composites: self-accelerating decomposition in a mild oxidative system, *Green Chem*., 2012, 14, 3260 - 3263

(64) Xu et al., Composites Science and Technology, 2013, 82, 54 – 59

(65) Yuqi, W. et al. Chemical recycling of carbon fiber reinforced epoxy resin composites via selective cleavage of carbon-nitrogen bond, *ACS Sustainable Chem. Eng*. 2015, 3, 3332−3337, DOI: 10.1021/acssuschemeng.5b00949

(66) T. Liu et al. Mild chemical recycling of aerospace fiber/epoxy composite wastes and utilization of the decomposed resin, Polymer Degradation and Stability 139 (2017) 20-27.

(67) Deng, T.; Ying L.; Xiaojing C.; Yongxing Y.; Shiyu J.; Yingxiong W.; Chunxiang L.; Debao L., Rong C. and Xianglin H., Cleavage of C–N bonds in carbon fiber/epoxy resin composites *Green Chem.*, 2015,17, 2141-2145.

(68) Palmer, J., Savage, L., Ghita, O.R., Evans, K.E., 2010. Sheet moulding compound (SMC) from carbon fibre recyclate. Compos. Part A *Appl. Sci. Manuf*. 41 (9), 1232e1237

(69) Li, Z.; Xing, M.; Zhao, L.; Li, Z.; Wang, Y. Recovery of carbon fiber-reinforced polymer waste using dimethylacetamide base on the resin swelling principle. *Front. Chem.* 2022, 10, 1050827.

(70) Montes-Moran, M. A.; Young, R. J. Raman spectroscopy study of HM carbon fibers: effect of plasma treatment on the interfacial properties of single fiber/epoxy composites – Part I: Fibre characterization. *Carbon*. 2002, 40 (6), 845–55.

(71) Malard, L.; Pimenta, M.; Dresselhaus, G.; and Dresselhaus, M. Raman spectroscopy in graphene. *Phys. Rep.* 2009, 473, 51–87.

(72) Ma, L.; Meng, L.; Wang, Y.; Wu, G.; Fan, D.; Yu, J.; Qi, M. and Huang, Y. Interfacial properties and impact toughness of dendritic hexamethylenetetramine functionalized carbon fiber with varying chain lengths. *RSC Adv.* 2014, 4, 39156–39166.

(73) Filik, J.; May, P.W.; Pearce, S. R. J.; Wild, R.K.; Hallam, K. R. XPS and laser Raman analysis of hydrogenated amorphous carbon films, *Diamond Relat. Mater.* 2003, 12(3–7), 974–978.

(74) Lee, S. M.; Lee, S. H.; Roh, J. S. Analysis of Activation Process of Carbon Black Based on Structural Parameters Obtained by XRD Analysis. *Crystals*. 2021, 11, 153.

(75) Kang, D. S.; Lee, S. M.; Lee, S. H.; Roh, J. S. X-ray diffraction analysis of the crystallinity of phenolic resin-derived carbon as a function of the heating rate during the carbonization process. *Carbon Lett.* 2018, 27(1), 108–111.

(76) Jiang, G.; Pickering, S. J. Structure–property relationship of recycled carbon fibers revealed by pyrolysis recycling process. *J. Mater. Sci.* 2016, 51, 1949–1958.

(77) Novoselov, K.S. Geim, A.K. Morozov, S.V., Jiang, D., Zhang, Y., Dubonos, S.V. , Grigorieva, I.V. , & Firsov, A.A. Electric Field Effect in Atomically Thin Carbon Films. Science, 306 (2004) 666-669. https://doi.org/10.1126/science.1102896

(78) Lee C., Wei, X., Kysar, J. W. & Hone, J. Measurement of the Elastic Properties and Intrinsic Strength of Monolayer Graphene *Science*, 321 (2008) 385. https://doi.org/10.1126/science.1157996

(79) Zhu, Y. Murali, S. Cai, W. Li, X. Suk, J. W. Potts, J. R. & Ruoff, R. S., Graphene and Graphene Oxide: Synthesis, Properties, and Applications, *Adv Mater*, 22 (2010) 3906. https://doi.org/10.1002/adma.201001068

(80) Moser, J. Barreiro, A.& Bachtold, A. Current-induced cleaning of graphene, *Appl Phys Lett*, 91 (2007) 163513. https://doi.org/10.1063/1.2789673

(81) Geim, A. K. & Novoselov, K. S. Nature Mater, The rise of graphene, 6 (2007) 183. https://doi.org/10.1038/nmat1849.

(82) Novoselov, K. S. Geim, A. K. Morozov, S. V. Jiang, D. Katsnelson, M. I. Grigorieva, I.V. Dubonos, S. V. & Firsov, A. A. Two-dimensional gas of massless Dirac fermions in graphene. *Nature*, 438 (2005), 197-200. https://doi.org/10.1038/nature04233

(83) Zhang, Y. Tan, Y.W. Stormer, H.L. & Kim, P. Experimental observation of the quantum Hall effect and Berry's phase in graphene. *Nature*, 438 (2005), 201-204. https://doi.org/10.1038/nature04235

(84) Balandin, A. A. Ghosh, S. Bao, W. Calizo, I. Teweldebrhan, D. Miao, F. and Lau, C. N. Superior Thermal Conductivity of Single-Layer Graphene, *Nano Letters*, 8(3) (2008) 902-907. https://doi.org/10.1021/nl0731872

(85) Yan, L. Zheng, YB Zhao, F. et al. Chemistry and physics of a single atomic layer: strategies and challenges for functionalization of graphene and graphene-based materials, *Chem. Soc. Rev*. 41(1) (2012) 97–114. https://doi.org/10.1039/c1cs15193b

(86) Sarkar, S. Bekyarova, E. Niyogi, S. Haddon, RC., Diels-Alder chemistry of graphite and graphene: graphene as diene and dienophile, *J. Am. Chem. Soc*. 133(10) (2011) 3324–3327. https://doi.org/10.1021/ja200118b

(87) Sarkar, S. Bekyarova, E. Haddon, RC. Chemistry at the Dirac point: Diels–Alder reactivity of graphene. *Acc. Chem. Res*. 45(4) (2012) 673–82. https://doi.org/10.1021/ar200302g

(88) Nicolau, K.C. Snyder, S.A. Montagnon, T. and Vassilikogiannakis, G. The Diels-Alder Reaction in Total Synthesis. Angewandte Chemie International Edition, 41(10) (2002) 1668–1698, https://doi.org/10.1002/1521-3773(20020517)41:10<1668: aid-anie1668>3.0.co;2-z

(89) Carruthers, W. and Coldham, I. in Cycloaddition Reactions in Organic Synthesis, Cambridge University Press, Cambridge, UK, 2004.

(90) Fringuelli, F. Taticchi, A. in The Diels–Alder Reaction: Selected Practical Methods, John Wiley & Sons, Chichester, UK 2002.

(91) Carreira, E.M. and Kvaerno, L. in Classics in Stereoselective Synthesis, Wiley-VCH, Weinheim, Germany, 2009.

(92) Santanu, S. Elena, B. and Haddon, R. C. Accounts of Chemical Research, Chemistry at the Dirac Point: Diels-Alder Reactivity of Graphene, 45 (2012) 673. https://doi.org/10.1021/ar200302g

(93) Willocq, B. Lemaur, V. Garah, M. El Ciesielski, A. Samori, P. Raquez, J. M. Dubois, P., and Cornil, J. The role of curvature in Diels–Alder functionalization of carbon-based materials, *Chem. Commun*. (Camb), 52 (2016) 7608-7611. https://doi.org/10.1039/C6CC01427E

(94) Yuan, J. Chen, G. Weng, W.and Xu, Y. One-step functionalization of graphene with cyclopentadienyl-capped macromolecules *via* Diels–Alder "click" chemistry, *Journal of Materials Chemistry*, 2012, 22 (2012) 7929. https://doi.org/10.1039/C2JM16433G

(95) Zydziak, N. Yameen, B. and Barner-Kowollik, C. Diels–Alder reactions for carbon material synthesis and surface functionalization, Polymer Chemistry, 4 (2013) 4072. https://doi.org/10.1039/c3py00232b

(96) Li, J. Li, M. Zhou, L. L. Lang, S. Y. Lu, H. Y. Wang, D. Chen, C. F. and Wan, L. J. Click and Patterned Functionalization of Graphene by Diels–Alder Reaction, *J. Am. Chem. Soc*., 138 (2016) 7448-7451. https://doi.org/10.1021/jacs.6b02209

(97) Denis, P. A. Chemical Physics Letters, Diels-Alder reactions onto fluorinated and hydrogenated graphene, 684 (2017) 79-85. https://doi.org/10.1016/j.cplett.2017.06.034

(98) Denis, P. A. Organic Chemistry of Graphene: The Diels-Alder Reaction. Chemistry - A European Journal, 19(46) (2013)15719-15725. https://doi.org/10.1002/chem.201302622

(99) Loh, K. P. Bao, Q. Ang, P.K. and Yang, J. The chemistry of graphene, *J. Mater. Chem.* 20 (2010) 2277-2289. https://doi.org/10.1039/B920539J

(100) Jiang, D. E. Sumpter, B. G. and Dai, S. Unique chemical reactivity of a graphene nanoribbon's zigzag edge, *J. Chem. Phys*. 126 (2007) 134701. https://doi.org/10.1063/1.2715558

(101) Wassmann, T. Seitsonen, A. P. Saitta, A.M. Lazzeri, M. and Mauri, F. Clar's Theory, π-Electron Distribution, and Geometry of Graphene Nanoribbons *J. Am. Chem. Soc*., 132 (2010) 3440-3451. https://doi.org/10.1021/ja909234y.

(102) Jie Z., Wenyuan W., Hua P., Jiangtao Q., Encai O., Weijian X., Water-soluble graphene dispersion functionalized by Diels–Alder cycloaddition reaction *J. IRAN CHEM. SOC*. (2017) 14:89–93

(103) Zhanbin F., Hongli Z., Jing H., Bing Y., Nanying N., Ming T., and Liqun Z., In Situ Exfoliation of Graphite into Graphene Nanosheets in Elastomer Composites Based on Diels−Alder Reaction during Melt Blending, *Ind. Eng. Chem. Res*. 2019, 58, 13182−13189

(104) Patrick P. Brisebois, ChristianKuss, Steen B. Schougaard, Ricardo Izquierdo, and Mohamed Siaj, New Insights intothe Diels–Alder Reaction of Graphene Oxide, *Chem. Eur*. J.2016, 22,5849–5852

(105) Sulleiro, M. V. Quiroga, S. Pen, D. Pe ´rez, D. Guitia, E. Criado, A. and Prato, M. Microwave-induced covalent functionalization of few-layer graphene with arynes under solvent-free conditions, *Chem. Commun*., 2018,54, 2086-2089

(106) Cho-Rong , Dae- Lee, , Jun-Hong Park , and Dai-Soo Lee, Thermally Healable and Recyclable Graphene-Nanoplate/Epoxy Composites Via an In-Situ Diels-Alder Reaction on the Graphene-Nanoplate Surface*;* *Polymers* 2019*,* 11(6), 1057; https://doi.org/10.3390/polym11061057

(107) Zhe J., Ji C., Liang H. and Gaoquan S., High-yield production of highly conductive graphene via reversible covalent chemistry, Chem. Commun., 2015,51, 2806--2809

(108) Xiaodong Z., Yuehua C. and Baoyan Z., Reduced graphene oxide/liquid crystalline oligomer composites based on reversible covalent chemistry, Phys. Chem. Chem. Phys., 2017, 19, 6082-6089

(109) Jeong-Min S. and Jong-Beom B., A solvent-free Diels–Alder reaction of graphite into functionalized graphene nanosheets, Chem. Commun., 2014, 50, 14651—14653

(110) Jianfeng X., Xiaomin Z., Feixiang L., Lun J. and Guohua C., Preparation of graphene via wet ball milling and in situ reversible modification with the Diels–Alder reaction, NewJ.Chem., 2020, 44, 1236-1244.

(111) Selvaraj M., Julio A., Adriana B., Volker A., Functionalization of Carbon Materials using the Diels-Alder Reaction, Macromol. Rapid Commun. 2010, 31, 574–579.

(112) Lucchese, M.M. Stavale, F. Ferreira, E.H.M. Vilani, C., Moutinho, M.V.O., Capaz, R.B. Achete, C.A., Jorio, A., Quantifying ion-induced defects and Raman relaxation length in graphene Carbon, 48(5) (2010) 1592-1597. https://doi.org/10.1016/j.carbon.2009.12.057

(113) Ferrari, A.C. Robertson, J., Interpretation of Raman spectra of disordered and amorphous carbon, *Phys. Rev*. B 61(2000) 14095. https://doi.org/10.1103/physrevb.61.14095

(114) Cui, T. Mukherjee, S. Cao, C. Sudeep, P.M. Tam, J. Ajayan, P.M. Singh, C.V. Sun, Y. Filleter, T. Effect of lattice stacking orientation and local thickness variation on the mechanical behavior of few-layer graphene oxide. *Carbon*, 136 (2018) 168–175. https://doi.org/10.1016/j.carbon.2018.04.074

(115) Ferrari, A.C. Meyer, J.C. Scardaci, V. Casiraghi, C. Lazzeri, M. Mauri, F. Piscanec, S. Jiang, D. Novoselov, K.S. Roth, S. Geim, A.K. Raman Spectrum of Graphene and Graphene layers. *Physical Review Letters*. 97 (2006) 187401. https://doi.org/10.1103/PhysRevLet.97.187401

(116) Cancado, L. G. Takai, K. Enoki, T. Endo, M. Kim, Y. A. Mizusaki, H. Speziali, N. L. Jorio, A.and Pimenta, M. A. Measuring the degree of stacking order in graphite by Raman spectroscopy, *Carbon*, 46(2) (2008) 272-275. https://doi.org/10.1016/j.carbon.2007.11.015

(117) Hernandez, Y. Nicolosi, V. Lotya, M. Blighe, F.M. Sun, Z. De, S. McGovern, I.T. Holland, B. Byrne, M. Gun'Ko, Y.K. Boland, J.J. Niraj, P. Duesberg, G. Krishnamurthy, S. Goodhue, R. Hutchison, J. Scardaci, V. Ferrari, A.C. Coleman, J.N. High-yield production of graphene by liquid-phase exfoliation of graphite, *Nature Nanotechnology*. 3(9) (2008) 563-568. https://doi.org/10.1038/nnano.2008.215

(118) Feng, C.P. Ni, H.Y. Chen, J. Yang, W. Facile Method to Fabricate Highly Thermally Conductive Graphite/PP Composite with Network Structures, Acs *Applied Materials & Interfaces*, 8(30) (2016) 19732-19738. https://doi.org/10.1021/acsami.6b03723.

(119) Chen, G. Wang, H. Zhao, W. Fabrication of highly ordered polymer/graphite flake composite with eminent anisotropic electrical property, *Polym. Adv. Technol*. 19(8) (2008) 1113-1117. https://doi.org/10.1002/pat.1093

(120) Mauro, M. Cipolletti, V. Galimberti, M. Longo, M. Guerra, G. Chemically Reduced Graphite Oxide with Improved Shape Anisotropy. *J. Phys. Chem*. C, 116(46) (2012) 24809–24813. https://doi.org/10.1021/jp307112k

(121) Fujimoto, H. Theoretical X-ray scattering intensity of carbons with turbostratic stacking and AB stacking structures, *Carbon*, 41(8) (2003) 1585–1592. https://doi.org/10.1016/s0008-6223(03)00116-7

(122) Rao, C. N. R. Biswas, K. Subrahmanyam, K. S. and Govindaraj, A. Graphene, the new nanocarbon, *J. Mater. Chem*., 19 (2009) 2457–2469. https://doi.org/10.1039/B815239J

(123) Scherrer, P. Nachrichten von der Gesellschaft der Wissenschaften zu Göttingen, Math. Klasse, 1918, 98–100.

(124) Machado, B. F. and Serp, P., Graphene-based materials for catalysis, *Catal. Sci. Technol*., 2 (2012) 54–75. https://doi.org/10.1039/C1CY00361E

(125) Tian, S. Li, L. Sun, W. Xia, X. Han, D. Li, J. and Gu, C. Robust adhesion of flower-like few-layer graphene nanoclusters, *Sci. Rep*., 2(1) (2012) 511. https://doi.org/10.1038/srep00511

(126) Yao, Y. Ren, L. Gao, S. Li, S., Histogram method for reliable thickness measurements of graphene films using atomic force microscopy (AFM). *J. Mater. Sci. Technol*., 33(8) (2017) 815–820. https://doi.org/10.1016/j.jmst.2016.07.020

(127) Hirsch Hadorn G., Hoffmann-Reim H., Biber-Klemm S., Gorssenbacher-Mansuy W., Joye D., Pohl C., et al., (Eds.), Handbook of transdisciplinary research, 2008, Springer; New York

(128) Gibbs, P., Neuhauser, L., Fam, D. (2018), the art of collaborative research and collective learning. http://doi.org/10.1007/978-3-319-93743-4_1

(129) Gibbons, M., Nowotny, H. (2001). An effective way for managing complexity (pp.67-80).

(130) Bergmann et al., 2012, P.35, methods for transdiciplinary research. A primer for practice.

(131) Horwath, I. Schweizer, S. (2023), Climate protection, resource efficiency and sustainable engineering.

(132) Horwath, I. Schweizer, S. (2023), Climate protection, resource efficiency and sustainable engineering. Application of transdisciplinarity in the context od sustainable product development. (p. 87)

(133) Horwath, I. Schweizer, S. (2023), Climate protection, resource efficiency and sustainable engineering. Interfacial design for catalytic recycling of CFRPs. (p. 149)

(134)) Horwath, I. Schweizer, S. (2023), Climate protection, resource efficiency and sustainable engineering. Henkes et al. Industry project. (p.105)

(135) United Nations, Department of Economic and Social Affairs. Population Facts, December 2019, No. 2019/6.

(136) Rockström, J.; Steffen, W.; Noone, K.; Persson, Â.; Chapin, F.S.; Lambin, E.; Lenton, T.M.; Scheffer, M.; Folke, C.; Schellnhuber, H.; et al. Planetary boundaries: Exploring the safe operating space for humanity. Ecol. Soc. 2009, 14, 32.

(137) Bjørn, A.; Chandrakumar, C.; Boulay, A.M.; Doka, G.; Fang, K.; Gondran, N.; Hauschild, M.Z.; Kerkhof, A.; King, H.; Margni, M.; et al. Review of life cycle-based methods for absolute environmental sustainability assessment and their applications. Environ. Res. Lett. 2020, 15, 083001.

(138) Mulder, K. Sustainable Development for Engineers: A Handbook and Resource Guide; Routledge: New York, NY, USA, 2006.

(139) Flangan, R. Whole-life Thinking and Engineering the Future, Frontiers of Engineering Management, 2014, 290-296, DOI 10.15302/J-FEM-2014040